WL-TR-96-2123

DYNAMIC BEHAVIOR OF A MENISCUS
SUBJECTED TO A TRANSIENT ACCELERATION FIELD

KIRK LEE YERKES

DECEMBER 1994
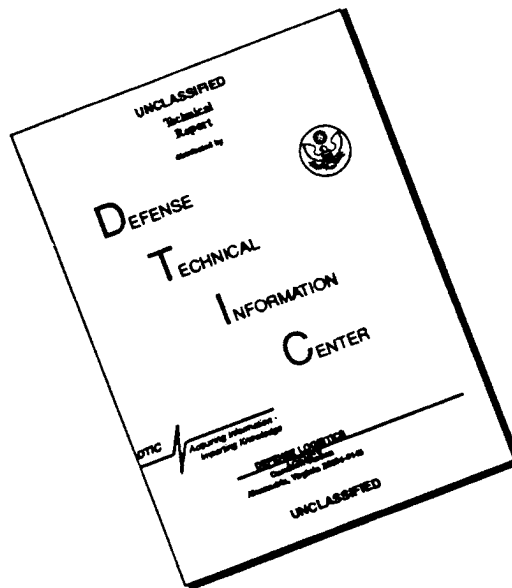
FINAL REPORT FOR 12/01/93-12/01/94

APPROVED FOR PUBLIC RELEASE; DISTRIBUTION IS UNLIMITED.

19961104 108

AEROPROPULSION AND POWER DIRECTORATE
WRIGHT LABORATORY
AIR FORCE MATERIEL COMMAND
WRIGHT PATTERSON AFB OH 45433-7251

DTIC QUALITY INSPECTED 1
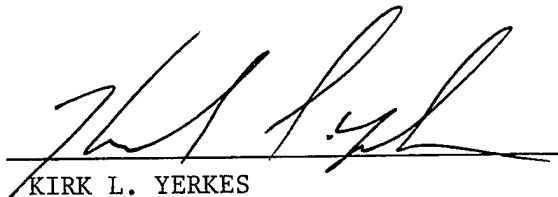
DISCLAIMER NOTICE

THIS DOCUMENT IS BEST QUALITY AVAILABLE. THE COPY FURNISHED TO DTIC CONTAINED A SIGNIFICANT NUMBER OF PAGES WHICH DO NOT REPRODUCE LEGIBLY.

NOTICE

WHEN GOVERNMENT DRAWINGS, SPECIFICATIONS, OR OTHER DATA ARE USED FOR ANY PURPOSE OTHER THAN IN CONNECTION WITH A DEFINITELY GOVERNMENT RELATED PROCUREMENT, THE UNITED STATES GOVERNMENT INCURS NO RESPONSIBILITY OR ANY OBLIGATION WHATSOEVER. THE FACT THAT THE GOVERNMENT MAY HAVE FORMULATED OR IN ANY WAY SUPPLIED THE SAID DRAWINGS, SPECIFICATIONS, OR OTHER DATA, IS NOT TO BE REGARDED BY IMPLICATION, OR OTHERWISE IN ANY MANNER CONSTRUED, AS LICENSING THE HOLDER, OR ANY OTHER PERSON OR CORPORATION; OR AS CONVEYING ANY RIGHTS OR PERMISSION TO MANUFACTURE, USE, OR SELL ANY PATENTED INVENTION THAT MAY IN ANY WAY BE RELATED THERETO.

THIS TECHNICAL REPORT HAS BEEN REVIEWED AND IS APPROVED FOR PUBLICATION.

KIRK L. YERKES
Research Engineer
Mechanical Branch
Aerospace Power Division

BURYL L. MCFADDEN,
Chief, Mechanical Branch
Aerospace Power Division
Aero Propulsion and Power Directorate

FOR THE COMMANDER

MICHAEL D. BRAYDICH, LT COL, USAF
Chief, Aerospace Power Division
Aero Propulsion and Power Directorate

REPORT DOCUMENTATION PAGE

Form Approved
OMB No. 0704-0188

1. AGENCY USE ONLY *(Leave blank)*	2. REPORT DATE	3. REPORT TYPE AND DATES COVERED	
	DEC 1994	FINAL	12/01/93--12/01/94

4. TITLE AND SUBTITLE DYNAMIC BEHAVIOR OF A MENISCUS SUBJECTED TO A TRANSIENT ACCELERATION FIELD

5. FUNDING NUMBERS
C
PE
PR   3145
TA   20
WU   49

6. AUTHOR(S) KIRK LEE YERKES

7. PERFORMING ORGANIZATION NAME(S) AND ADDRESS(ES)

AEROPROPULSION AND POWER DIRECTORATE
WRIGHT LABORATORY
AIR FORCE MATERIEL COMMAND
WRIGHT PATTERSON AFB OH 45433-7251

8. PERFORMING ORGANIZATION REPORT NUMBER

9. SPONSORING/MONITORING AGENCY NAME(S) AND ADDRESS(ES)

AEROPROPULSION AND POWER DIRECTORATE
WRIGHT LABORATORY
AIR FORCE MATERIEL COMMAND
WRIGHT PATTERSON AFB OH 45433-7251

10. SPONSORING/MONITORING AGENCY REPORT NUMBER

WL-TR-96-2123

11. SUPPLEMENTARY NOTES

12a. DISTRIBUTION/AVAILABILITY STATEMENT

APPROVED FOR PUBLIC RELEASE; DISTRIBUTION IS UNLIMITED.

12b. DISTRIBUTION CODE

13. ABSTRACT *(Maximum 200 words)*

The dynamic response of an unheated meniscus within a capillary tube subjected to single and multiple cycle transient acceleration induced forces was studied experimentally and analytically. A capillary tube was partially filled with either water or ethyl alcohol and mounted on a centrifuge for visual observation of the dynamic response of the meniscus subject to an acceleration transient. A one-dimensional mathematical model was formulated to predict the dynamic response of the meniscus and compared with experimental results. For the case in which the meniscus was heated, thermocapillary stresses in the near contact line region were accounted for in the model by a change in contact angle.

14. SUBJECT TERMS

Transient Acceleration, Thin Film, Meniscus, Contact Angle, Capillary Tube

15. NUMBER OF PAGES
220

16. PRICE CODE

17. SECURITY CLASSIFICATION OF REPORT	18. SECURITY CLASSIFICATION OF THIS PAGE	19. SECURITY CLASSIFICATION OF ABSTRACT	20. LIMITATION OF ABSTRACT
UNCLASSIFIED	UNCLASSIFIED	UNCLASSIFIED	SAR

DYNAMIC BEHAVIOR OF A MENISCUS SUBJECTED TO A TRANSIENT
ACCELERATION FIELD

Approved by:

_____
Kevin P. Hallinan, Ph.D.
Associate Professor
Mechanical Engineering
Committee Chairperson

_____
Jamie S. Ervin, Ph.D.
Assistant Professor
Mechanical Engineering
Committee Chairperson

_____
Thomas J. Kelly, Ph.D.
Assistant Professor
Aerospace Engineering
Committee Chairperson

_____
Paul W. Eloe, Ph.D.
Associate Professor
Mathematics
Committee Chairperson

_____
Won S. Chang, Ph.D.
Research Scientist
Wright Laboratory, USAF
Committee Chairperson

_____
Donald L. Moon, Ph.D
Associate Dean/Director
Graduate Engineering & Research
School of Engineering

_____
Joseph Lestingi, D. Eng., P.E.
Dean
School of Engineering

ii

ABSTRACT

DYNAMIC BEHAVIOR OF A MENISCUS SUBJECTED TO A TRANSIENT ACCELERATION FIELD

Name: Yerkes, Kirk, Lee
University of Dayton, 1994

Advisor: Dr. Kevin P. Hallinan

The dynamic response of an unheated and heated meniscus within a capillary tube subjected to single and multiple cycle transient acceleration induced forces was studied experimentally and analytically. A capillary tube was partially filled with either water or ethyl alcohol and mounted on a centrifuge for visual observation of the dynamic response of the meniscus subject to an acceleration transient. A one-dimensional mathematical model was formulated to predict the dynamic response of the meniscus and compared with experimental results. For the case in which the meniscus was heated, thermocapillary stresses in the near contact line region were accounted for in the model by a change in contact angle.

Comparison of the experimental results and analytical calculations for the case of an unheated meniscus showed that a combined axial and elevated transverse acceleration significantly altered the dynamic response of the meniscus and resulting in an increased meniscus velocity and subsequently lower meniscus position. Systems characterized by large Bond numbers, greater than 1.5, as distinguished by the larger capillary tube

diameters, were particularly sensitive to an elevated transverse acceleration component greater than 2g. Systems typified by a low Bond number, less than 1.5, tended to be insensitive to a transverse acceleration component due to the small capillary tube diameter. For systems typified by the combination of a low Bond number, less than 1.5, and high capillary number, greater than 10^{-5}, there was a significant amount of lag and retardation in the meniscus position, when compared to an inviscid solution.

The effect of heating the capillary tube on the dynamic response was also studied. Experimental results and analytical calculations were compared for a Bond number of 1.47 and a capillary number of 3.00×10^{-6}. Experimental data of the meniscus recession and advance agreed well with a one-dimensional equation of motion accounting for the "dynamic" contact angle.

ACKNOWLEDGMENTS

PREFACE

Recent technological advances in such areas as high power electronics and electric motor design have provided the impetus for the Air Force to develop more electric technologies in high performance aircraft. In doing so, the thermal management of electrical components, such as might be developed for actuation systems, may play a key role in the viability of a more electric concept. The use of passive thermal management concepts are currently being addressed to take advantage of the inherent reliability and simplicity in design. Such devices may incorporate capillary structures to aid heat transfer and have been generally thought of as being unreliable in high acceleration environments. However, little is known of the actual performance of capillary driven devices in a transient acceleration environment typical of high performance aircraft. It is the objective of this research to address and identify fundamental physical concepts which will ultimately aid in predicting the performance and design parameters of capillary driven heat transfer devices subject to transient accelerations.

This manuscript is the compilation of three papers (chapters I-III) for publication in the *Journal of Thermophysics and Heat Transfer* and the 9th International Heat Pipe Conference. As a result, there is some repetition in the text and figures to maintain clarity in each chapter. The reader is encouraged, along with the introduction and chapter IV (summary and conclusions), to treat chapters I, II, or III as independent investigations.

TABLE OF CONTENTS

LIST OF TABLES

LIST OF SYMBOLS

a = capillary tube radius

B = coefficient

Bo = Bond number, $(2a)^2 g_{pk} \rho / \sigma$

$\bar{b}$ = acceleration vector

Ca = capillary number, $\mu V_c / \sigma$

$\hat{e}$ = unit vector

$\bar{F}$ = force vector

F_{b_z} = body force, axial component

F_{s_z} = surface force, axial component

f = frequency of angular velocity

g = gravitational acceleration

g_{pk} = peak radial acceleration component

h_o = static wicking height, $2\sigma \cos\theta / \rho a g \sin\phi$

m = mass of liquid column in inclined capillary tube

Re = Reynolds number, $(2a) \rho V_c / \mu$

R_m = spherical radius of curvature

r = radial coordinate

r_o' = radial location of capillary tube pivot point

T = temperature

t = time

tf = angular velocity cycle period

$\bar{t}^{(\hat{n})}$ = surface traction vector

$\bar{V}$ = velocity vector

V_c = characteristic velocity, $2h_o/tf$

v = velocity component

We = Weber number, $Re \times Ca$

z = capillary tube axial directional coordinate

z_1 = capillary tube axial pivot location

ΔT = temperature difference over 1 cm

ζ = dimensionless meniscus position, η/h_o

η = meniscus position

Θ = dimensionless time, t/tf

θ = equivalent contact angle

θ_s = equivalent static contact angle

θ_d = dynamic contact angle (recession or advancing) or

contact angle, $\theta_{s,\ heat}$, with heat addition

μ = dynamic viscosity

ρ = density

σ = surface tension

$\tilde{\sigma}$ = stress tensor

τ_w = wall shear stress

ϕ = inclination angle

Ω = angular velocity as a function of Θ

ω = angular velocity

Subscripts

ave = average

b = body

lv = liquid-vapor interface

R = capillary tube transverse direction

r_T = centrifuge radial direction

s = surface

sl = solid-liquid interface

sv = solid-vapor interface

T = centrifuge tangential direction

y = vertical direction

z = capillary tube axial direction

INTRODUCTION

The static and dynamic behavior of two- and three-phase interfaces constitute a range of problems that have been frequently addressed in textbooks[1-4] and by investigators[5-8] over the last several years. These interfaces, which may be referred to as contact lines, often involve the displacement of one immiscible fluid in another along a solid surface, the spreading of a liquid drop on a solid, the displacement of gas or vapor by a liquid in a capillary tube, etc. There are many processes that require information with regard to the static and dynamic behavior of contact lines, such as the spreading of viscous liquids like paint, adhesive technologies, lubrication technologies, oil recovery, and processes utilizing contact lines and capillarity to enhance heat and mass transfer. The latter relates to condensation and evaporation processes associated with a wetting liquid on planar surfaces and within wicking structures consisting of porous media, grooved structures, and screens. In these cases, it is typical to have length-scales associated with the size of droplets, grooves, or pores on the order of several millimeters or less, resulting in a dominant surface tension force which controls the shape of the fluid-fluid interface close to the contact line.

Additional difficulties arise when devices incorporating these processes are subjected to elevated steady state and transient acceleration fields. Elevated steady state acceleration fields resulting in forces on the same order of magnitude or greater than

1

surface tension forces (more properly, the adhesion forces between the liquid and solid in the vicinity of the near contact line region) may affect the shape of the fluid interface. Transient acceleration induced forces (both transverse and axial), in addition to altering the fluid interface shape, will cause motion of the contact line as the gravitational potential associated with the liquid filled pore or groove changes. In such instances, the contact line velocity is functionally dependent on these transient acceleration induced forces as well as surface tension. The inclusion of these elevated steady state and transient acceleration fields defines a class of problems that are unique in the study of the static and dynamic behavior of contact lines.

If the problem of a static meniscus in a capillary tube is considered (discounting the near contact line region where the solid-liquid intermolecular forces may dominate the force field at the fluid interface), the equilibrium equation

$$\nabla \cdot \tilde{\sigma} + \rho \bar{b} = 0 \tag{1}$$

must be satisfied. A traction stress vector boundary condition in terms of surface tension is imposed on the free-surface interface. If this interface is assumed to have a spherical shape

$$\bar{t}^{(\hat{n})} \cdot \hat{n} = \frac{\sigma}{R_m} \tag{2}$$

is also satisfied. With this assumption, the "apparent" contact angle at the contact line is also required as a boundary condition to determine the radius of curvature and therefore

the interface shape. The specification of an apparent contact angle is intended to macroscopically describe the contribution of the physics of the extended meniscus region.

However, the contact angle as described by Young[9] is dependent on the free energy state at the contact line. Young was the first to derive an expression for contact angle using a force balance at the contact line and represented by the expression

$$\sigma_{lv}\cos\theta_e = \sigma_{sv} - \sigma_{sl} \tag{3}$$

This shows that the contact angle is functionally dependent on the free energy state at the contact line and may be used as an indirect determination of this minimum free energy state. Furthermore the difference between the free energy of the liquid-solid and liquid-gas to that of the solid-gas is defined as a spreading parameter

$$S = \sigma_{sv} - (\sigma_{sl} + \sigma_{lv}) \tag{4}$$

or

$$S = \sigma_{lv}(\cos\theta_e - 1) \tag{5}$$

When $S < 0$, the solid-gas interface has a lower free energy than the liquid-solid and liquid-gas and therefore the free energy is already minimized and the liquid will not spread.

Although static contact angles have been reported, early experimenters such as Padday[10] used direct methods of photography and indirect methods using measurements

3

from the vertical position of the contact line with respect to the undisturbed free surfaces. Others attempted to deduce its value from dynamic experimental measurements using tangent measurements along the free-surface at a point removed from the contact line. These investigations treated the contact line as a region of zero thickness intersecting the solid wall along a line with constant surface tension and, as such, were unable to consider the physics governing the contact line region. Hansen and Toong[11] concluded that classical laws of fluid motion were not applicable at the contact line and that observed contact angles may not be the appropriate contact angle of interest.

Concus[12] investigated the effect of Bond number on the shape of this interface in a right circular cylinder. Several contact angles were specified and the equilibrium equation was solved for the interface shape as a function of contact angle. His results showed that the interface shape was not necessarily spherical in nature, but was strongly dependent on the specified contact angle and corresponding Bond number.

Several different approaches, either macroscopic or microscopic, have been used to describe the dynamics associated with an advancing or receding unheated meniscus. In the macroscopic approach, the details of the near contact line region are ignored. Elliott and Riddiford[13] and Phillips and Riddiford[14] investigated the advancing and receding contact angle for a growing bubble between two flat plates as a function of interfacial velocity. They found a definitive relationship between the advancing or receding contact angle on interfacial velocity. For single liquid systems spreading on a dry surface, the advancing contact angle was found to be independent of the velocity for interfacial velocities up to 1 mm/min. For interfacial velocities greater than 1 mm/min.,

4

the advancing contact angle increased linearly to a limiting value. Qualitative molecular considerations were used to explain the velocity dependence of advancing contact angles. Relaxation of the contact angle from a dynamic value to a static value, when the fluid drive system was removed, was described as a molecular reorientation of the liquid molecules at the contact line.

Hoffman[15] investigated the shape of an advancing interface in a capillary tube for which viscous and interfacial forces are the dominant salient features defining the system. He found a relationship between the advancing contact angle and the capillary number ($Ca = \mu V/\sigma$) plus a shift factor determined by the static contact angle.

Recently, Calvo et al.[16] examined the advancing meniscus in a horizontal capillary tube attached to a liquid reservoir. It was found that the advance of the meniscus was controlled by: (i) the gravity head of the liquid above the capillary tube; and (ii) the line force associated with the apparent contact line equal to $(2\sigma/r)\cos\theta_d$, where θ_d is the apparent contact line angle for dynamic conditions. Their results indicated that for capillary numbers less that 10^{-5}, $\theta_d \sim \theta_s$, the static contact angle. With increasing capillary numbers the dynamic contact angle increases for advancing menisci and decreases for receding menisci. The macroscopic predictions of the advancing rate of the meniscus showed good agreement with experimental data.

The microscopic approach has focused on the details of the thin film region near the contact line. Instead of prescribing a line force, this approach has sought to determine the total dissipation in the thin film where the velocity gradients will be maximum. Thus, the viscous losses in the thin film will control the motion of the meniscus. Relative to

these microscopic approaches, de Gennes et al.[17], Ngan and Dussan, V.[18], and Dussan, V. et al.[19] have performed many of the most recent investigations concerning contact line dynamic behavior. In particular, de Gennes et al.[6] considered the dynamic behavior of the contact line associated with the spreading of a partially wetting fluid on an inclined moving plate. They distinguished four sub-regions, as shown in Fig. 1, consisting of: (i) a molecular region where the continuum description is no longer valid; (ii) a proximal region dominated by the long-range van der Waals forces; (iii) a central region dominated by viscous and capillary forces; and (iv) a distal region dominated by viscous and gravitational body forces. Their solution approach was to use matched asymptotic expansions to describe each distinct sub-region such that the boundary conditions of neighboring sub-regions were satisfied. The problem for each sub-region was formulated such that the physics was correctly defined (i.e., proper length-scales and appropriately dominant salient features). They solved for the static fluid thickness in the proximal and central region, then considered the contact line velocity as a perturbation and determined a first order correction to the static profile. Finally they matched this profile to that of the distal region profile.

Ngan and Dussan, V.[18] presented an investigation whose objective was to determine the appropriate boundary-value problem in an outer region (analogous to de Gennes' central and distal regions) excluding the inner region (analogous to de Gennes's proximal and central regions) in the immediate vicinity of the moving contact line between two parallel glass plates. The formulation of this boundary-value problem was based on the predication that the velocity field has an asymptotic structure near the

6

moving contact line. It was proposed that this structure contains only one parameter made up of terms consisting of the experimentally measurable quantities of apex height and intermediate contact angle, θ_R at $r = R$ (slightly removed from the contact line). The boundary-value problem was posed such that its validity in the outer region was maintained while a slip boundary condition was applied in the inner region along the solid surface. Further conditions required that the Bond number, capillary number, and Reynolds number approach zero. Their investigation dealt primarily with the extent to which this formulation accurately described the shape of the fluid interface asymptotically near the moving contact line in the outer region as $r \rightarrow 0$, and for small capillary numbers, $Ca \rightarrow 0$. The validity of this approach was verified in conjunction with experimental data.

Ngan and Dussan, V.[18] also found a systematic deviation between the predicted and experimental observations due in part from the fact that the theory accounted for only the two lowest orders in the asymptotic expansion in the capillary number and hence indicated that the capillary number used, on the order of 10^{-2}, may have been too large. A subsequent experimental investigation was performed by Dussan, V. et al.[19] to verify these hypotheses. Experiments were performed for capillary numbers ranging from 2.8×10^{-4} to 8.3×10^{-3}. The capillary numbers used for this investigation were lower by an order of magnitude than previous investigations in an attempt to verify that the systematic deviation between experimental results and analytical calculations was due to the neglect of higher-order terms in the capillary number expansions. They found good agreement between the experimental results and the theoretical predictions with the systematic deviations appearing only at the higher capillary numbers.

With the addition of heat to the meniscus region, the dynamics associated with an advancing or receding meniscus may be significantly altered from that of the unheated case. In addition to evaporation, surface tension will decrease with increased temperature and temperature gradients will result in a spatial surface tension gradient along the meniscus surface. These surface tension gradients cause interfacial tangential stresses or thermocapillary stresses to develop at the meniscus surface. The induced stresses due to thermocapillary effects have the effect of altering the contact angle. Modifying the equation by Young[9], eq. (3), to account for the thermocapillary stress, σ_{tc}, results in

$$(\sigma_{lv} - \sigma_{tc}) \cos \theta_e = \sigma_{sv} - \sigma_{sl} \qquad (6)$$

If non-isothermal conditions exist, thermocapillary stresses at the interface may have a net effect of either increasing or decreasing the contact angle depending on the direction of the spatial surface tension gradient.

There have been many noteworthy investigations with regard to the evaporating meniscus with and without the inclusion of thermocapillary effects.[20-26] Derjaguin et al.[20] was first to develop a theory of evaporation from a capillary with verification from experimental results. Holm and Goplen[21] developed an approximate method for predicting the surface heat transfer coefficients in the vicinity of the extended meniscus (analogous to de Gennes' proximal and central regions) in a capillary groove structure. They concluded that heat transfer through the extended meniscus accounted for approximately 80% of the total heat dissipation from the wall. Moosman and Homsy[22] used perturbation theory to model a horizontal non-isothermal extended meniscus. They showed that there

8

is a potential for large heat fluxes to occur near the contact line with a subsequent thinning of this region and an increase in the apparent contact angle. However, none of these investigators considered thermocapillary effects.

Investigations taking into account thermocapillary effects have been primarily mathematical in nature without experimental verification. Sen and Davis[23] analytically demonstrated thermocapillary flows in a two-dimensional slot induced as a result of an applied temperature gradient to the free surface. They assumed either a fixed contact line or a fixed contact angle as a basis for their analytical solutions. Swanson and Herdt[24] developed a mathematical model of an evaporating meniscus in a capillary tube taking into account thermocapillary effects for small heat inputs. They observed no change in the apparent contact angle and noted that the meniscus profile remained spherical. Hallinan et al.[25] considered the same geometry as Swanson and Herdt also allowing for non-isothermal extended meniscus. Results were comparable with other investigators and they identify conditions necessary for thermocapillary stresses to have an effect on the flow into the extended meniscus region.

Pratt and Hallinan[26] present an experimental and analytical approach on the thermocapillary effects on a heated meniscus in a capillary tube. They experimentally demonstrate their claim that thermocapillary stresses induce a meniscus recession and present the critical ΔT or Marangoni number required for the meniscus to recede. The critical ΔT was analytically shown to have the effect of increasing the apparent contact angle resulting in a meniscus recession.

To date, these formulations have been limited to situations where the Bond number

is small (e.g., inside of capillary tubes) or where it is infinite (such as exists for draining films[27]). While acceleration induced forces are considered conservative and long-range in nature, they affect the free surface shape and the slope for which solutions to the sub-regions as described by de Gennes et al.[17] must be asymptotically matched. Furthermore, it is not known what potential effects these forces may have on the precursor film thickness and stability in both static and dynamic conditions.

In general, prior investigations with regard to the dynamic behavior of the contact line have specified a contact line velocity consistent with a moving solid boundary. Transient acceleration induced forces will induce a contact line velocity posing a problem such that the contact line dynamics is dependent only on the temporal acceleration fields and not on a moving solid boundary. There has been limited research with regard to the effects of acceleration induced forces. Most of these have addressed the equilibrium free-surface shape.[12] This investigation addresses the dynamic behavior of a unheated and heated meniscus and contact line region in a capillary tube subjected to a transient acceleration field.
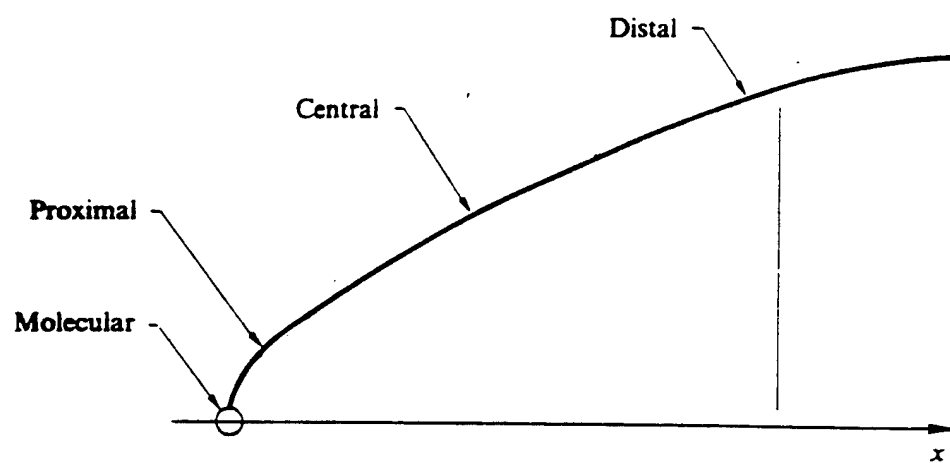
Fig. 1 The contact line region divided into four sub-regions.

11

CHAPTER I

DYNAMIC BEHAVIOR OF AN UNHEATED MENISCUS SUBJECTED TO A TRANSIENT ACCELERATION FIELD

Abstract

This study experimentally and analytically investigates the effects of acceleration transients on the dynamic response of an unheated meniscus in a capillary tube. A capillary tube partially filled with either water or ethyl alcohol was mounted on a centrifuge to observe the dynamic response of the meniscus subject to an acceleration transient. It was found that for a transverse acceleration component of less than 2g, experimental data of the meniscus advance or recession agreed well with a one-dimensional formulation of the equation of motion which assumed a spherical shaped meniscus. However, for transverse accelerations greater than 2g, there was an increase in the observed meniscus velocity both upon recession and advancement resulting in a lower meniscus position when compared to the analytically predicted position. Water exhibited a significant amount of "sticking" and hysteresis which appeared to intensify with increasing transverse acceleration.

Experimental

Acceleration Field

Transient acceleration fields were generated using a 2.4-m diameter centrifuge table (Fig. 1.1) rotating with a time variant angular velocity. Angular velocity transients were generated at a specified cyclic frequency of 0.0015 Hz ($tf = 1/0.0015$ s) using a signal or waveform generator as a control input to the centrifuge. The angular velocity was increased linearly to a peak value at the midpoint of the cycle and subsequently decreased as shown in Fig. 1.2a. A tri-axis accelerometer (Columbia Research Laboratories, Inc.) was used to monitor the time variant acceleration components in a cartesian reference frame affixed to the centrifuge table. Figure 1.2b shows a typical accelerometer output to the experimentally generated acceleration field for each of the three coordinate directions. For this investigation, the peak angular velocity was specified such that a 4.2-g ± 0.1-g peak radial acceleration was generated ($g_{pk} = 41.20$ m/s^2).

Capillary Test Cell

A sealed test cell containing a glass capillary tube and reservoir was positioned on the centrifuge as shown in Fig. 1.3. The test cell was mounted to a motorized optics rotation stage (Newport) such that the capillary tube was allowed to pivot about its center of mass. This pivot point was displaced vertically from the centrifuge surface at a fixed radial location, r_o', as shown in Fig. 1.4a. Angles of inclination of the capillary tube were determined from the output of a calibrated angular displacement transducer (Trans-Tek, Inc.) accurate to within ±0.2 degrees.

13

Experiments were conducted by fixing the capillary tube at a specified inclination angle while subjecting it to the aforementioned transient acceleration field. Increasing the inclination angle elevates the transverse acceleration component referenced to the capillary tube. This allowed the dynamic response of the meniscus subjected to an increasing transverse acceleration component to be observed experimentally. The dynamic response of the meniscus to the transient acceleration field was observed using an 8-mm CCD camera (Sony) mounted adjacent to the test cell as shown in Fig. 1.3b. The meniscus height relative to the reservoir meniscus, η, was measured as a function of time to within ± 1.0 mm. An equivalent contact angle, θ, was calculated from the experimentally determined static wicking height, h_o, for conditions when the transverse acceleration component was zero ($h_o \rho g \sim (2\sigma/a)\cos\theta$).

Water (reverse osmosis) and ethyl alcohol were used as the test fluids to demonstrate the importance of the equilibrium contact angle on the advance and recession of the meniscus due to a transient acceleration field. Properties of these fluids were assumed to be that of the bulk reservoir fluid corresponding to a experimental temperature of 30°C.

The test cell and capillary tube were cleaned using potassium hydroxide and rinsed with distilled water. The test cell was filled and subsequently sealed resulting in a fill that had a combination of air, fluid vapor, and liquid.

Analytical Formulation

The goals of the analytical formulation were to: (i) mathematically describe the transient nature of the acceleration field referenced to the capillary tube in the meniscus region; (ii) mathematically describe the dynamic behavior of the meniscus as a result of the temporal acceleration induced forces using a simplified one-dimensional model with a constant line force; and (iii) determine the relative importance of the transverse acceleration component, Bond number, and capillary number on the meniscus motion by comparing experimental results and analytical calculations.

Acceleration Vector

Acceleration measurements were obtained with regard to a three-dimensional cartesian non-inertial reference frame affixed to the centrifuge. The acceleration field was then referenced to fixed locations on the capillary tube and subsequently decomposed into transverse and axial acceleration components relative to the capillary tube as shown in Fig. 1.4b.

The transient acceleration vector in a cartesian coordinate reference frame from the viewpoint of an observer on the centrifuge is of the form

$$\bar{b} = b_{r_T}\hat{e}_{r_T} + b_y\hat{e}_y + b_T\hat{e}_T = b_z\hat{e}_z + b_R\hat{e}_R \tag{1}$$

where for a fixed radial location, r_T, the following acceleration components are realized:

radial component, $\quad b_{r_T}(t) = \omega^2(t)\, r_T,$

15

tangential component, $b_T(t) = \dfrac{d\omega(t)}{dt} r_T$,

vertical component, $b_y(t) = -g$.

After an appropriate transformation to the capillary tube reference frame, the acceleration vector can be decomposed into an axial component, b_z, and a transverse component, b_R, which results in

$$\bar{b} = \left[-\omega^2(r'_o + (z_1 - z)\cos\phi)\cos\phi + (-g)\sin\phi\right]\hat{e}_z +$$
$$\left[\left[-\omega^2(r'_o + (z_1 - z)\cos\phi)\sin\phi - (-g)\cos\phi\right]^2 + \left[(r'_o + (z_1 - z)\cos\phi)\frac{d\omega}{dt}\right]^2\right]^{1/2}$$

(2)

Here, the transverse component, b_R, is a magnitude with no reference to direction due to the axisymmetric nature of the capillary tube.

Equation of Motion

A simple analytical model is described which predicts the motion of the meniscus subjected to transient accelerations. The analytical formulation of the equation of motion was simplified assuming bulk flow only in the axial direction of the capillary tube. Effectively the liquid column in the capillary tube is assumed to undergo a slug flow. From the conservation of momentum,

$$\Sigma\bar{F} = \bar{F}_s + \bar{F}_b = \frac{d(m\bar{V})}{dt},$$ (3)

the surface and body forces in the axial direction combine resulting in the axial force

$$F_z = F_{s_z} + F_{b_z}.$$ (4)

The surface force, F_{s_z}, is formulated by accounting for the cumulative effect of solid-liquid intermolecular forces in the near contact line region and the wall shear stress associated with Poiseuille flow in the liquid column. The contact line force is defined assuming a spherical meniscus and a constant equivalent or apparent contact angle such that

$$F_{s_z} = \sigma(2\pi a)\cos\theta + \tau_w(2\pi a)\eta.$$ (5)

Note that such an assumption implies a non-changing apparent contact angle under dynamic conditions. A great deal of work has established a relationship between the dynamic contact angle, θ_d, and the capillary number (for low Bond numbers) as summarized by Hoffman[15]. These results have shown little change in the contact angle for capillary numbers less than 10^{-5}.

The shear stress at the wall is defined using the Darcy friction factor assuming laminar tube flow where

$$\tau_w = \frac{64}{Re}\left(\frac{\rho V_{ave}^2}{8}\right).$$ (6)

This results in the following surface force formulation while using a slug flow

17

approximation to describe the flow of liquid in the column, i.e., $V_{ave} = d\eta/dt$.

$$F_{s_z} = \sigma(2\pi a)\cos\theta - 8\pi\mu\eta\frac{d\eta}{dt} \qquad (7)$$

The total body force,

$$F_{b_z} = \int_0^\eta \int_0^a b_z\rho(2\pi)\,r\,dr\,dz, \qquad (8)$$

is formulated by integrating over the volume of the liquid column the axial acceleration component, b_z, from eq. (2) as defined by

$$b_z = -\omega(t)^2\cos\phi\left(r_o' + (z_1 - z)\cos\phi\right) - g\sin\phi. \qquad (9)$$

The transient angular velocity is of the form

$$\begin{aligned}\omega(t) &= Bt, & 0 \le t \le \frac{tf}{2} \\ &= B(tf - t), & \frac{tf}{2} \le t \le tf\end{aligned} \qquad (10)$$

where

$$B = \left(\frac{4\,g_{pk}}{(tf)^2 r_o'}\right)^{\frac{1}{2}}. \qquad (11)$$

Assuming that the axial fluid velocity is also defined by $v_z = d\eta/dt$ (due to the slug

18

flow assumption) and the mass in the capillary tube as $m = \rho\,(\pi a^2)\,\eta$, the relation for the time rate of change in momentum is defined as

$$\frac{d(mv_z)}{dt} = \rho\,(\pi a^2)\left[\eta\,\frac{d^2\eta}{dt^2} + \left(\frac{d\eta}{dt}\right)^2\right]. \tag{12}$$

Combining eqs.(7), (8), and (12), the momentum equation becomes

$$\left[\frac{2\sigma\cos\theta}{\rho a}\right] - \left[\frac{8\mu}{\rho a^2}\eta\,\frac{d\eta}{dt}\right] + \left[\int_0^\eta b_z\,dz\right] = \left[\eta\,\frac{d^2\eta}{dt^2} + \left(\frac{d\eta}{dt}\right)^2\right]. \tag{13}$$

Integrating the axial acceleration term, b_z, and rearranging, the momentum equation becomes

$$\frac{2\sigma\cos\theta}{\rho a} = \left[\eta\,\frac{d^2\eta}{dt^2} + \left(\frac{d\eta}{dt}\right)^2\right] + \left[\frac{8\mu}{\rho a^2}\eta\,\frac{d\eta}{dt}\right]$$
$$+ \eta\left[\omega(t)^2\,\cos\phi\left(\left(z_1 - \frac{\eta}{2}\right)\cos\phi + r_o'\right) + g\sin\phi\right]. \tag{14}$$

A non-dimensional form of the momentum equation can now be derived using the following dimensionless parameters

$$\zeta = \frac{\eta}{h_o},\quad 0 \le \zeta \le 1$$
$$\Theta = \frac{t}{tf},\quad 0 \le \Theta \le 1, \tag{15}$$

with the following initial conditions

$$\zeta = 1, \quad \frac{d\zeta}{d\Theta} = 0, \quad \Theta = 0.$$

A new angular velocity, Ω, is formed by factoring g_{pk} out of the coefficient B (defined by eq. (11)) in eq. (10) and casting it in terms of the non-dimensional time, Θ, where

$$
\begin{aligned}
\Omega(\Theta) &= \left(\frac{4}{r_o'}\right)^{\frac{1}{2}} \Theta, & 0 \leq \Theta \leq \frac{1}{2} \\
&= \left(\frac{4}{r_o'}\right)^{\frac{1}{2}} (1-\Theta), & \frac{1}{2} \leq \Theta \leq 1.
\end{aligned}
\tag{16}
$$

The non-dimensional form of the momentum equation in terms of a transient dimensionless meniscus position becomes

$$
\frac{g}{g_{pk}}\sin\phi = \left[\frac{a}{h_o}\right]\left[\frac{Re\,Ca}{2Bo}\right]\left[\zeta\frac{d^2\zeta}{d\Theta^2}+\left(\frac{d\zeta}{d\Theta}\right)^2\right]+\left[\frac{16\,Ca}{Bo}\right]\left[\zeta\frac{d\zeta}{d\Theta}\right]
$$
$$
+\zeta\left[\Omega(\Theta)^2\cos\phi\left(\left(z_1-\frac{h_o\zeta}{2}\right)\cos\phi+r_o'\right)+\frac{g}{g_{pk}}\sin\phi\right].
\tag{17}
$$

The first and second terms of eq. (17) represent the inertial and viscous effects, respectively, with the coefficients formed as the products of the dimensionless parameters of Reynolds, capillary, and Bond numbers. The Reynolds and capillary numbers are referenced to a characteristic velocity, V_c, which is the maximum attainable velocity over one-half of the acceleration cycle period assuming $\eta = 0$ at g_{pk}. The Bond number is referenced to the peak radial acceleration component, g_{pk}.

For small inertial and viscous effects, the momentum equation can be reduced to

the following quadratic form for the transient dimensionless meniscus position.

$$\zeta^2 - \left(\frac{\Omega(\Theta)^2 \cos\phi \, (z_1\cos\phi + r_o') + \dfrac{g}{g_{pk}}\sin\phi}{\Omega(\Theta)^2 \dfrac{h_o}{2} \cos^2\phi} \right) \zeta + \left(\frac{\dfrac{g}{g_{pk}}\sin\phi}{\Omega(\Theta)^2 \dfrac{h_o}{2} \cos^2\phi} \right) = ($$

(18)

Results

Equations (17) and (18) were solved for the dimensionless meniscus position using a central-difference scheme and as a quadratic respectively. These solutions were obtained as a result of specifying a static wicking height, h_o, based on the experimentally determined equivalent contact angle, θ. Solutions to eqs. (17) and (18) were identical for the experimental parameter range specified in this investigation. This supports the use of the closed form solution of eq. (18) in instances where inertial and viscous effects can be assumed to be negligible.

Experiments were performed and the results compared with solutions to the analytical model. Uncertainty in the experimentally obtained dimensionless meniscus position, ζ, and time, Θ, was on the order of ζ, $\Theta \pm 0.02$ based on the accuracy and resolution of the experimentally measured quantities. In general, the comparison between the model and the experiment is surprisingly good, given the simplicity of the model. However, a number of interesting deviations from the model help to provide insight into the physical phenomena associated with the advancing/receding meniscus.

Figure 1.5 compares the experimentally obtained dimensionless meniscus position

21

to the analytical results for water at varying angles of inclination. Also shown are the axial and transverse acceleration components. The equivalent contact angle was 22.2° with an experimental Bond number of 2.05. Experimental parameters ranged from

$5.9 \times 10^{-7} \leq Ca \leq 1.5 \times 10^{-6}$, $0.11 \leq Re \leq 0.28$, and

$2.3 \times 10^{-2} \leq a/h_o \leq 5.7 \times 10^{-2}$ as the inclination angle varied from 20° to 60°.

There was a significant amount of "sticking" of the advancing meniscus for water as evidenced by the discontinuous nature of the meniscus position curves, Fig. 1.5. There also was a permanent hysteresis in the meniscus position at the completion of the test cycle resulting in a lower wicking height. This "sticking" of the meniscus appeared to become more significant with an increased transverse acceleration component, as demonstrated in Fig. 1.5e. For a peak transverse acceleration component greater than 2.5g the experimental results showed an increase in the meniscus velocity for both the receding and advancing meniscus from that predicted by the analytical results, Figs. 1.5d and 5e. At the midpoint of the acceleration cycle the meniscus position was also lower in Figs. 1.5d and 1.5e than that predicted analytically.

Also, for all cases using water as the test fluid the initial meniscus recession speed tended to be under-predicted. Since the contact line force in the predictions is controlling the receding and advancing velocities it is apparent that it is slightly over-predicting the actual contact line dissipation. Using an equivalent contact angle to describe the line force at the contact line neglects the fact that, as the meniscus recedes, some fluid is left behind rather that being dragged over the tube wall.[27] Thus, the line force is physically less than predicted by the model. Conversely, for the advancing contact line, since it is

presumed that a film of liquid is already present on the inside diameter of the tube, it is easier for the meniscus to advance relative to that predicted for an advancing meniscus over a dry surface (such as is associated with using the equivalent contact angle).

Figure 1.6 compares the experimentally obtained dimensionless meniscus position to the analytical results for ethyl alcohol at varying angles of inclination. As with Figure 1.5, also shown are the axial and transverse acceleration components. The equivalent contact angle was 16.7° with an experimental Bond number of 1.47. Experimental parameters ranged from $1.7 \times 10^{-6} \leq Ca \leq 3.6 \times 10^{-6}$, $3.0 \times 10^{-2} \leq Re \leq 6.1 \times 10^{-2}$, and $1.9 \times 10^{-2} \leq a/h_o \leq 4.0 \times 10^{-2}$.

The experimentally obtained dimensionless meniscus position for ethyl alcohol agrees well with the analytical results to within experimental error for a peak transverse acceleration component less than 2g. No "sticking" of the meniscus was observed and there was no observable hysteresis. As shown in Figs. 1.6 c-e, there was an observable increase in the meniscus velocity relative to the model for both the receding and advancing meniscus for a peak transverse acceleration component greater than 2g. This increase in meniscus velocity resulted in a meniscus position lower than that predicted analytically.

The effects of capillary number for a fixed Bond number and inclination angle on the dimensionless meniscus position are shown in Fig. 1.7. A comparison of the analytical results, using eq. (17), for a Bond number of 0.42 and capillary numbers of 10^{-6}, 10^{-5}, and 10^{-4} at a 20° inclination angle demonstrates that, for capillary numbers less than 10^{-5}, viscous losses outside of the contact line had only a small effect on the

23

meniscus position. However, for capillary numbers on the order of 10^{-4} and greater there is a significant lag in the meniscus position due to viscous effects. Capillary numbers less than 10^{-5} and Bond numbers ranging from 0.42 to 2.1 were predicted to have no effect on the dynamic response of the meniscus. Analytical results, using eq. (17), for a capillary number of 10^{-4} and Bond numbers of 0.42, 0.84, and 1.26 at angles of inclination ranging from 20° to 60° are compared in Fig. 1.8. Figure 1.8a shows the dimensionless meniscus position at varying angles of inclination for a fixed Bond number of 0.42 and a capillary number of 10^{-4}. For decreasing angles of inclination, viscous effects outside the contact line region become significant resulting in the characteristic lag in meniscus position. These analytical results do not take into account the significance of the transverse acceleration component at the higher angles of inclination and to the extent at which this transverse component affects the dynamic response of the meniscus. Figure 1.8b compares the dimensionless meniscus position for a varying Bond number with that of the inviscid solution, using eq. (18), neglecting inertial effects at a 20° inclination angle. Here, a decrease in Bond number resulted in the increased importance of viscous effects yielding a lag in the meniscus position when compared to the low inertia inviscid solution. For Bond numbers less than 1.3 and capillary numbers greater than 10^{-4}, there were significant viscous effects resulting in a lag in the meniscus position. However, these results assume a constant contact line force, as a result of specifying a constant equivalent contact angle, and does not account for the functional dependence of the contact angle on capillary number as discussed by Hoffman[15]. However, for experimental and analytical results with capillary numbers less than 10^{-5}, this dependence

24

can be assumed to be negligible.

The magnitude of the transverse acceleration component had a significant effect on the dynamic response of the meniscus. This is in part attributed to the use of the constant equivalent contact angle to define a constant contact line force in the analytical formulation. While the meniscus shape may remain relatively spherical in nature with an increased axial acceleration component for the relatively low Bond numbers considered, the transverse acceleration component will serve to reorient the meniscus in a transverse direction and distend it in the axial direction. This variation in the meniscus shape and position in the capillary tube will result in an increased contact line length which will tend to be elliptical rather than spherical, as shown in Fig. 1.9. Therefore, one might expect an increase in the net contact line force due to the increased length of the contact line. Theoretically, the predicted recession and advancing rates would be differ from those shown, actually moving in a direction opposite of that seen experimentally in the water and ethyl alcohol tests. Such observations point to the need for a closer examination of the near contact line region fluid physics with regard to the transverse acceleration component to completely describe the motion of the meniscus. Therefore, use of an equivalent contact angle to define the contact line force is an approximation at best. Instead, the contact angle, rather than being constant, is a function of the transverse acceleration component and angular position on the capillary tube wall.
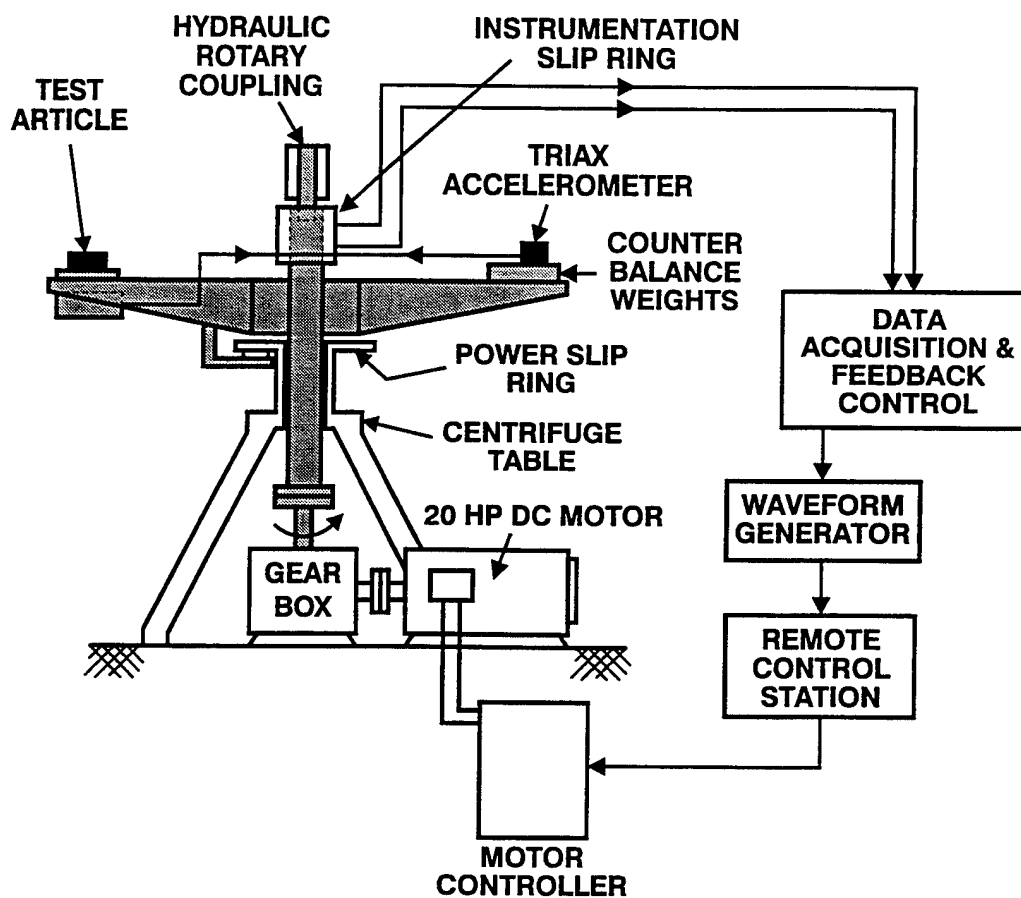
Fig. 1.1 Schematic of centrifuge.

a)
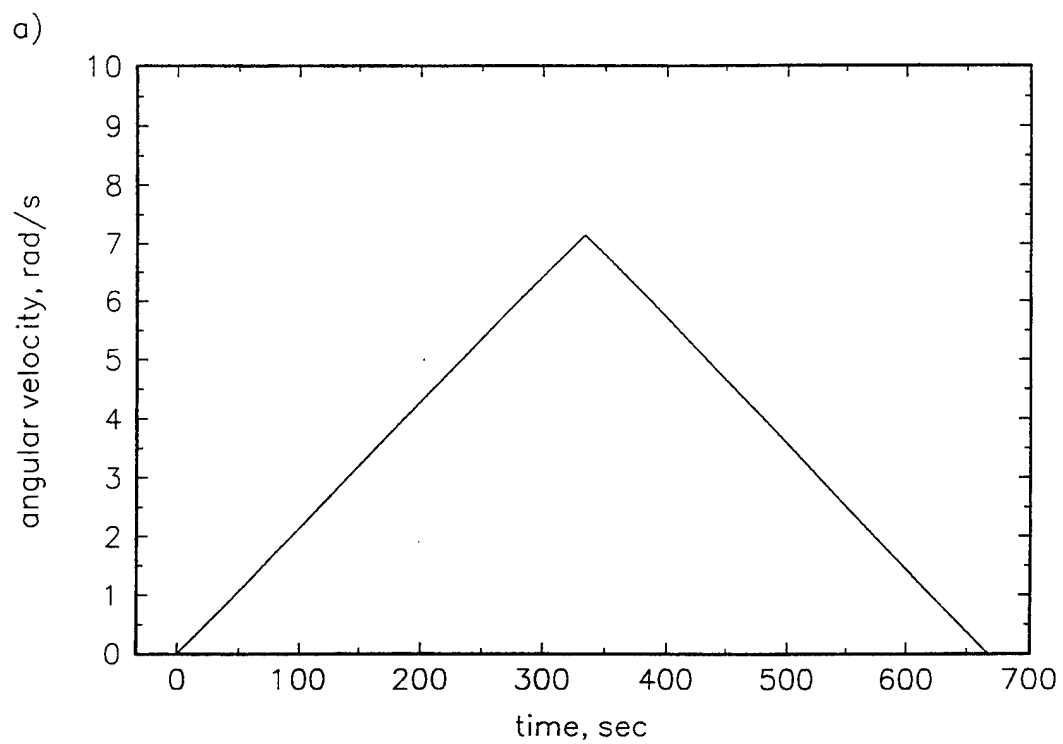
Fig. 1.2 Plot of the centrifuge test cycle (0.0015 Hz): a) angular velocity,

b)
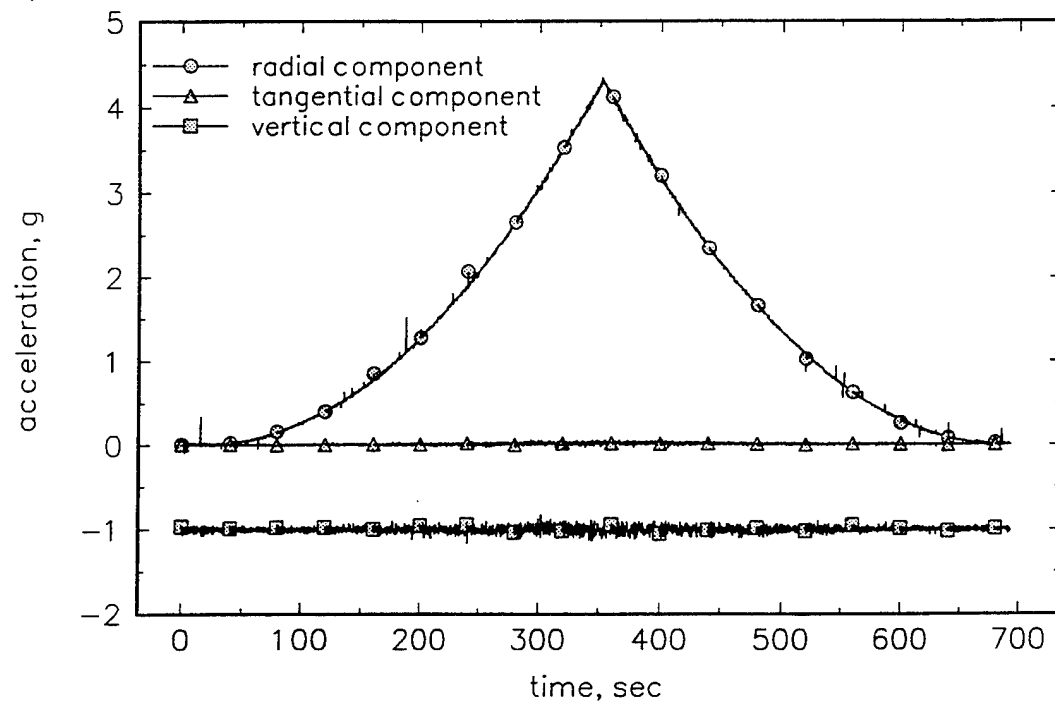
Fig. 1.2(contd) b) resulting acceleration field.

28

a)

$\bar{b}$

spring
loaded
clamp

capillary
tube

pivot
point

reservoir

b)

8mm CCD
camera

optics
rotation
stage

angular
position
transducer

test cell w/
capillary tube

accelerometer
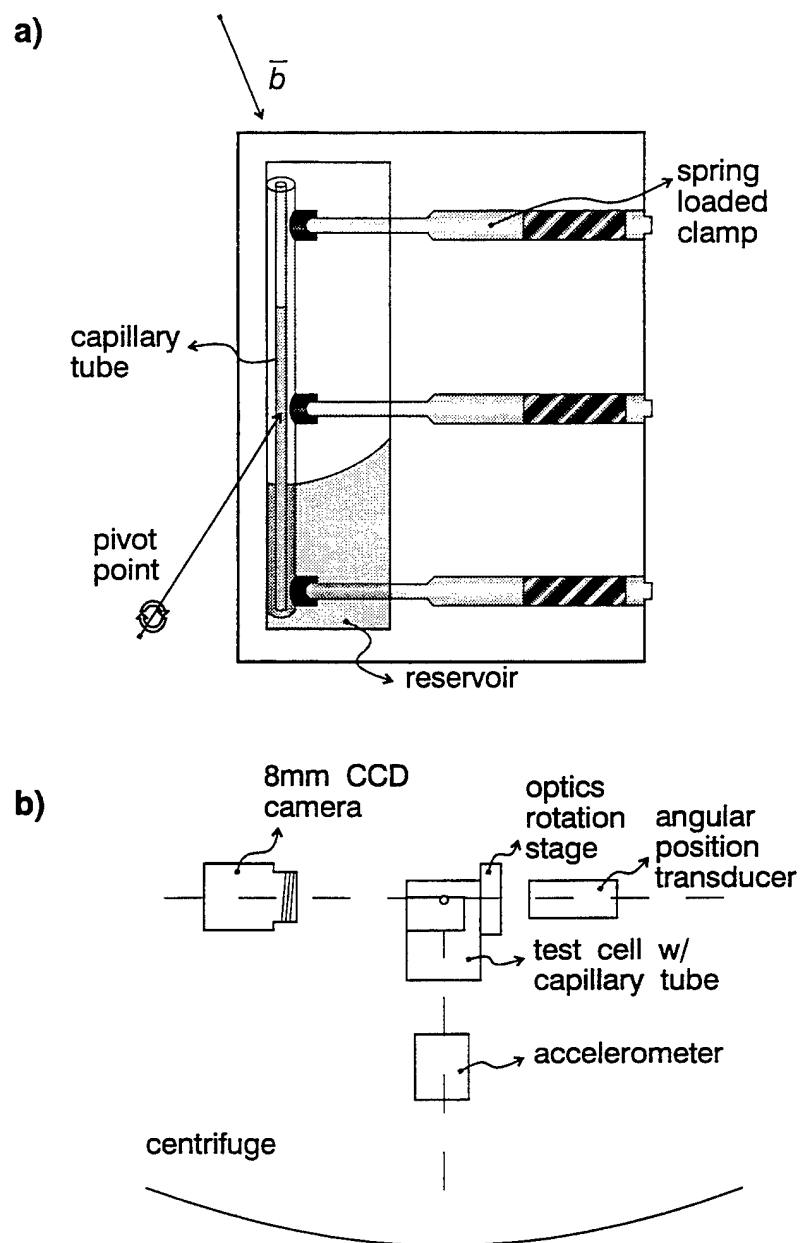
centrifuge

Fig. 1.3 Experimental apparatus: a) sealed test cell
and b) schematic of experimental apparatus as mounted on the centrifuge.

29
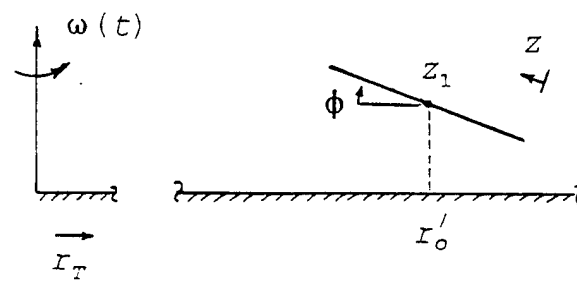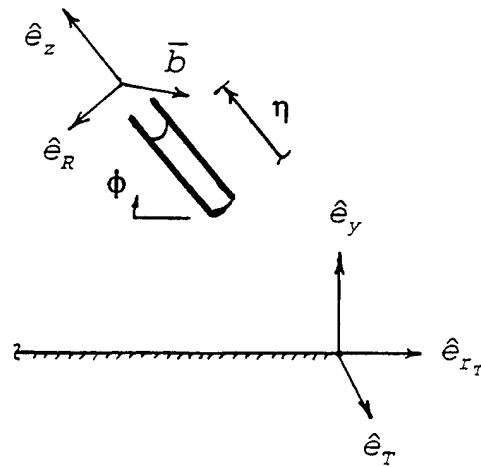
Fig. 1.4 Capillary tube orientation: a) pivot point location, directional coordinates and b) coordinate systems as referenced to the centrifuge accelerometer and capillary tube.

30

$\varphi = 20°$
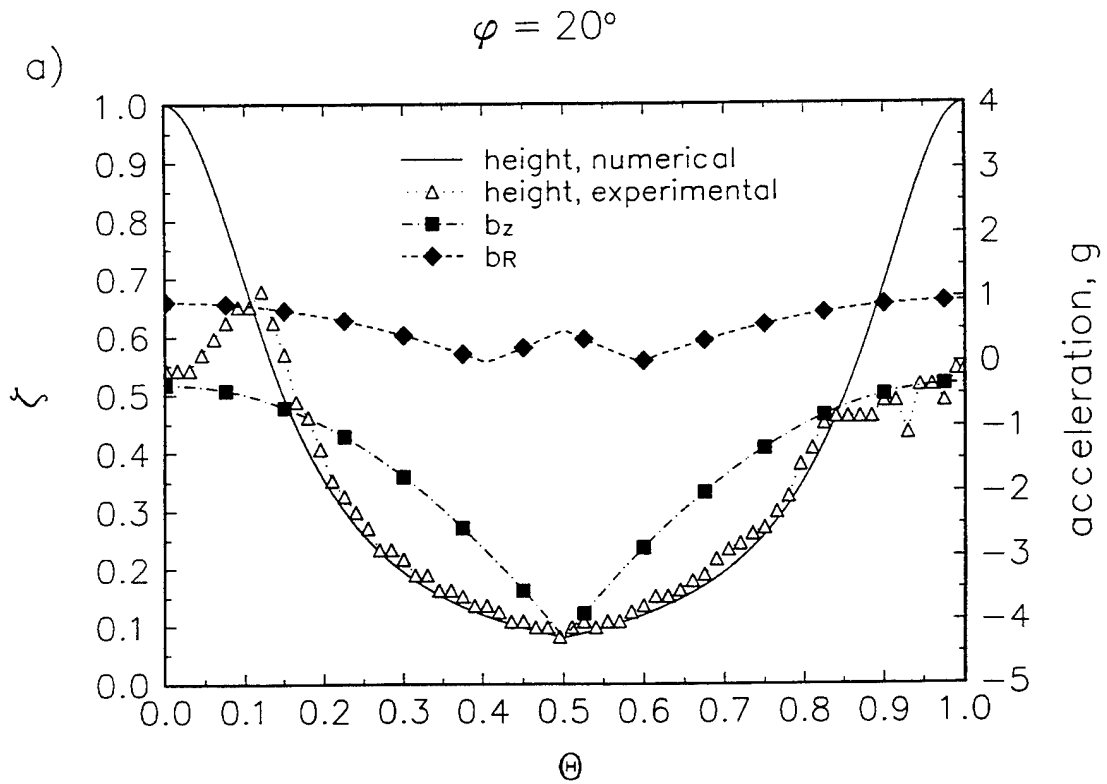
Fig. 1.5 Experimental data compared to analytical results for water at $Bo = 2.05$:
a) $\phi = 20°$, $Ca = 1.50 \times 10^{-6}$, $Re = 0.278$, $a/h_o = 2.25 \times 10^{-2}$,

$\varphi = 30°$
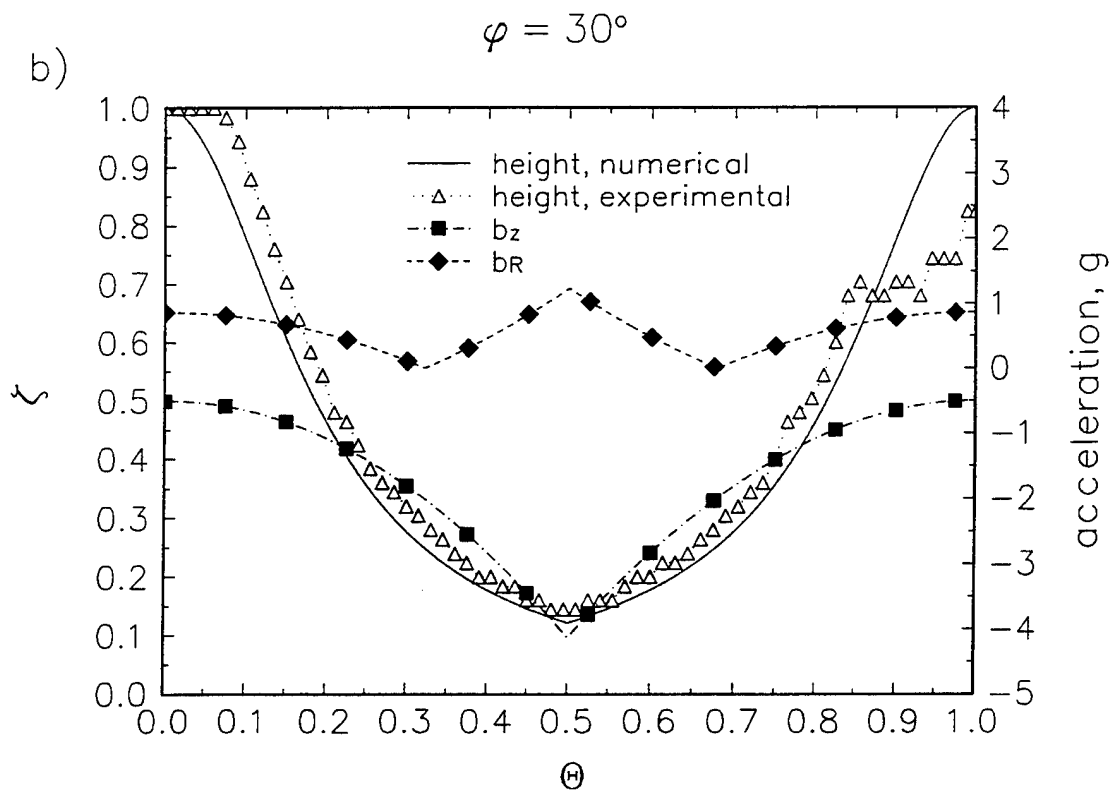
Fig. 1.5(contd)

b) $\phi = 30°$, $Ca = 1.03 \times 10^{-6}$, $Re = 0.191$, $a/h_o = 3.30 \times 10^{-2}$,

$\varphi = 40°$
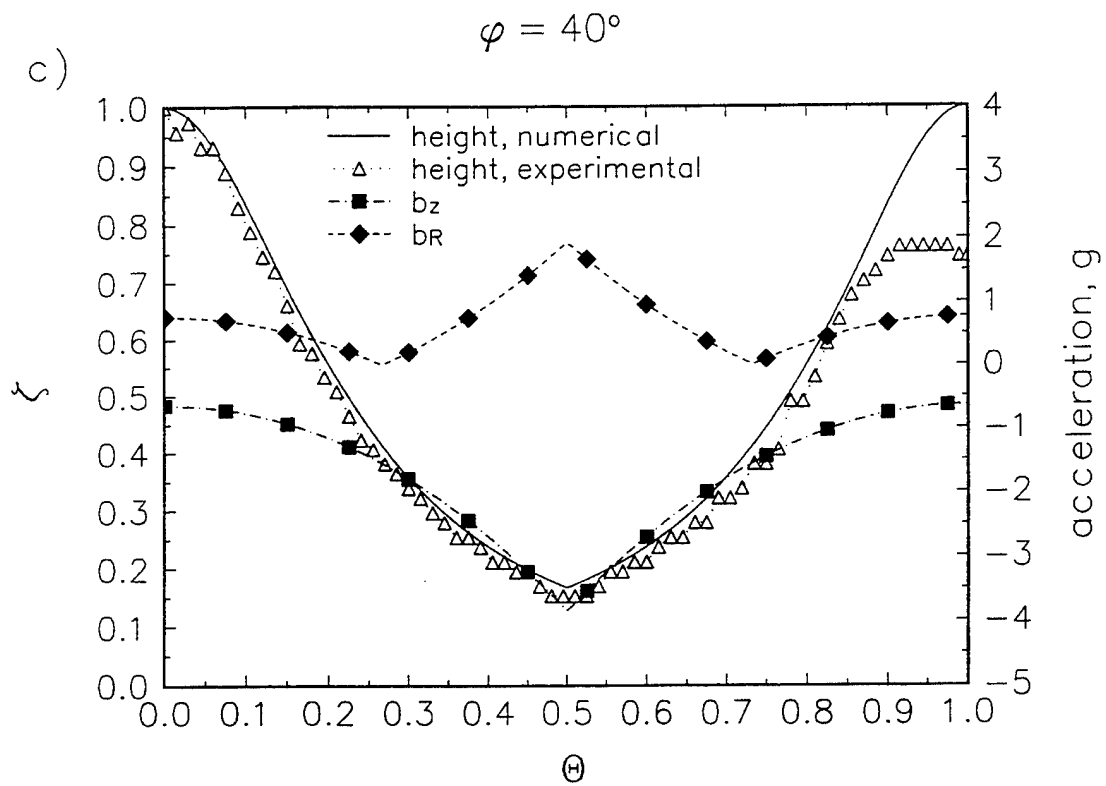
Fig. 1.5(contd)

c) $\varphi = 40°$, $Ca = 7.99 \times 10^{-7}$, $Re = 0.148$, $a/h_o = 4.24 \times 10^{-2}$,

33

$\varphi = 50°$
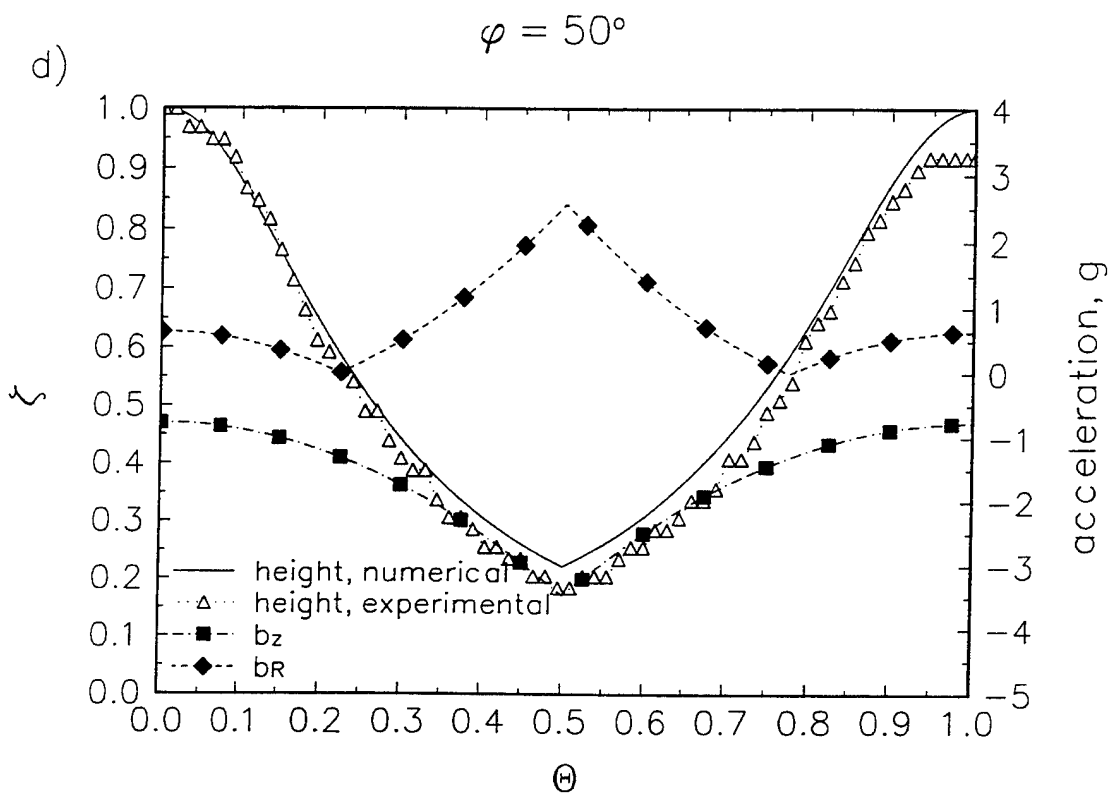
Fig. 1.5(contd)

d) $\phi = 50°$, $Ca = 6.70 \times 10^{-7}$, $Re = 0.124$, $a/h_o = 5.05 \times 10^{-2}$,

34
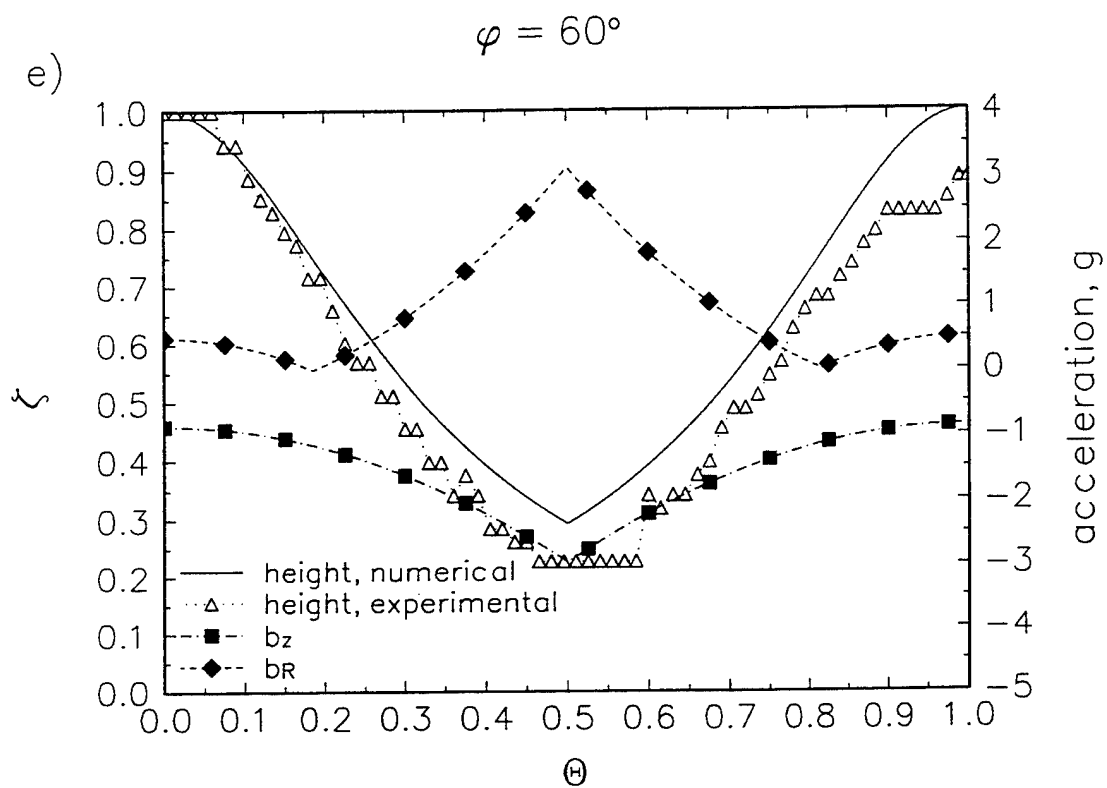
Fig. 1.5(contd)

e)$\phi = 60°$, $Ca = 5.93 \times 10^{-7}$, $Re = 0.110$, $a/h_o = 5.71 \times 10^{-2}$.
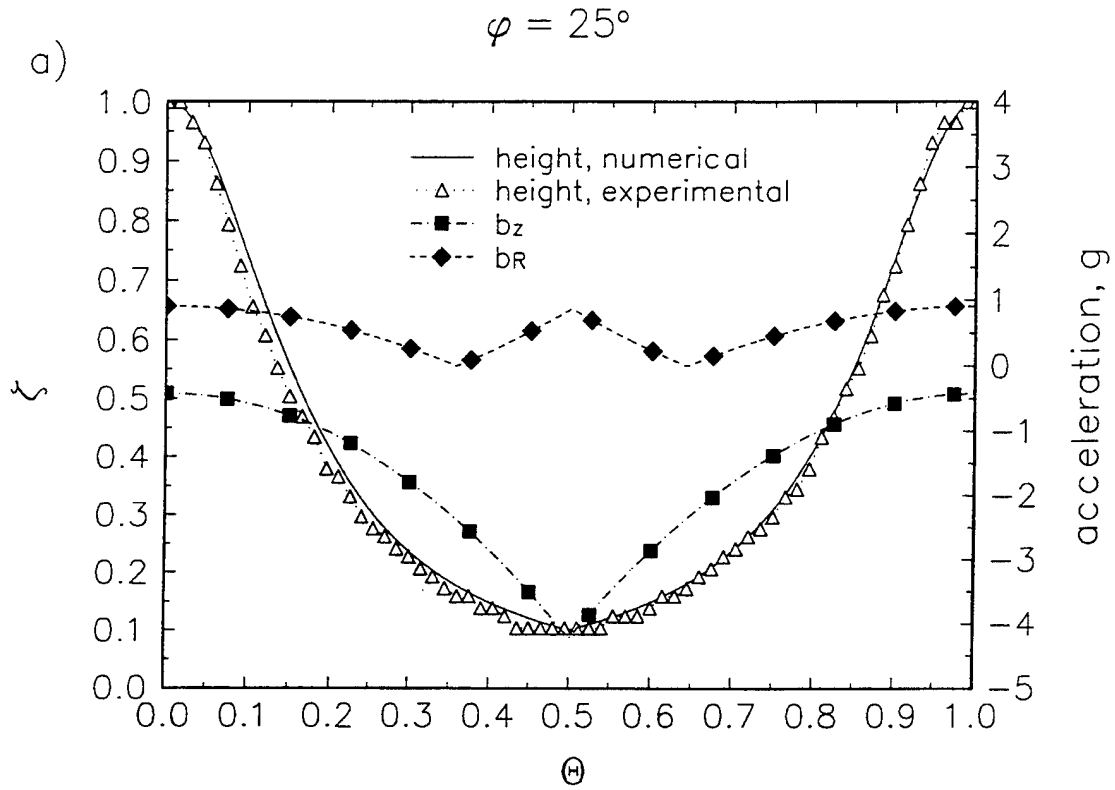
Fig. 1.6 Experimental data compared to analytical results
for ethyl alcohol at $Bo = 1.47$:
a) $\phi = 25°$, $Ca = 3.55 \times 10^{-6}$, $Re = 6.07 \times 10^{-2}$, $a/h_o = 1.93 \times 10^{-2}$,

$\varphi = 30°$

b)
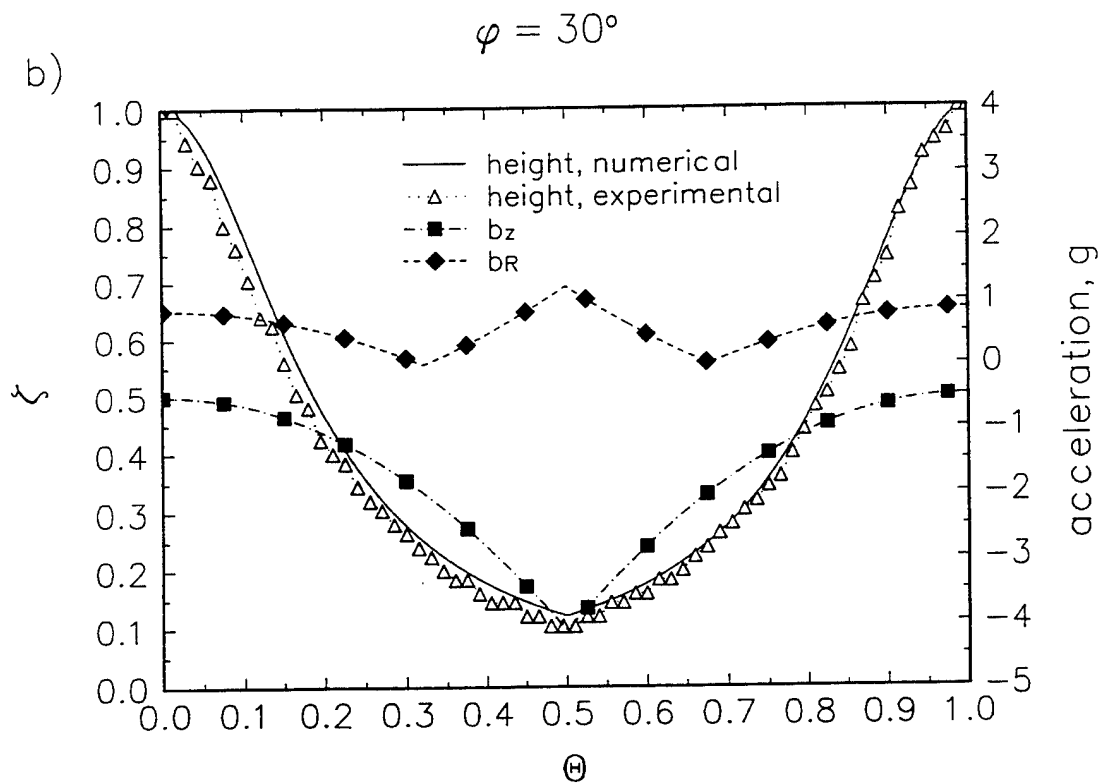
Fig. 1.6(contd)

b) $\phi = 30°$, $Ca = 3.00 \times 10^{-6}$, $Re = 5.13 \times 10^{-2}$, $a/h_o = 2.28 \times 10^{-2}$,

$\varphi = 40°$
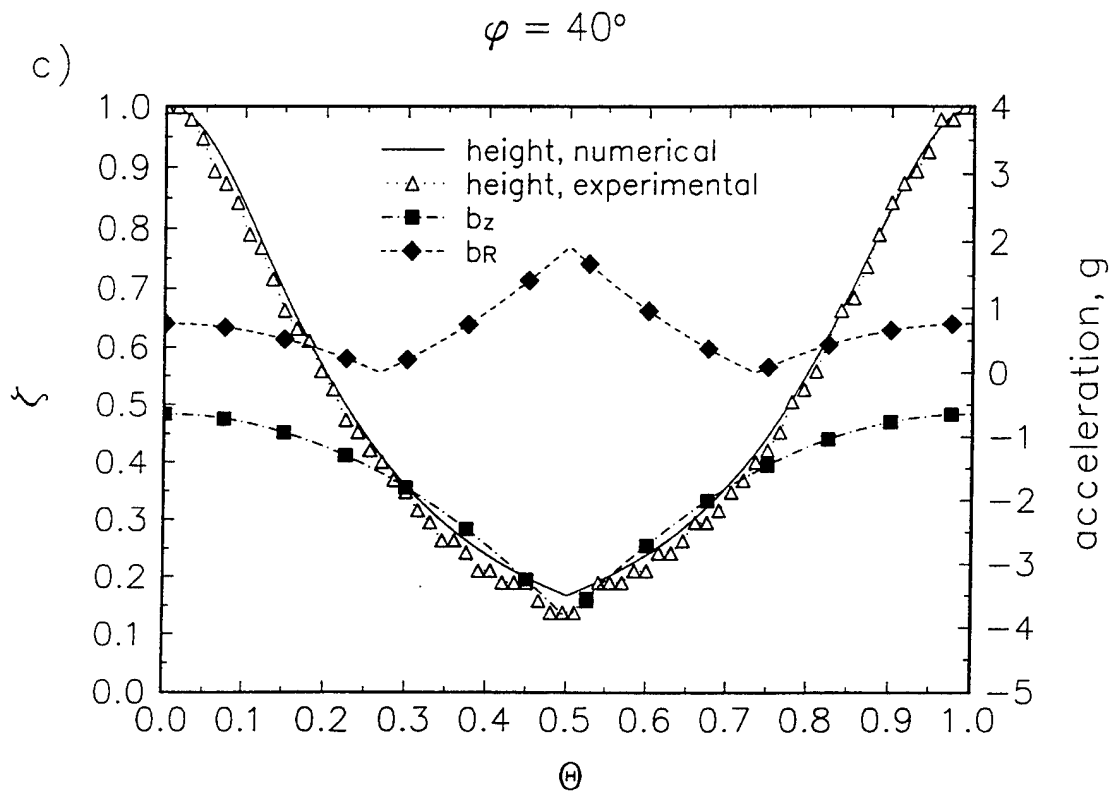
Fig. 1.6(contd)

c) $\phi = 40°$, $Ca = 2.33 \times 10^{-6}$, $Re = 3.98 \times 10^{-2}$, $a/h_o = 2.94 \times 10^{-2}$,

$\varphi = 50°$

d)
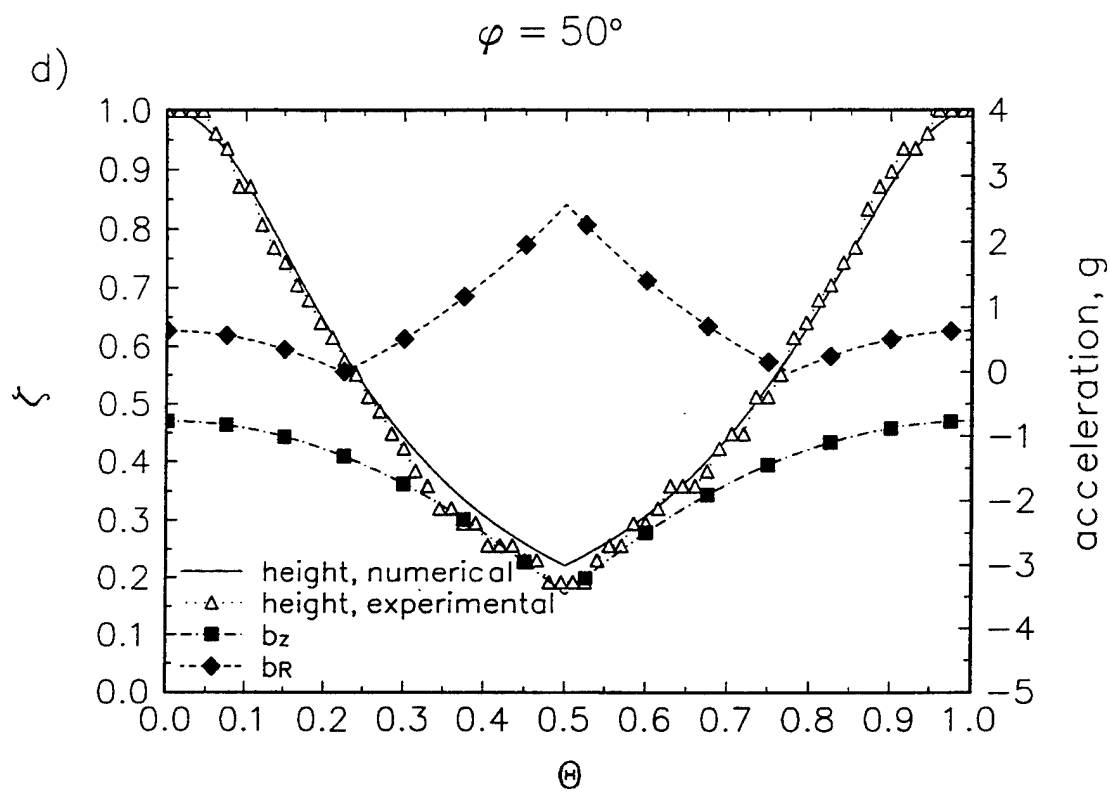
Fig. 1.6(contd)

d) $\phi = 50°$, $Ca = 1.96 \times 10^{-6}$, $Re = 3.35 \times 10^{-2}$, $a/h_o = 3.50 \times 10^{-2}$,

$\varphi = 60°$
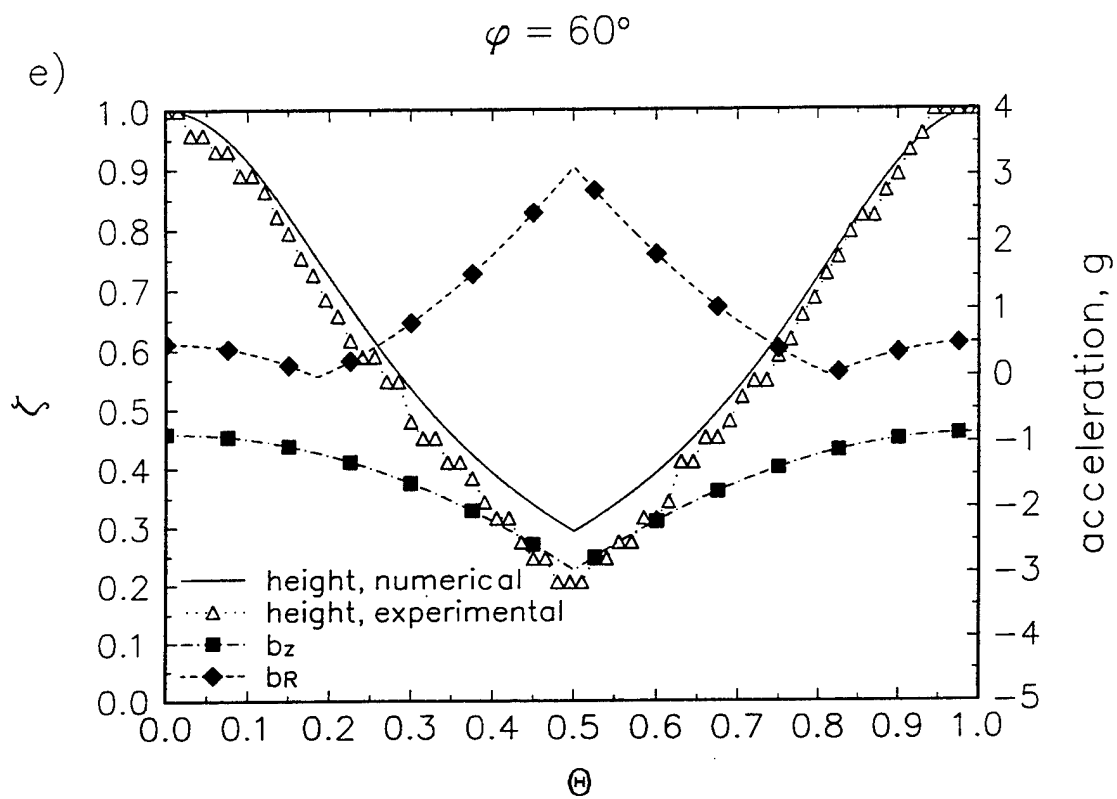
Fig. 1.6(contd)

e) $\phi = 60°$, $Ca = 1.73 \times 10^{-6}$, $Re = 2.96 \times 10^{-2}$, $a/h_o = 3.96 \times 10^{-2}$.
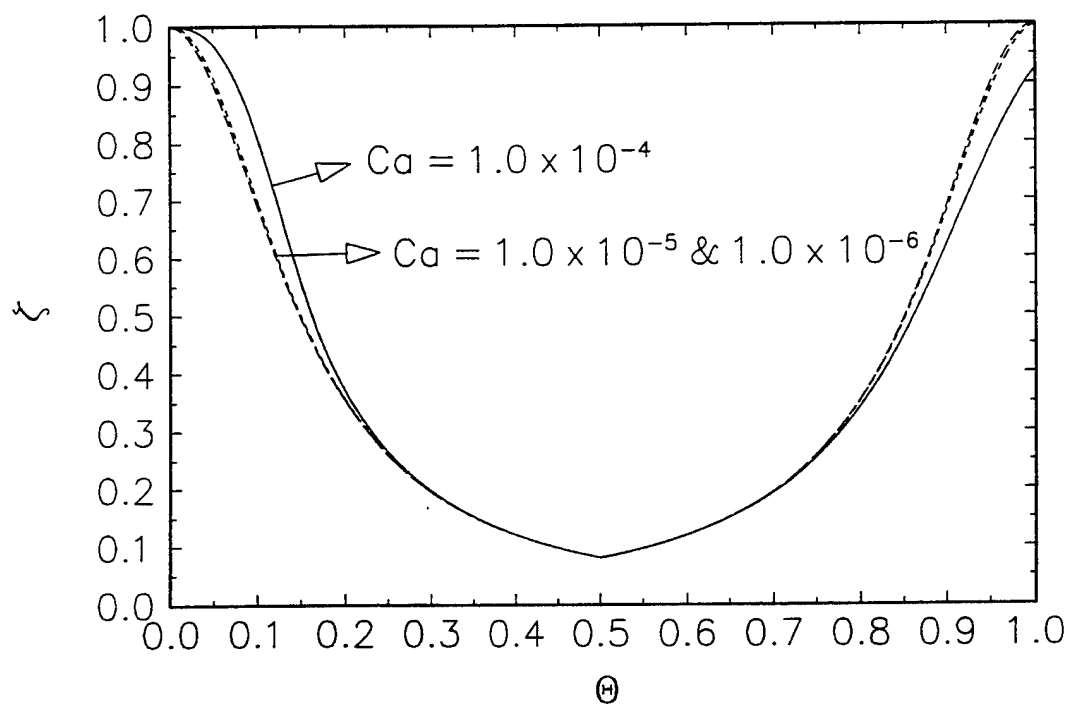
Fig. 1.7 Analytical results for $\phi = 20°$, $Bo = 0.42$ and varying capillary number.
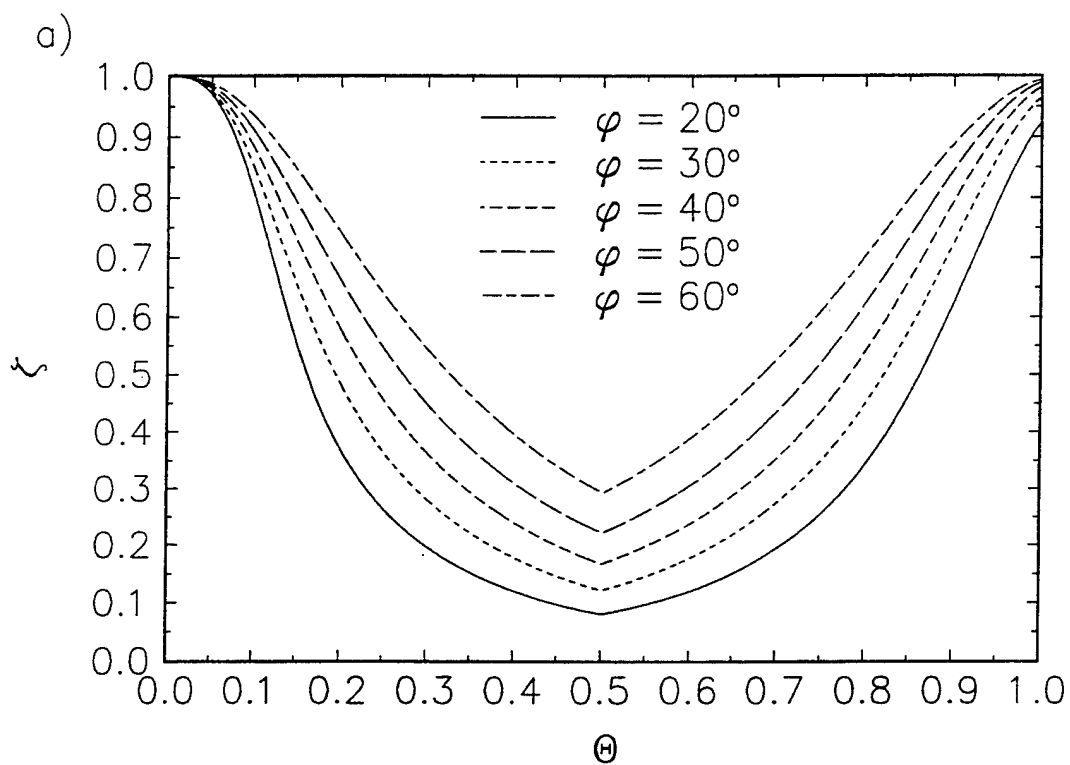
Fig. 1.8 Analytical results:
a) varying angle of inclination (Bo = 0.42, Ca = 1.0×10⁻⁴),

b)
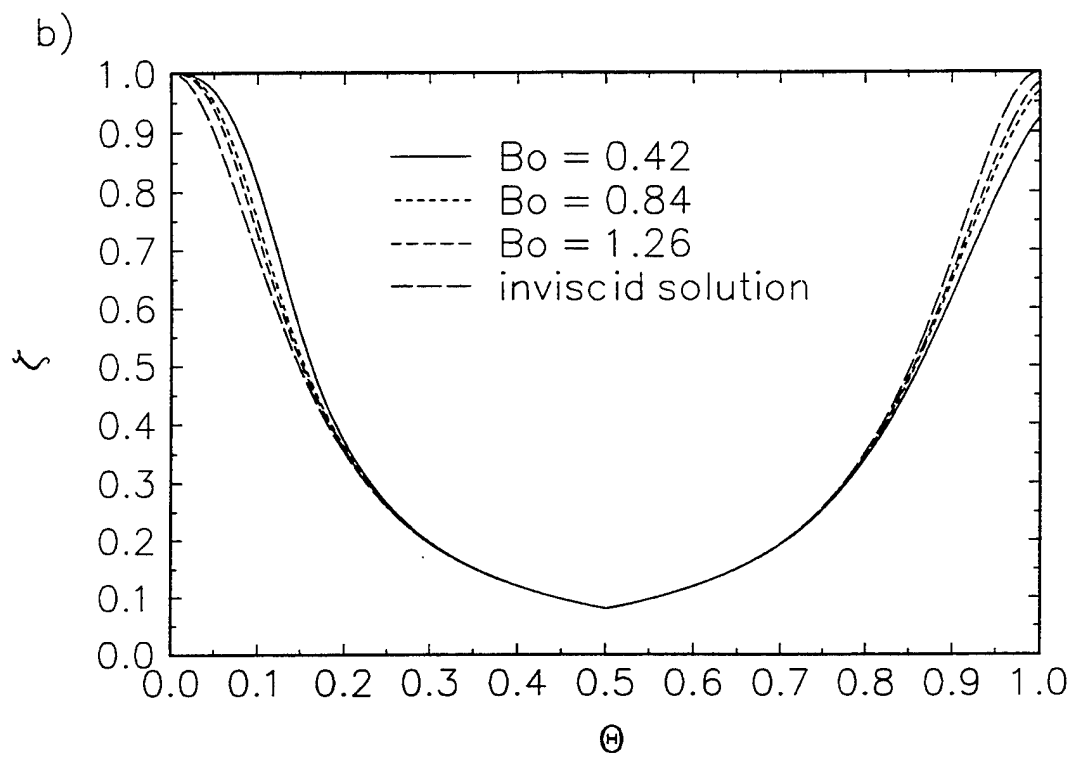
Fig. 1.8(contd) b) varying Bond number (ϕ = 20°, Ca = 1.0×10⁻⁴).

43
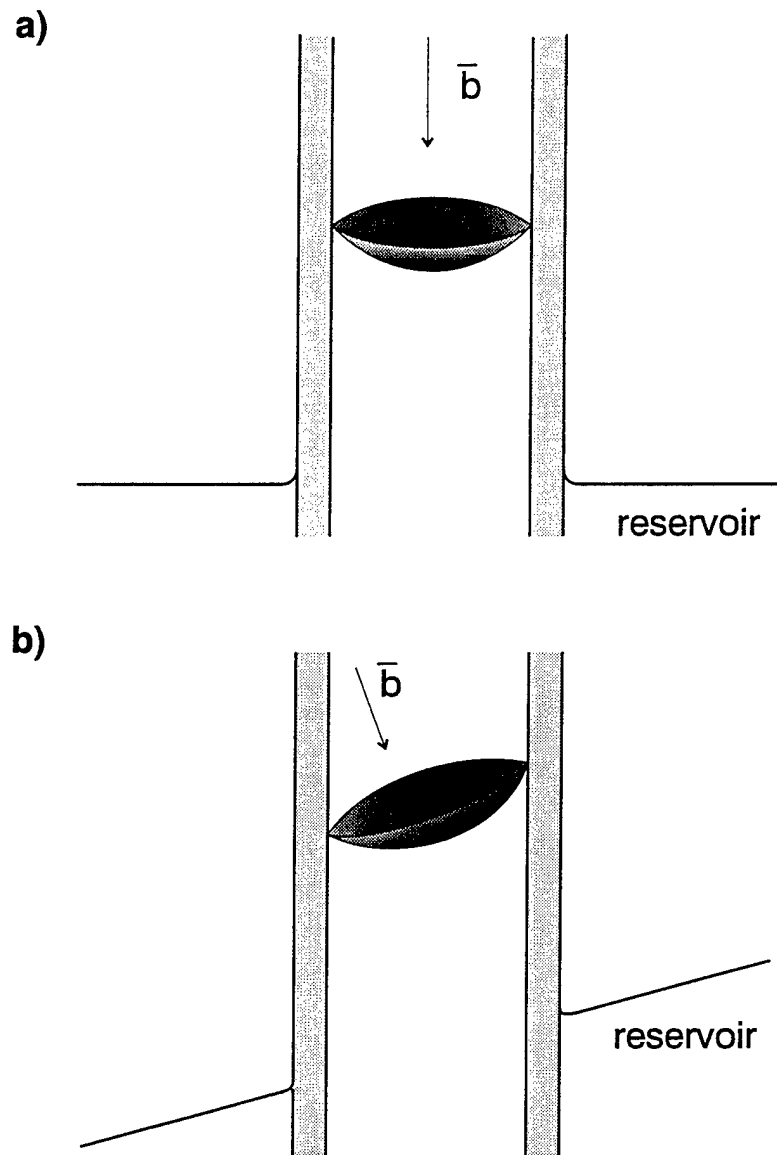
Fig. 1.9 Meniscus position in capillary tube: a) axial acceleration component only and b) combined axial and transverse acceleration components.

44

CHAPTER II

DYNAMIC BEHAVIOR OF AN UNHEATED MENISCUS
SUBJECTED TO A TRANSIENT ACCELERATION FIELD:
EFFECT OF A LOW BOND NUMBER

Abstract

This study experimentally and analytically investigates the effects of acceleration

transients on the dynamic response of an unheated meniscus in a capillary tube. A

capillary tube partially filled with ethyl alcohol was mounted on a centrifuge to observe

the dynamic response of the meniscus subject to single and multiple cycle acceleration

transients. Experimental data of the meniscus recession and advance agreed well with a

one-dimensional equation of motion accounting for changes in the receding and advancing

contact angle assuming a spherically shaped meniscus. Systems typified by a low Bond

number, as distinguished by a small capillary tube diameter, tended to be insensitive to

transverse acceleration components. It was found that the combined effects of a Bond

number, Bo, less than 1.5 (distinguished by a small capillary tube diameter), and capillary

number, Ca, greater than 10^{-5} resulted in a retardation of the meniscus position, relative

to the inviscid solution, due to acceleration transients. An additional retardation in the

advancing meniscus position, indicated by experimental results, appeared to be due to an

increase in the advancing contact angle with increasing capillary number.

Experimental

Acceleration Field

Transient acceleration fields were generated using a 2.4-m diameter centrifuge table (Fig. 2.1) rotating with a time variant angular velocity. Angular velocity transients were generated at a specified cyclic frequency, $0.0015\,Hz \leq f \leq 0.10\,Hz$, using a signal or waveform generator as a control input to the centrifuge. The angular velocity was increased linearly to a peak value at the midpoint of the cycle and subsequently decreased as shown in Fig. 2.2 for single and multiple cycles. A tri-axis accelerometer (Columbia Research Laboratories, Inc.) was used to monitor the time variant acceleration components in a cartesian reference frame affixed to the centrifuge table. Figure 2.3 shows typical accelerometer outputs to the experimentally generated acceleration fields at varying frequencies, f, for single and multiple cycles in each of the three coordinate directions. For this investigation, the peak angular velocity was specified such that a 4.2-g ± 0.1-g peak radial acceleration was generated ($g_{pk} = 41.20$ m/s^2).

Capillary Test Cell

A sealed test cell containing a glass capillary tube and reservoir was positioned on the centrifuge as shown in Fig. 2.4. The test cell was mounted to a motorized optics rotation stage (Newport) such that the capillary tube was allowed to pivot about its center of mass. This pivot point was displaced vertically from the centrifuge surface at a fixed radial location, r_o', as shown in Fig. 2.5a. Angles of inclination of the capillary tube were determined from the output of a calibrated angular displacement transducer (Trans-

Tek, Inc.) accurate to within ±0.2 degrees.

Experiments were conducted by fixing the capillary tube at a specified inclination angle while subjecting it to the transient acceleration field. Increasing the inclination angle elevates the transverse acceleration component referenced to the capillary tube. This allowed the dynamic response of the meniscus subjected to an increasing transverse acceleration component to be observed experimentally. The dynamic response of the meniscus to the transient acceleration field was observed using an 8-mm format CCD camera (Sony, 30 frames/s) mounted adjacent to the test cell as shown in Fig. 2.4b. Video images were used to provide a record of the meniscus height relative to the reservoir meniscus, η, as a function of time to within ±1.0 mm. An equivalent static contact angle, θ_s, was calculated from the experimentally determined static wicking height, h_o, for conditions when the transverse acceleration component was zero $(h_o \rho g \approx (2\sigma/a)\cos\theta_s)$.

Ethyl alcohol was used as the test fluid to demonstrate the importance of the equilibrium contact angle on the advance and recession of the meniscus due to a transient acceleration field for low Bond numbers. Two capillary tubes, 1.0 mm and 0.5 mm in diameter, were used in order to vary the experimental Bond number. Properties of the ethyl alcohol were assumed to be that of the bulk fluid corresponding to a experimental temperature of 30° C.

The test cell and capillary tube were cleaned using potassium hydroxide and thoroughly rinsed with ethyl alcohol. The test cell was filled and subsequently sealed resulting in a fill that had a combination of air, fluid vapor, and liquid.

47

Analytical Formulation

The goals of the analytical formulation were to expand the mathematical formulation described in chapter I to: (i) mathematically describe the dynamic behavior of the meniscus as a result of the temporal acceleration induced forces using a simplified one-dimensional model with a constant line force accounting for changes in the recession and advancing contact angles; and (ii) determine the relative importance of the transverse acceleration component and capillary number for low Bond numbers on the meniscus motion by comparing experimental results and analytical calculations.

Acceleration Vector

Acceleration measurements were obtained with regard to a three-dimensional cartesian non-inertial reference frame affixed to the centrifuge as described in chapter I. The acceleration field was then referenced to fixed locations on the capillary tube and subsequently decomposed into transverse and axial acceleration components relative to the capillary tube as shown in Fig. 2.5b.

The resulting transient acceleration vector decomposed into an axial component, b_z, and a transverse component, b_R, becomes

$$\bar{b} = \left[-\omega^2 \left(r_o' + (z_1 - z)\cos\phi\right)\cos\phi + (-g)\sin\phi\right]\hat{e}_z +$$
$$\left[\left[-\omega^2\left(r_o' + (z_1 - z)\cos\phi\right)\sin\phi - (-g)\cos\phi\right]^2 + \left[\left(r_o' + (z_1 - z)\cos\phi\right)\frac{d\omega}{dt}\right]^2\right]^{1/2}$$

(1)

Here, the transverse component, b_R, is a magnitude with no reference to direction due to the axisymmetric nature of the capillary tube. This form of the acceleration vector does

48

not include the Coriolis acceleration (see Appendix A) which would be embodied in the transverse acceleration component. The Coriolis acceleration is induced from the motion of the fluid column or meniscus in the axial direction in the capillary tube. Therefore prior knowledge of the meniscus dynamics, specifically the velocity, is required to evaluate the Coriolis acceleration. The one-dimensional equation of motion for the meniscus formulated for this investigation assumes that the transverse acceleration component has a negligible effect on the dynamic behavior of the meniscus and therefore does not account for tangential and Coriolis acceleration effects.

Equation of Motion

The simple analytical model described in chapter I was used to predict the motion of the meniscus subjected to transient accelerations. The analytical formulation of the equation of motion was simplified assuming bulk flow only in the axial direction of the capillary tube. Effectively, the liquid column in the capillary tube was assumed to undergo a slug flow.

The surface force, F_{s_z}, was formulated by accounting for the cumulative effect of solid-liquid intermolecular forces in the near contact line region and the wall shear stress associated with the predominantly Poiseuille flow in the liquid column. This approach has been used since the work of West[28] and Washburn[29] and as described by Kafka and Dussan, V.[30] has been surprisingly good in modelling steady capillary flows when Ca and Re are small. The contact line force is defined assuming a spherical meniscus and a constant equivalent or apparent contact angle such that

$$F_{s_z} = \sigma (2\pi a) \cos\theta_s + \tau_w (2\pi a)\eta . \qquad (2)$$

Note that such an assumption implies a non-changing apparent contact angle under dynamic conditions ($\theta_d \sim \theta_s$).

The resulting dimensional form of the momentum equation is

$$\frac{2\sigma\cos\theta}{\rho a} = \left[\eta \frac{d^2\eta}{dt^2} + \left(\frac{d\eta}{dt}\right)^2\right] + \left[\frac{8\mu}{\rho a^2}\eta \frac{d\eta}{dt}\right]$$
$$+ \eta\left[\omega(t)^2 \cos\phi\left((z_1 - \frac{\eta}{2})\cos\phi + r_o'\right) + g\sin\phi\right]. \qquad (3)$$

The transient angular velocity is of the form

$$\omega(t) = Bt, \qquad 0 \le t \le \frac{tf}{2}$$
$$= B(tf - t), \qquad \frac{tf}{2} \le t \le tf \qquad (4)$$

where

$$B = \left(\frac{4 g_{pk}}{(tf)^2 r_o'}\right)^{\frac{1}{2}}. \qquad (5)$$

Using the following dimensionless parameters,

$$\zeta = \frac{\eta}{h_o}, \quad 0 \le \zeta \le 1$$

$$\Theta = \frac{t}{tf}, \quad 0 \le \Theta \le 1,$$

(6)

with the following initial conditions

$$\zeta = 1, \quad \frac{d\zeta}{d\Theta} = 0, \quad \Theta = 0,$$

the non-dimensional form of the momentum equation in terms of a transient dimensionless meniscus position becomes

$$\frac{g}{g_{pk}}\sin\phi = \left[\frac{a}{h_o}\right]\left[\frac{Re\,Ca}{2Bo}\right]\left[\zeta\frac{d^2\zeta}{d\Theta^2} + \left(\frac{d\zeta}{d\Theta}\right)^2\right] + \left[\frac{16\,Ca}{Bo}\right]\left[\zeta\frac{d\zeta}{d\Theta}\right]$$

$$+ \zeta\left[\Omega(\Theta)^2 \cos\phi\left(\left(z_1 - \frac{h_o\zeta}{2}\right)\cos\phi + r_o'\right) + \frac{g}{g_{pk}}\sin\phi\right].$$

(7)

where the angular velocity, Ω, is defined by

$$\Omega(\Theta) = \left(\frac{4}{r_o'}\right)^{\frac{1}{2}}\Theta, \qquad 0 \le \Theta \le \frac{1}{2}$$

$$= \left(\frac{4}{r_o'}\right)^{\frac{1}{2}}(1-\Theta), \qquad \frac{1}{2} \le \Theta \le 1.$$

(8)

The first and second terms of eq. (7) represent the inertial and viscous effects, respectively, with the coefficients formed as the products of the Reynolds number, capillary number, Bond number, and aspect ratio. The Reynolds and capillary numbers

51

are referenced to a characteristic velocity, V_c, which is the maximum attainable velocity over one-half of the acceleration cycle period assuming $\eta = 0$ at g_{pk}. The Bond number is referenced to the peak radial acceleration component, g_{pk}.

The momentum equation can be easily modified to include a constant receding or advancing contact angle, θ_d, differing from that of the static contact angle, θ_s, resulting in

$$\frac{g}{g_{pk}} \frac{\cos\theta_d}{\cos\theta_s} \sin\phi = \left[\frac{a}{h_o}\right] \left[\frac{ReCa}{2Bo}\right] \left[\zeta \frac{d^2\zeta}{d\Theta^2} + \left(\frac{d\zeta}{d\Theta}\right)^2\right] + \left[\frac{16Ca}{Bo}\right] \left[\zeta \frac{d\zeta}{d\Theta}\right]$$
$$+ \zeta \left[\Omega(\Theta)^2 \cos\phi\left(\left(z_1 - \frac{h_o\zeta}{2}\right)\cos\phi + r'_o\right) + \frac{g}{g_{pk}} \sin\phi\right].$$

(9)

It may be noted that the general form of the dynamic contact angle is known to be functionally dependent on the contact line receding and advancing velocity, $\theta_d = \theta_d(d\zeta/d\Theta)$. Equation (9) can be modified to include any specific form for the dynamic contact angle and solved numerically.

Results

Equation (9) was solved for the dimensionless meniscus position, ζ, using a central-difference scheme. Solutions were obtained by first specifying a static wicking height, h_o, based on the experimentally determined equivalent contact angle, $\theta_s = 16.7°$. Numerical solutions were consistent with the experimental parameters for $Bo = 0.3675$, 1.47 and $3.47 \times 10^{-6} \le Ca \le 4.00 \times 10^{-4}$ with single or multiple acceleration transient cycles. Numerical solutions were also calculated for various

advancing contact angles in order to address deviations between experimental results and analytical calculations based upon the assumption that the contact angle is equivalent to the static contact angle, θ_s. All numerical solutions assumed a constant recession contact angle equivalent to the static contact angle, $\theta_d = \theta_s = 16.7°$.

Experiments were performed and the results compared with solutions to the analytical model. Uncertainty in the experimentally obtained dimensionless meniscus position, ζ, and time, Θ, was on the order of ζ, $\Theta \pm 0.02$ based on the accuracy and resolution of the experimentally measured quantities.

Figure 2.6 compares the experimentally obtained dimensionless meniscus position to the analytical results at varying angles of inclination. Also shown are the axial and transverse acceleration components. Experimental parameters in this figure ranged from $3.47 \times 10^{-6} \leq Ca \leq 6.00 \times 10^{-6}$, $2.96 \times 10^{-2} \leq Re \leq 5.13 \times 10^{-2}$, and $5.71 \times 10^{-3} \leq a/h_o \leq 9.89 \times 10^{-3}$ as the inclination angle varied from 30° to 60°. The experimentally obtained dimensionless meniscus position agreed well with the analytical calculations. There was a slight deviation from the predicted values due to the transverse acceleration component as shown in Fig. 2.6d as was observed in chapter one. A small Bond number tended to decrease the sensitivity of the meniscus position to the transverse acceleration component as a result of the small capillary tube diameter.

Figure 2.7 compares the experimental results and analytical calculations for $4.00 \times 10^{-5} \leq Ca \leq 4.00 \times 10^{-4}$ with $Bo = 1.47$ at 25° inclination and $Bo = 0.3675$ at 30° inclination. Table 2.1 shows a summary of the dimensionless parameters corresponding to Fig. 2.7.

Table 2.1
Values of dimensionless numbers.

Bo	Ca	Re	We	a/h_o	ϕ
0.3675	4.00×10^{-4}	3.42	1.37×10^{-3}	5.71×10^{-3}	30°
	2.00×10^{-4}	1.71	3.42×10^{-4}		
	1.00×10^{-4}	0.855	8.55×10^{-5}		
	4.00×10^{-5}	0.342	1.37×10^{-5}		
	6.00×10^{-6} *	5.13×10^{-2}	3.08×10^{-7}		
1.47	2.37×10^{-4}	4.05	9.60×10^{-4}	1.93×10^{-2}	25°
	1.18×10^{-4}	2.02	2.38×10^{-4}		
	5.92×10^{-5}	1.01	5.98×10^{-5}		
	3.55×10^{-6} **	6.07×10^{-2}	2.15×10^{-7}		

*Fig. 2.6a
**Fig. 1.6a

As shown in Fig. 2.7a, there was no significant deviation between the predicted and observed meniscus position for $Bo = 1.47$. For $Bo = 0.3675$, as shown in Fig. 2.7b, the predicted and observed meniscus position agreed well for meniscus recession with an increase in the retardation in meniscus position corresponding to an increase in the capillary number. For the advancing meniscus, there was a retardation in the observed meniscus position, in response to the acceleration transient, from that of the predicted values. The retarded position for the advancing meniscus was not evident for $Ca = 4.00 \times 10^{-5}$ but became significant for $Ca \geq 1.00 \times 10^{-4}$ and increased with

54

increasing capillary number.

The variation between the predicted and observed advancing meniscus velocity is in part due to the dependence of the contact angle on capillary number and/or Reynolds number. Figure 2.8 compares the analytical calculations for a 16.7° receding contact angle while varying the advancing contact angle. Also shown in Fig. 2.8 are the transient acceleration fields decomposed into the axial and transverse components at the pivot point of the capillary tube. The experimental results agree very well with that of the analytical calculations when a change in the advancing contact angle is taken into account.

Hoffman[15] and Phillips and Riddiford[14] discuss systems in which the interfacial forces between the solid and the liquid change when flow occurs under conditions where inertia is assumed to be negligible. For very low velocities the apparent contact angle is usually independent of velocity, but as the interfacial velocity is increased above a critical velocity, the apparent contact angle will change until a limiting value is reached. Phillips and Riddiford postulated that there is a change in the interfacial forces as the critical velocity is reached thereby resulting in a shift in the apparent contact angle. Figures 2.8b and 8c show that the advancing velocity agrees well with the analytical calculations up to $\Theta \sim 0.75$, corresponding to an inflection in the transverse acceleration component. The meniscus velocity at $\Theta \sim 0.75$ suddenly decreases (from ~ 3 mm/s for $Ca = 2.00 \times 10^{-4}$ and ~ 6 mm/s for $Ca = 4.00 \times 10^{-4}$) and subsequently increases again resulting in a retarded meniscus position compared to the analytical solution. The sudden decrease in the meniscus velocity at time $\Theta \sim 0.75$ and subsequent increase may be due to the combined effects of the transverse acceleration component and the Coriolis

acceleration which is dependent on the velocity of the meniscus. In addition, the analytical formulation takes into account the opposing viscous force at the tube wall and general inertial effects but does not take into account the opposing viscous force at the contact line region and a possible increase in the radius of curvature of the meniscus as a result of inertial effects. Analytical calculations and experimental results show that the motion of the meniscus along the contact line and fluid along the tube wall is retarded due to viscous effects. However, the motion of the central core of fluid, due to inertia, likely results in the "pushing forward" of the central portion of the meniscus relative to the contact line yielding an increased radius of curvature and therefore an increased contact angle. This change in contact angle further retards the meniscus motion.

In addition, with the removal of the acceleration transient, there is a rapid but noticeable relaxation time ($\approx$4-5 seconds) when the contact angle returns to the static value and the column of alcohol returns to the initial static wicking height. The existence of a relaxation time agrees with observations by Phillips and Riddiford.[14]

Figure 2.9 compares the analytically calculated advancing contact angle required to match experimental results to the results presented by Hoffman[15]. The shifting function described by Hoffman was determined to be approximately $F(\theta_s) = 2.5 \times 10^{-4}$. Using a capillary number as defined in this investigation (really an average capillary number), $Ca + F(\theta_s)$ was plotted against the advancing contact angle. The deviation from that of Hoffman's results may be in part due to the fact that Hoffman is characterizing the shape of the liquid-air interface for viscous fluids (i.e. oils) in motion when only the viscous and interfacial forces are important. This investigation considers motion of the

liquid-air interface for ethyl alcohol as a result of acceleration induced forces which results in inertial as well as the viscous and interfacial forces.

Figure 2.10 shows the percent deviation in meniscus position from the inviscid solution, at the end of a cycle, relative to the viscous term, Ca/Bo. The effect of increasing the angle of inclination resulted in a reduction in the percent deviation from the inviscid solution. As shown in Fig. 2.10, the experimental results showed an increased deviation over the analytical solutions which appears as a vertical shift from the analytical results. This shift between the experimental results and analytical predictions provides credibility to the hypothesis that inertial forces may result in a change in the contact angle and that viscous forces alone are not sufficient to induce the observed increase in the deviation (or attenuation) from the inviscid prediction.

Figure 2.11 compares analytical calculations and experimental results for three cycles in the transient acceleration for $Bo = 0.3675$, $Ca = 2.00 \times 10^{-4}$ and 4.00×10^{-4}, $g_{pk} = 2.1g$, $4.2g$, $8.4g$, and at a 30° inclination angle. As shown in Fig. 2.11a, there is an attenuation and phase shift in meniscus position due to viscous effects from an inviscid or low capillary number solution as the capillary number is increased. Again, there is good agreement between the observed and predicted receding meniscus position. The deviation between the observed and predicted advancing meniscus position is apparent, however, when an advancing contact angle of 30° is accounted for in the numerical solution. The predicted and observed meniscus positions agree very well. As shown in Fig. 2.11b, there is an increased attenuation from the initial meniscus height and a slight phase shift with increasing peak radial acceleration.
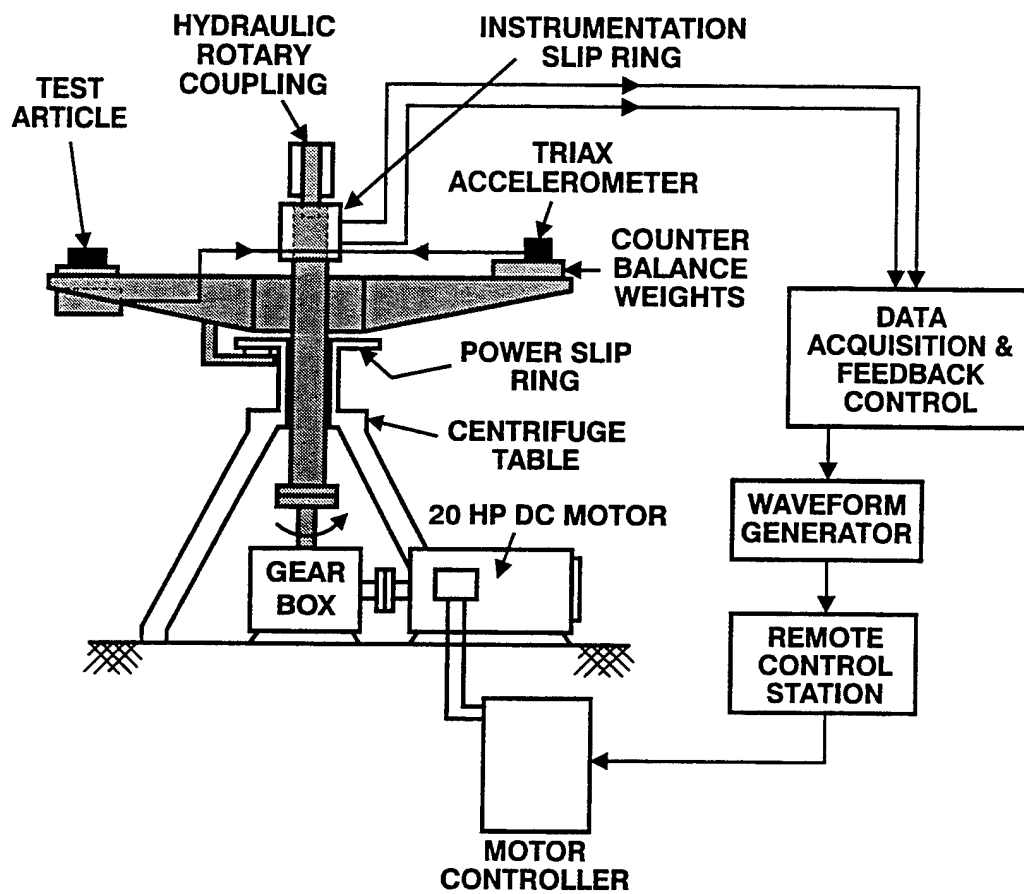
Fig. 2.1 Schematic of centrifuge.
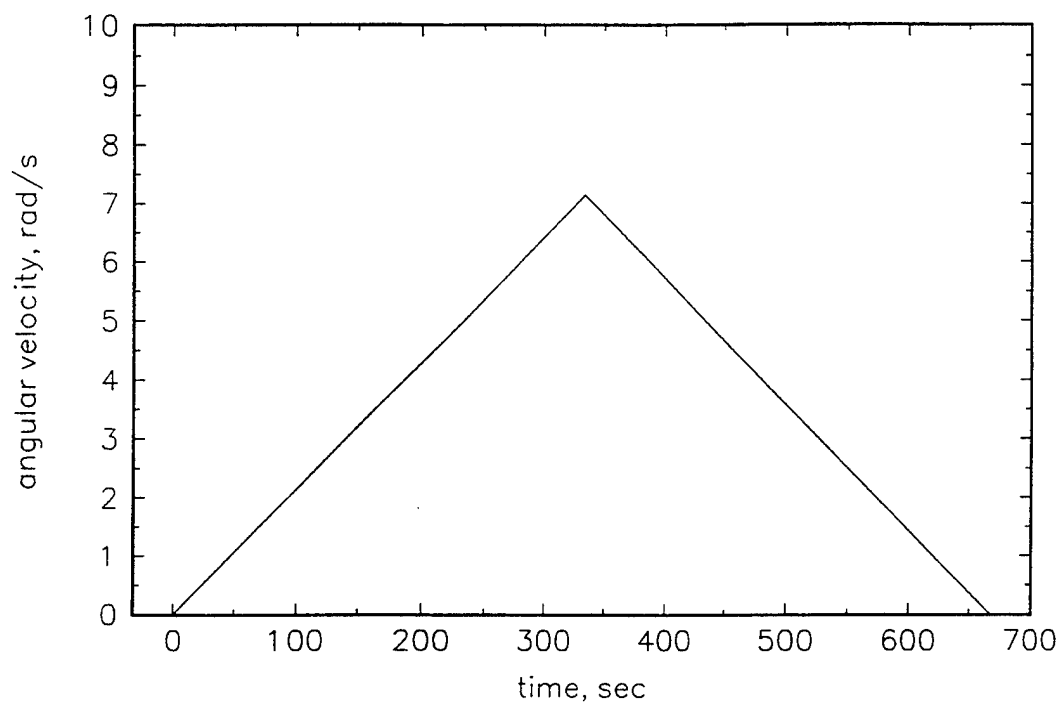
Fig. 2.2 Plot of the centrifuge angular velocity test cycle ($f = 0.0015\ Hz$).

a)
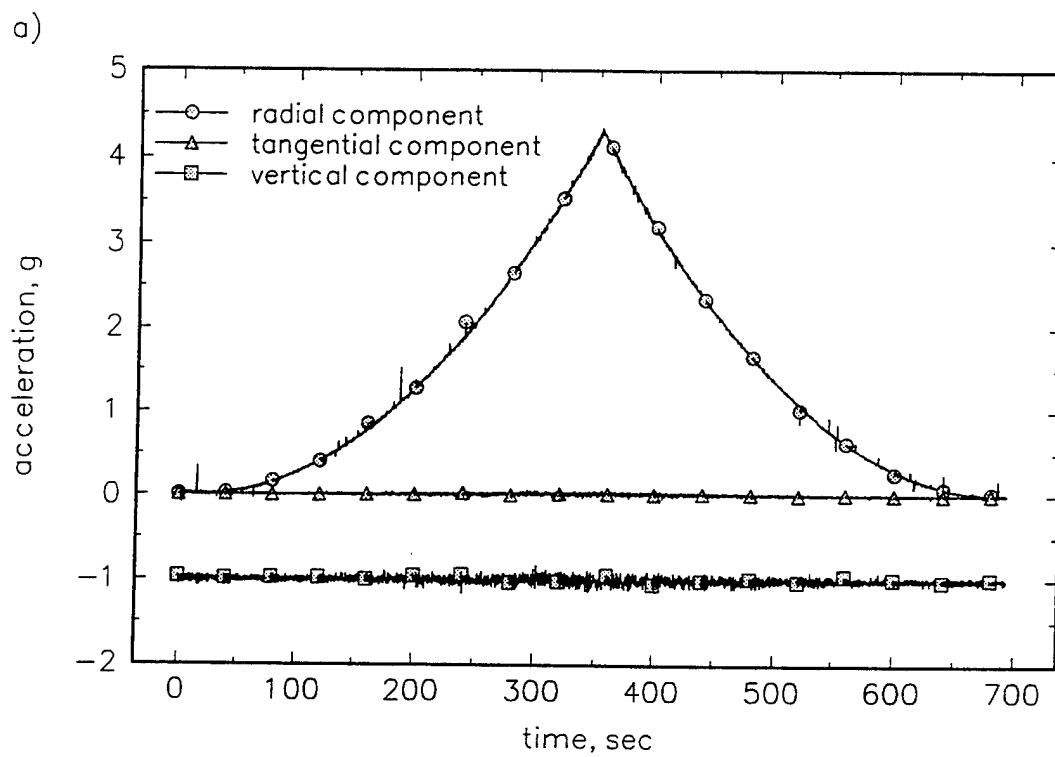
Fig. 2.3 Experimentally generated acceleration field (accelerometer output):
a) $f = 0.0015$ Hz, single cycle,

b)
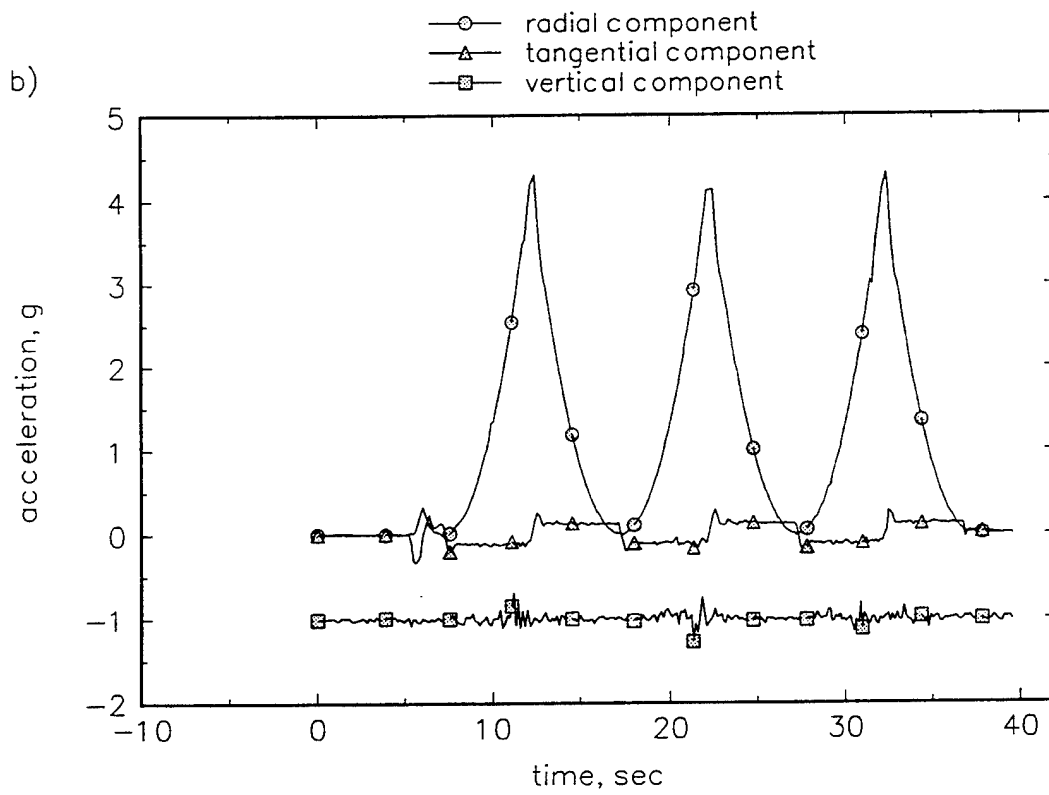
Fig. 2.3(contd) b) $f = 0.1$ Hz, multiple cycle,

61
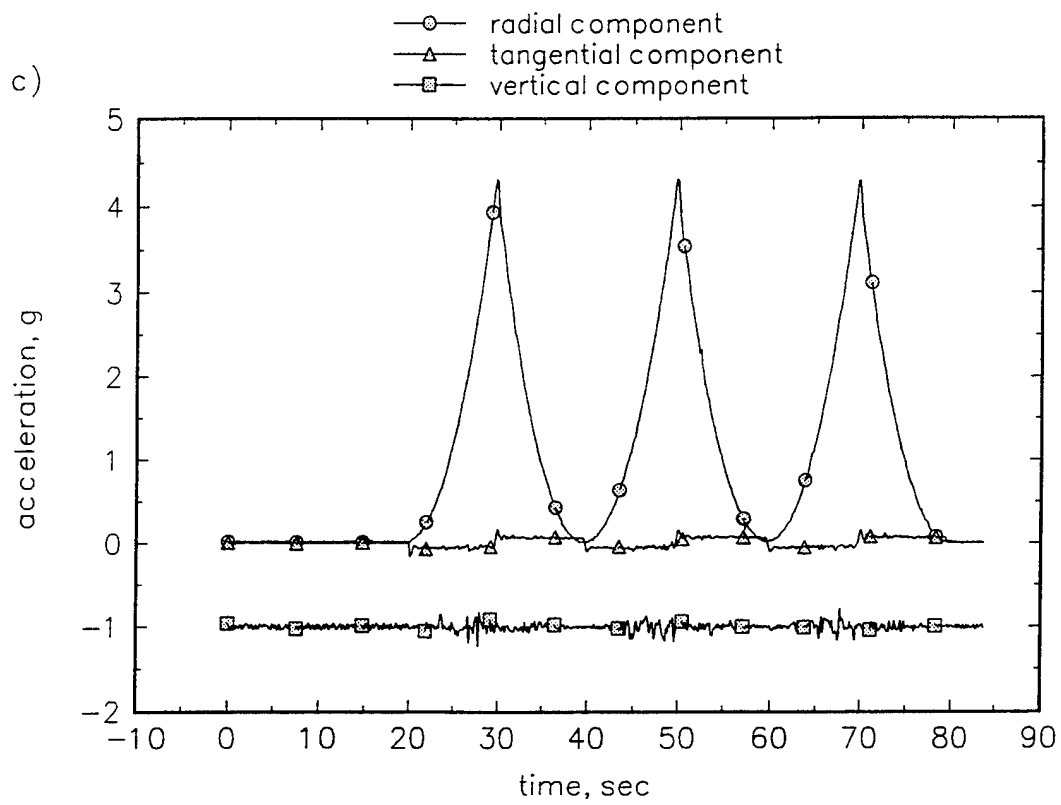
Fig. 2.3(contd) c) f = 0.05 Hz, **multiple cycle,**
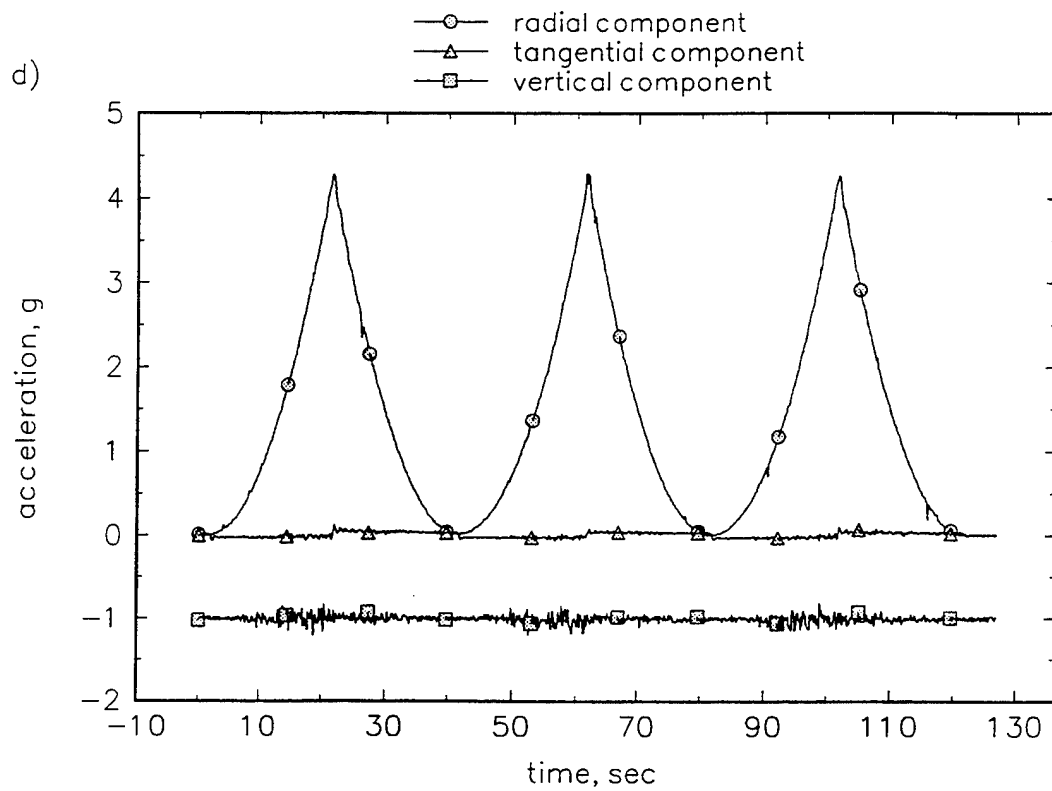
Fig. 2.3(contd) d) $f = 0.025$ Hz, multiple cycle,
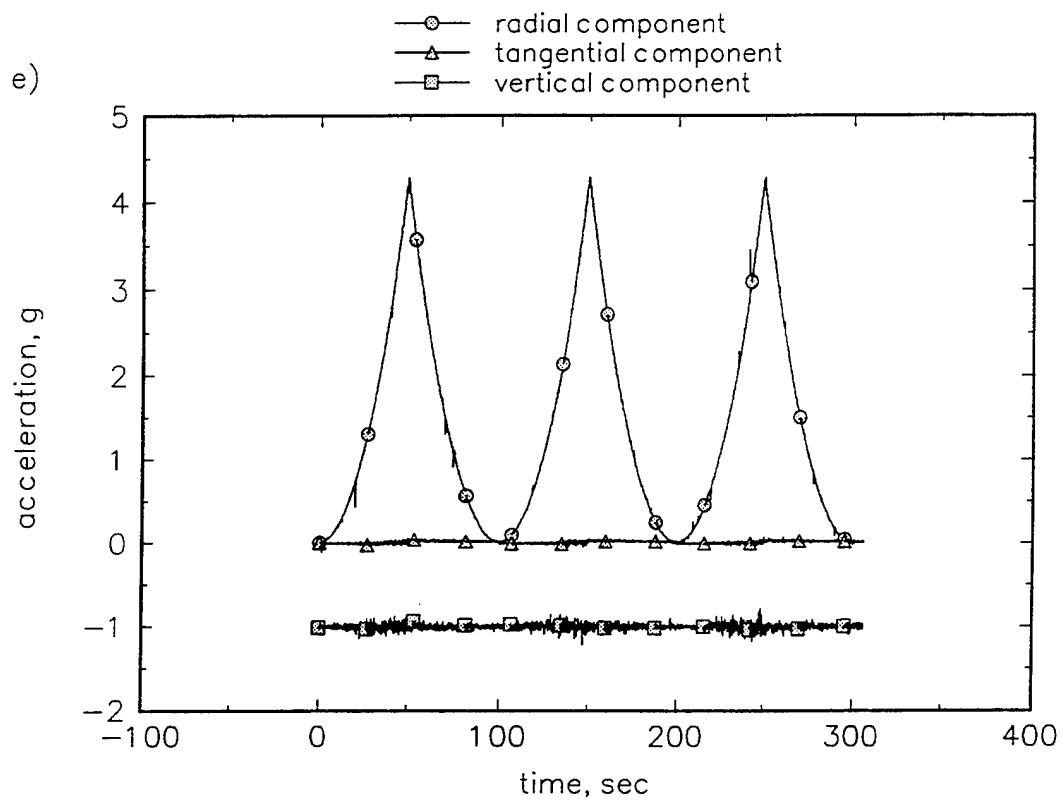
Fig. 2.3(contd) e) $f = 0.01$ Hz, multiple cycle.

64

a)

$\bar{b}$

spring
loaded
clamp

capillary
tube

pivot
point

reservoir

b)

8mm CCD
camera

optics
rotation   angular
stage   position
           transducer

test cell w/
capillary tube

accelerometer
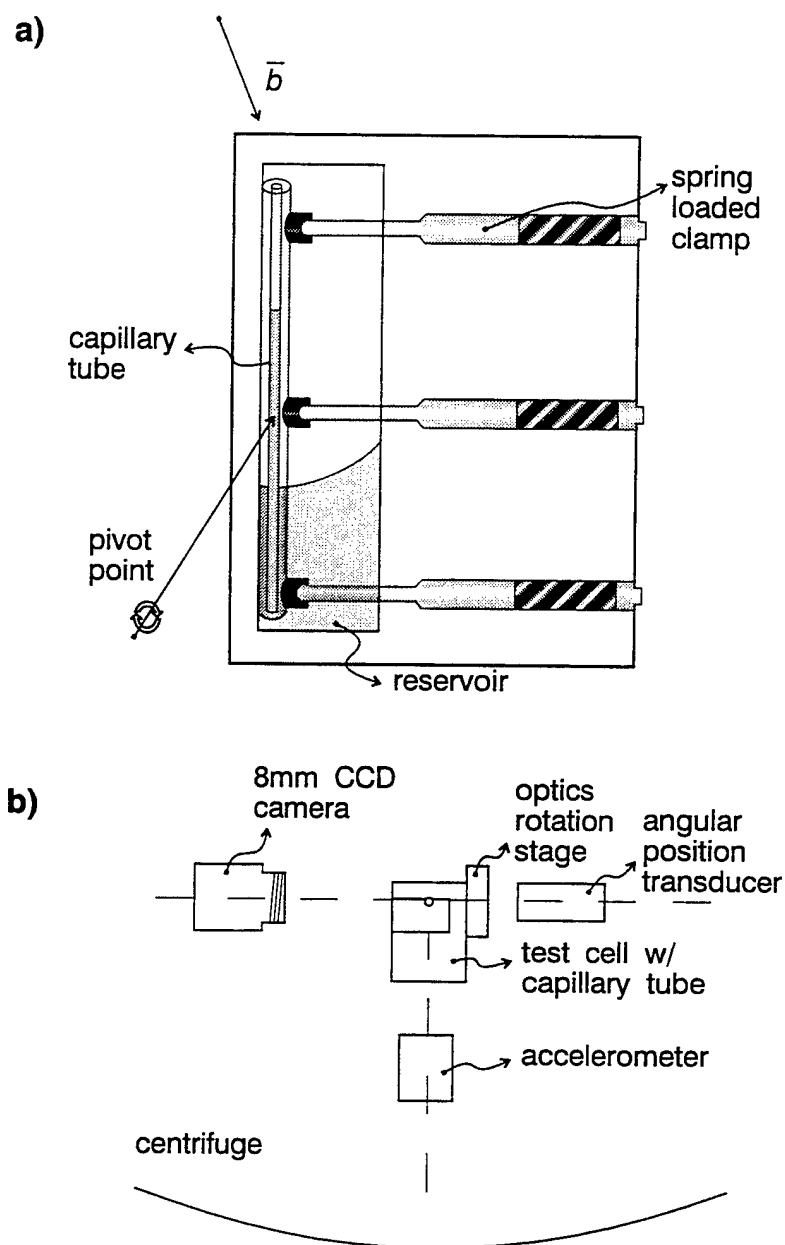
centrifuge

Fig. 2.4 Experimental apparatus: a) sealed test cell
and b) schematic of experimental apparatus as mounted on the centrifuge.

65
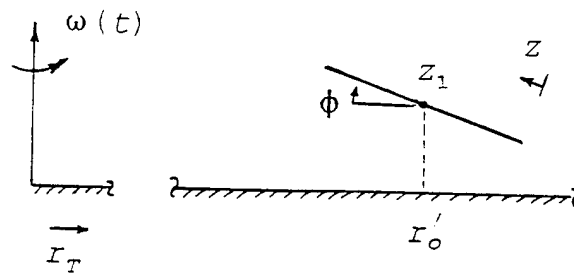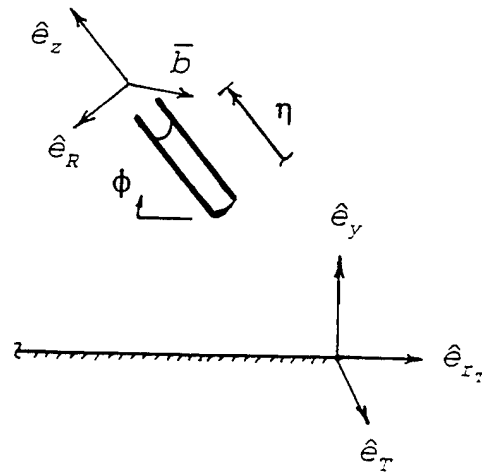
Fig. 2.5 Capillary tube orientation: a) pivot point location, directional coordinates and b) coordinate systems as referenced to the centrifuge accelerometer and capillary tube.
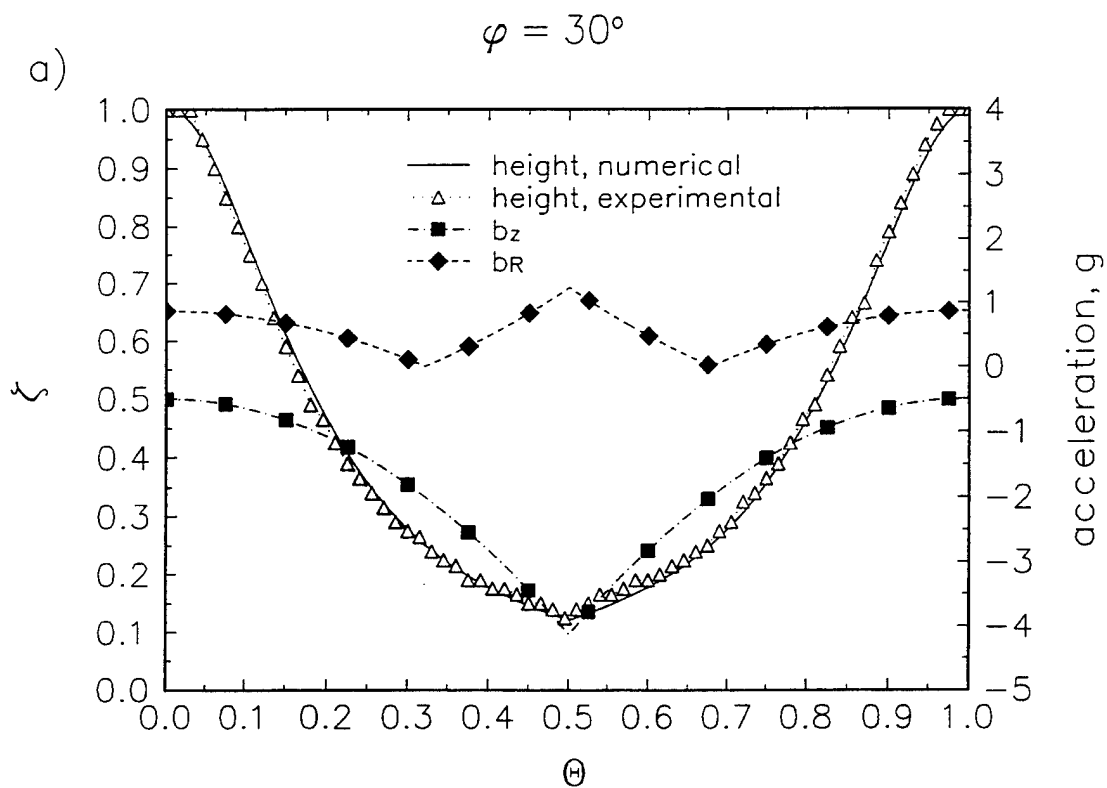
Fig. 2.6 Experimental data compared to analytical calculations
for ethyl alcohol at $Bo = 0.3675$:

a) $\phi = 30^\circ$, $Ca = 6.00 \times 10^{-6}$, $Re = 5.13 \times 10^{-2}$, $a/h_o = 5.71 \times 10^{-3}$,

$$\varphi = 40°$$
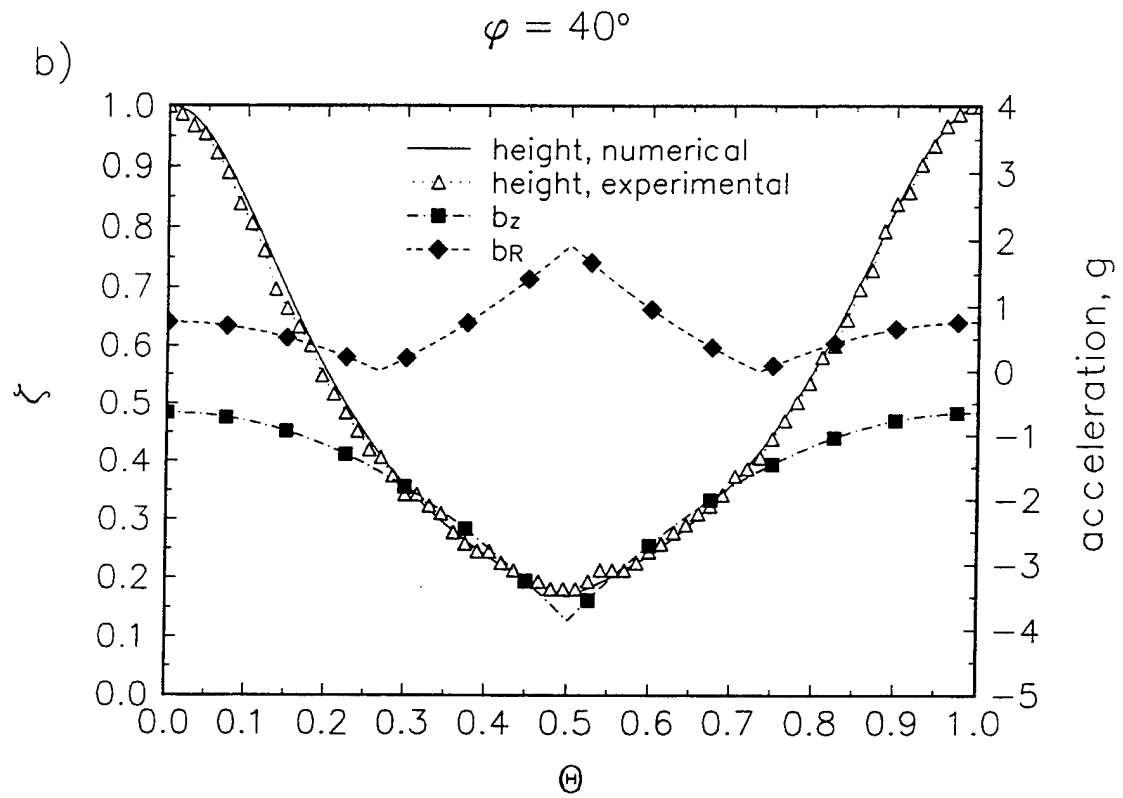
Fig. 2.6(contd)

b) $\phi = 40°$, $Ca = 4.67 \times 10^{-6}$, $Re = 3.99 \times 10^{-2}$, $a/h_o = 7.34 \times 10^{-3}$,
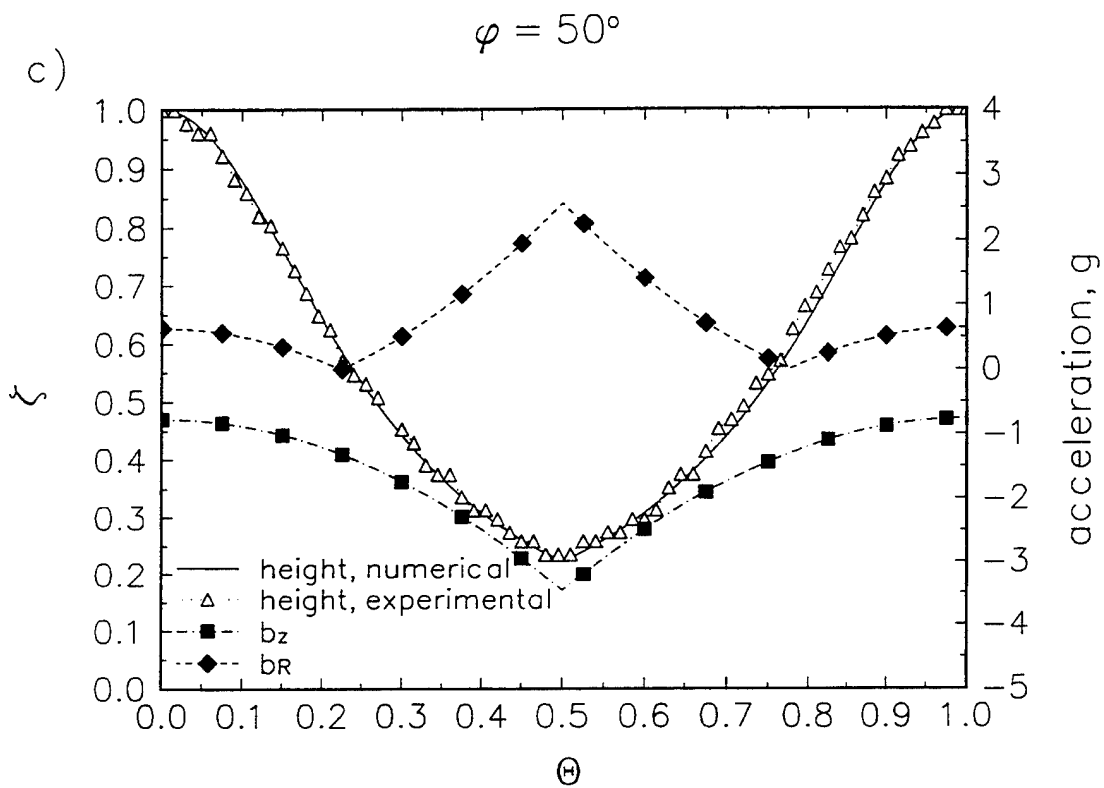
Fig. 2.6(contd)

c) $\phi = 50°$, $Ca = 3.92 \times 10^{-6}$, $Re = 3.35 \times 10^{-2}$, $a/h_o = 8.75 \times 10^{-3}$,

$\varphi = 60°$

d)
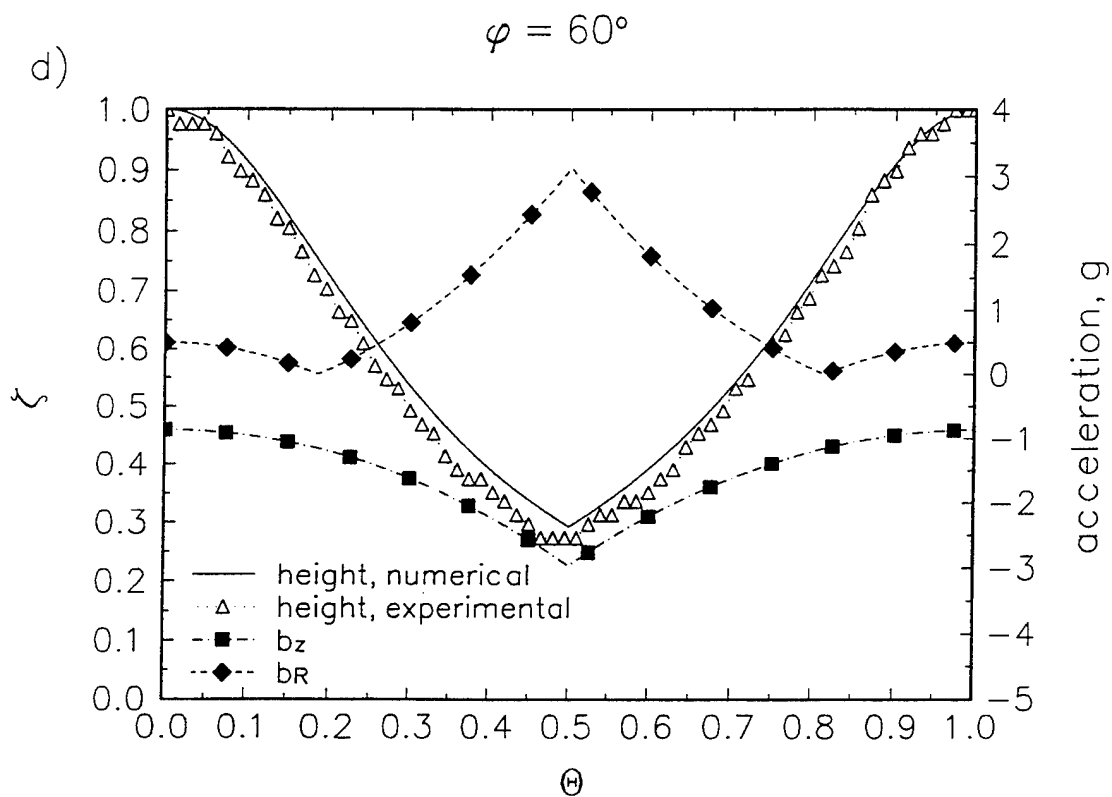
Fig. 2.6(contd)

d) $\varphi = 60°$, $Ca = 3.47 \times 10^{-6}$, $Re = 2.96 \times 10^{-2}$, $a/h_o = 9.89 \times 10^{-3}$.
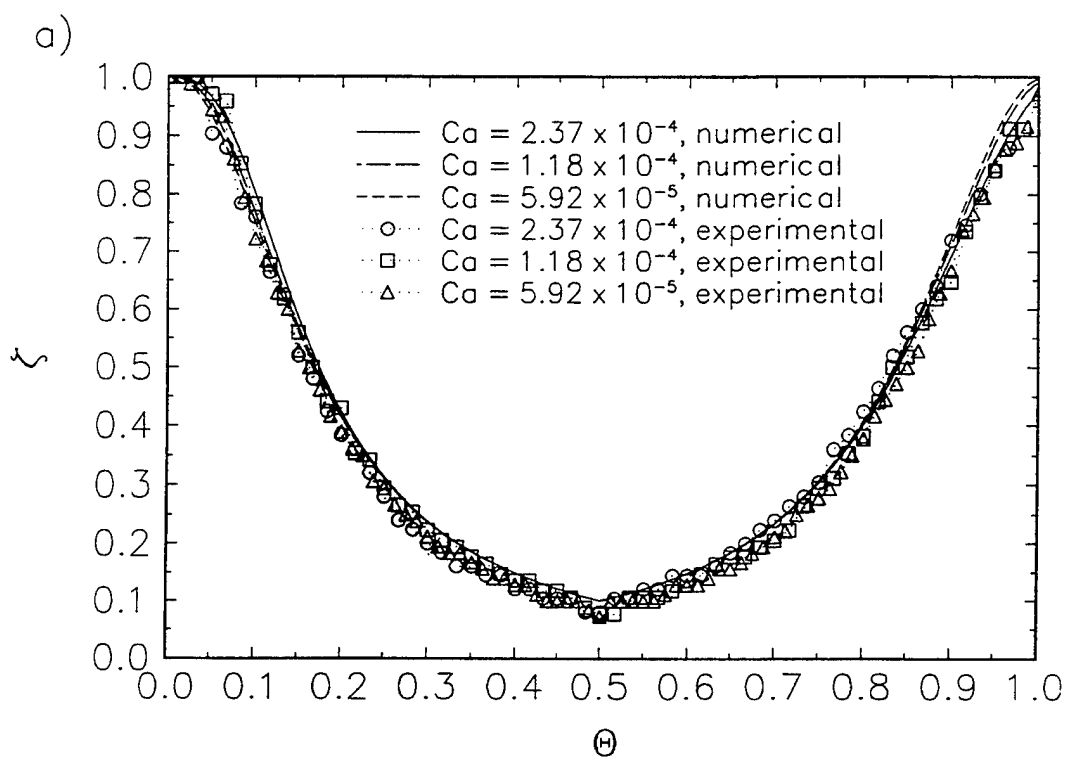
Fig. 2.7 Experimental data compared to analytical calculations
for varying capillary number:

a) $\phi = 25^\circ$, $Bo = 1.47$,
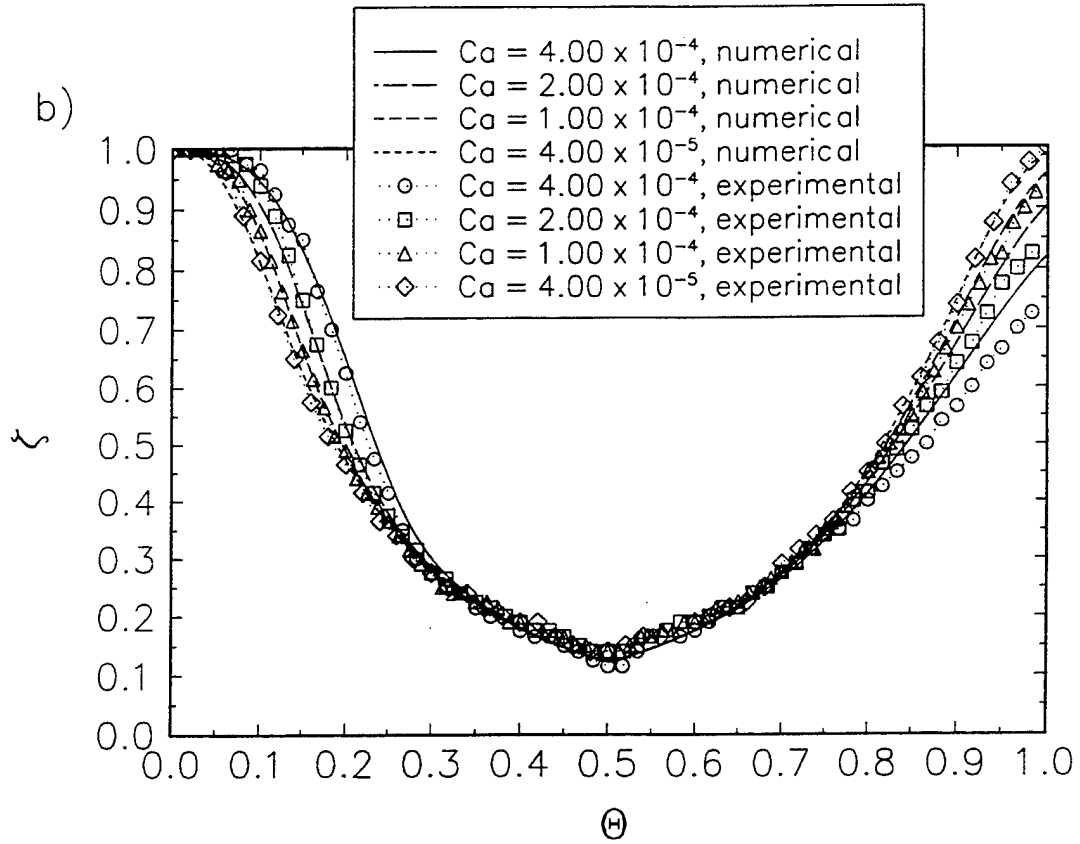
Fig. 2.7(contd) b) $\phi = 30°$, $Bo = 0.3675$.

72
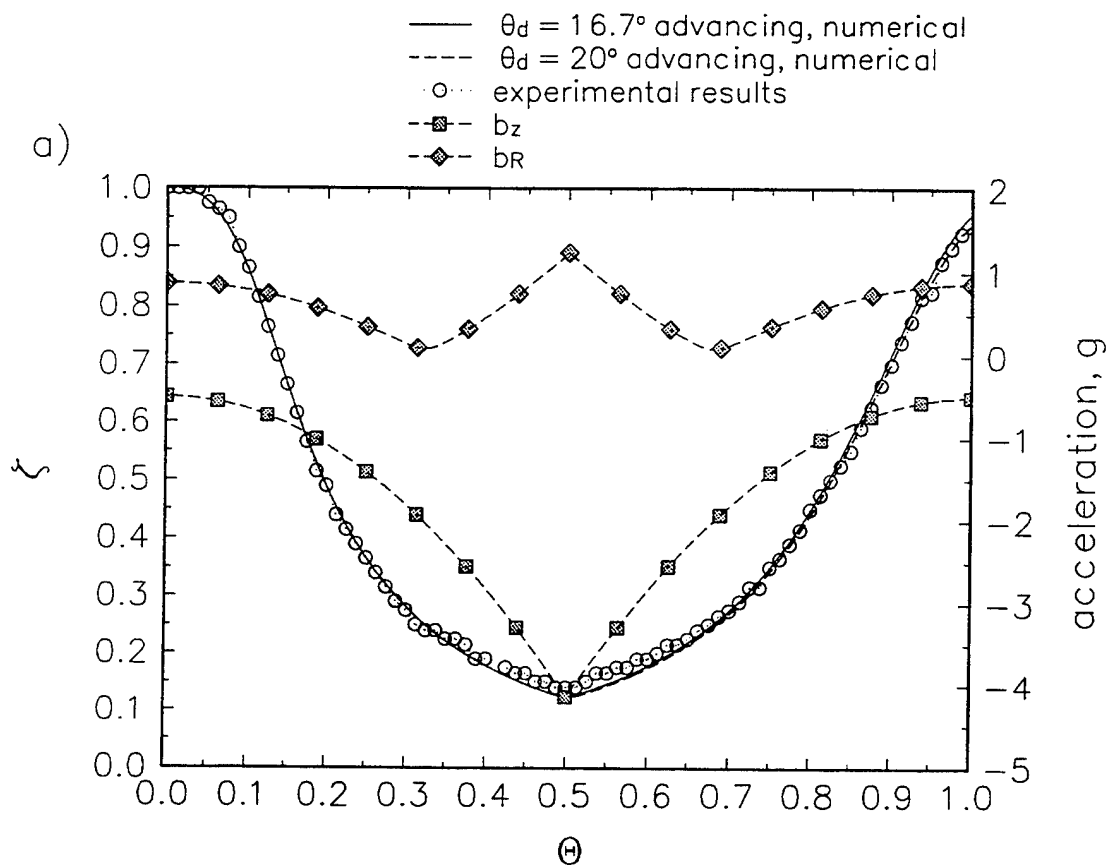
Fig. 2.8 Experimental data compared to analytical calculations
for varying advancing contact angle, $\phi = 30°$, $Bo = 0.3675$ (16.7° receding
contact angle) and acceleration field: a) $Ca = 1.00 \times 10^{-4}$,
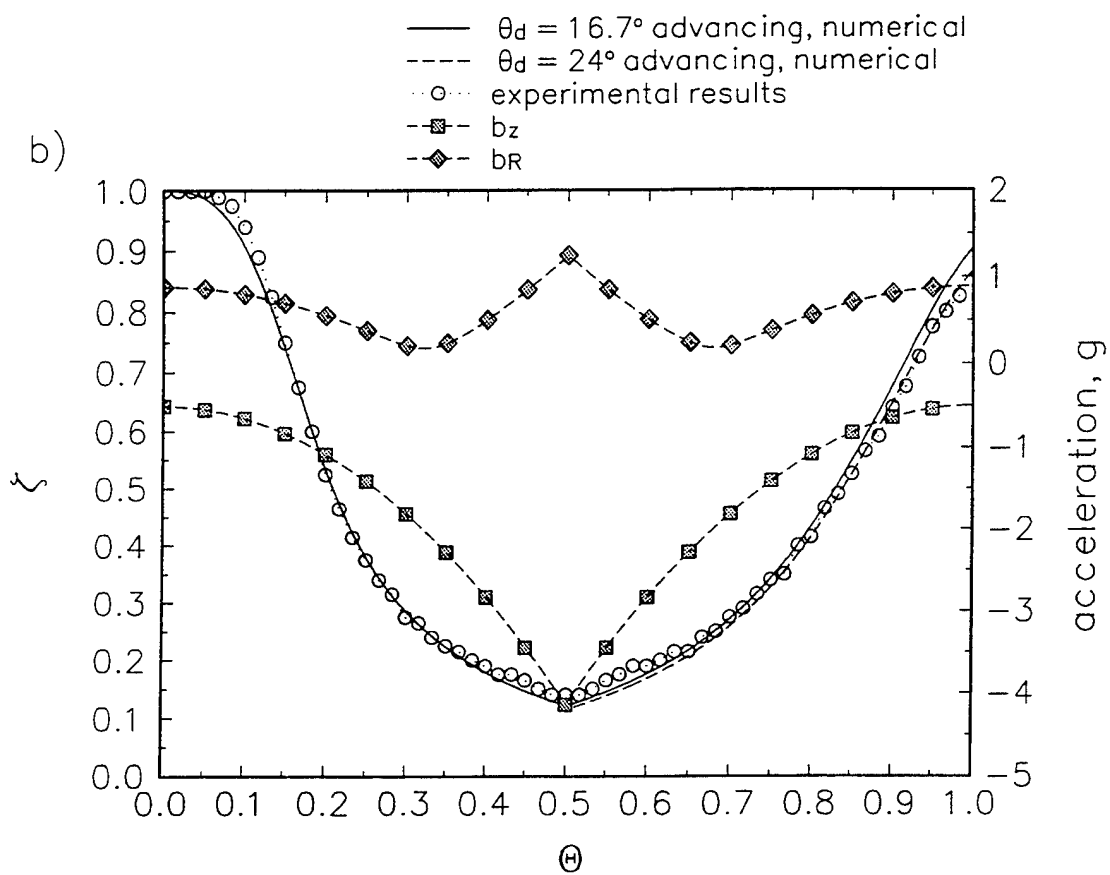
Fig. 2.8(contd) b) $Ca = 2.00 \times 10^{-4}$,
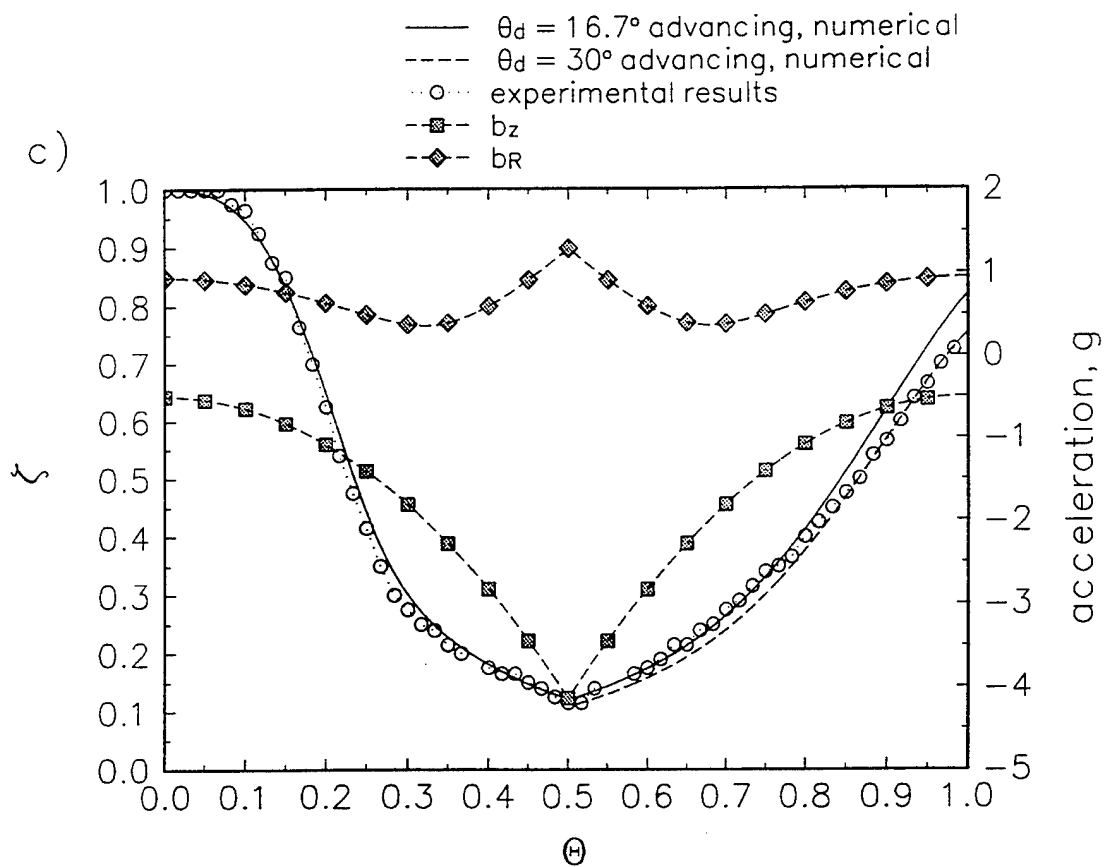
Fig. 2.8(contd) c) $Ca = 4.00 \times 10^{-4}$.

75
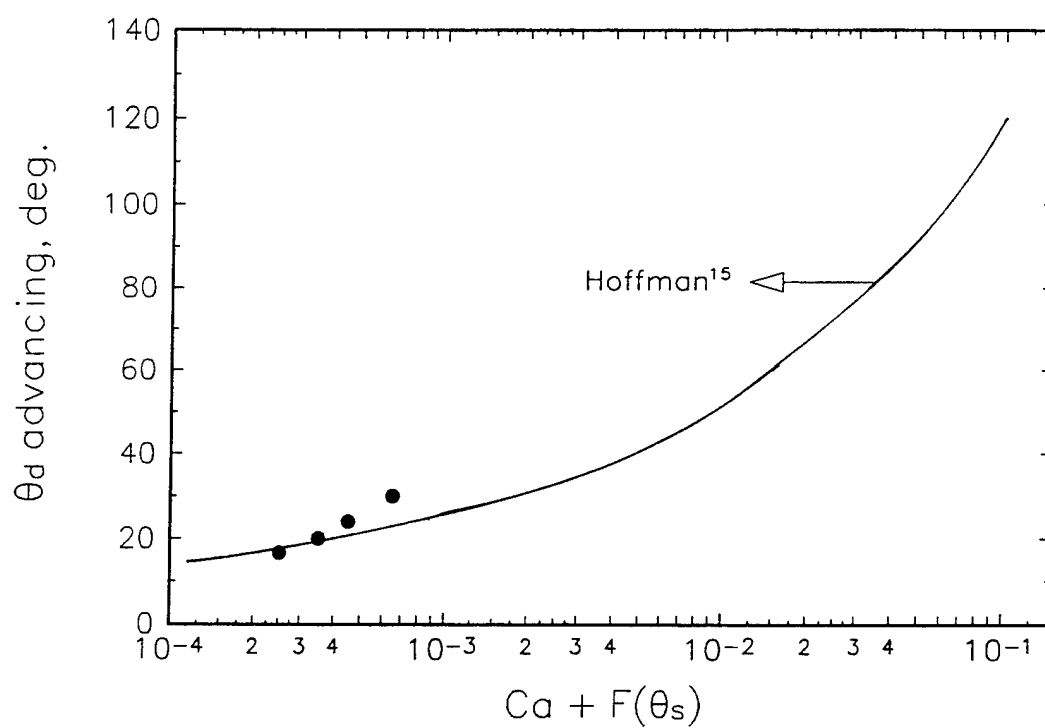
Fig. 2.9 Comparison of Hoffman's[15] results and advancing contact angle
required to match experimental results.
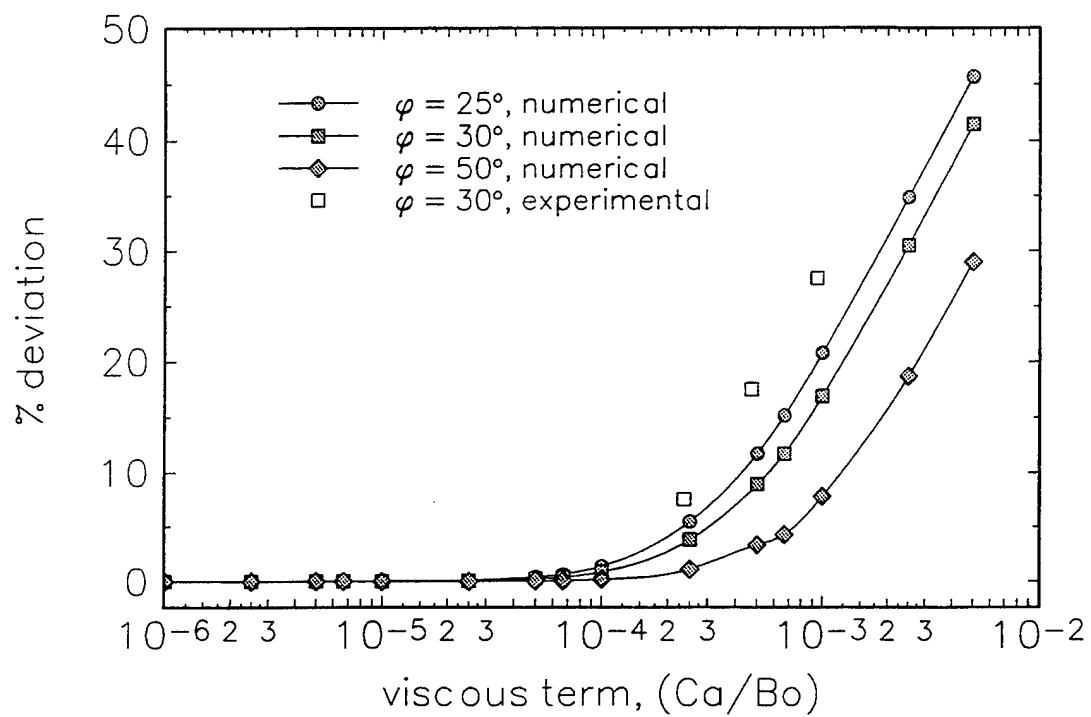
Fig. 2.10 Percent deviation from the inviscid solution at the end of a cycle.
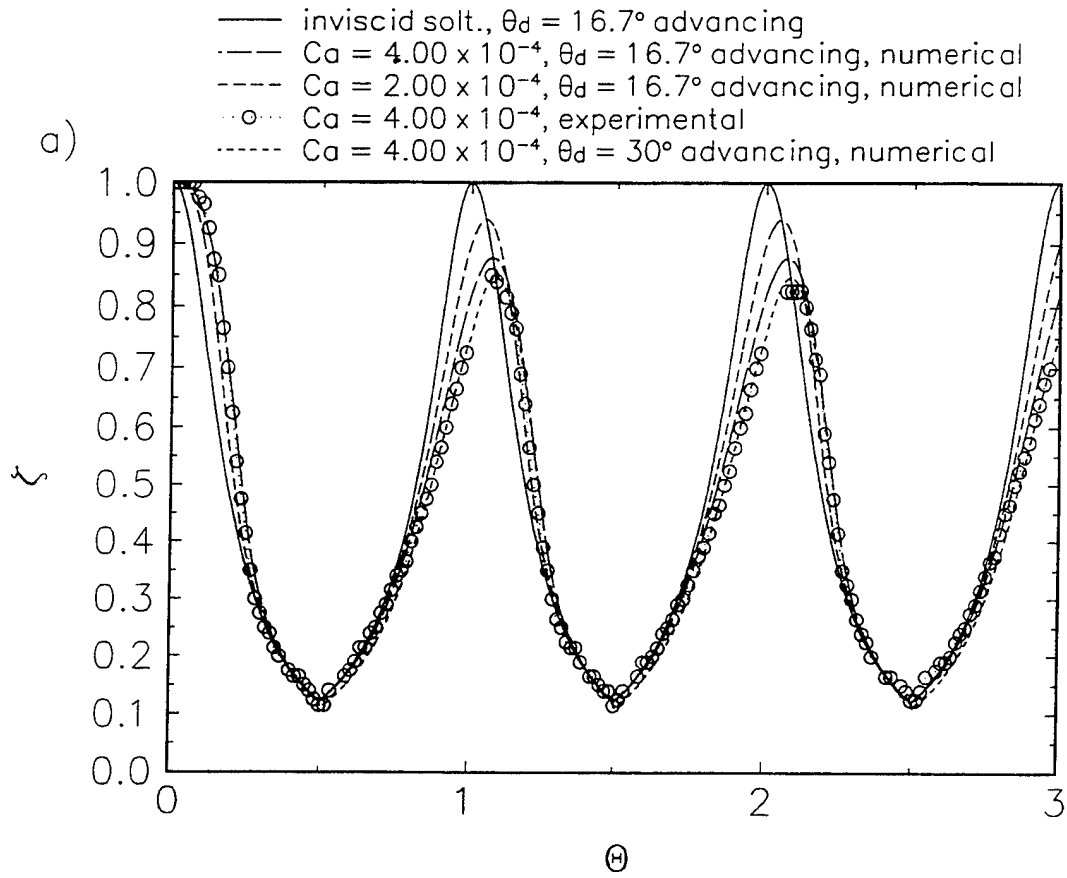
Fig. 2.11 Experimental data compared to analytical calculations for multiple acceleration cycles ($\phi = 30\,^\circ$, $Bo = 0.3675$): a) varying capillary number, $g_{pk} = 4.2\,g$,
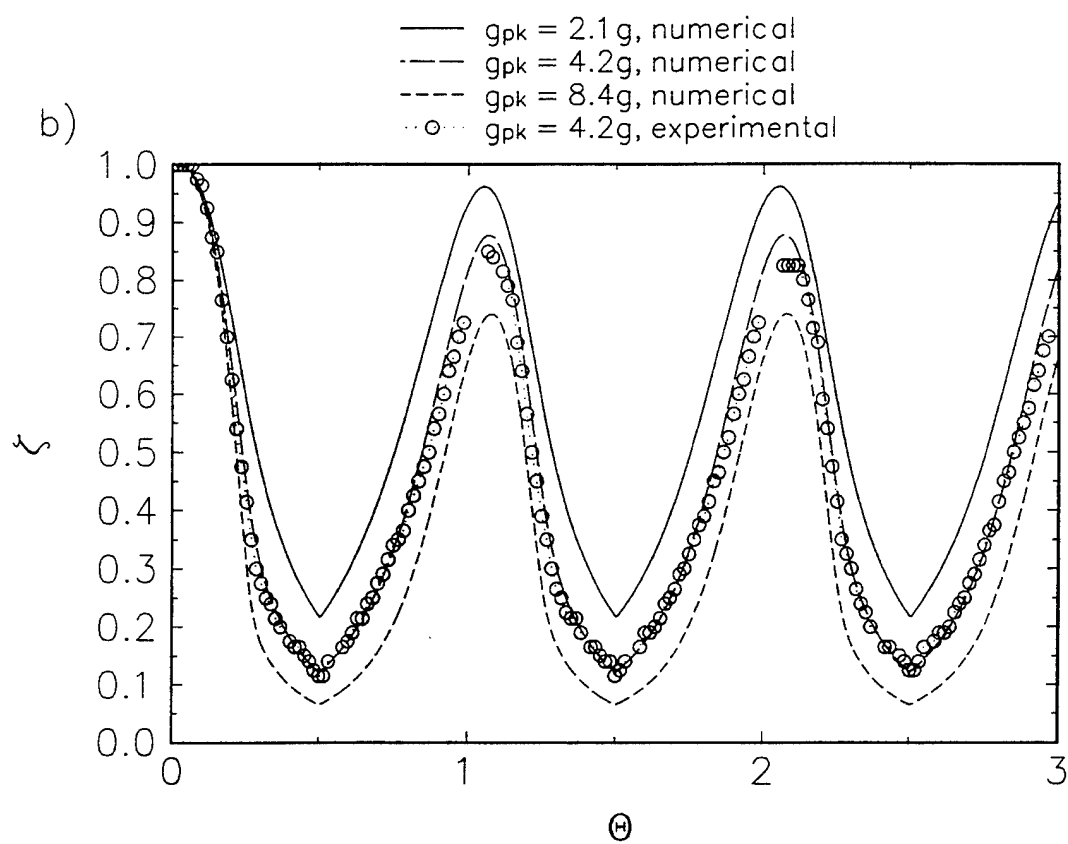
Fig. 2.11(contd) b) varying g_{pk}, $Ca = 4.00 \times 10^{-4}$.

CHAPTER III

DYNAMIC BEHAVIOR OF A HEATED MENISCUS
SUBJECTED TO A TRANSIENT ACCELERATION FIELD

Abstract

This study experimentally and analytically investigates the effects of acceleration

transients on the dynamic response of a heated meniscus in a capillary tube. A capillary

tube partially filled with ethyl alcohol was mounted on a centrifuge to observe the

dynamic response of a heated meniscus subject to an acceleration transient. An initial

recession of the meniscus due to heat input was treated as a change in contact angle due

to thermocapillary effects as a result of non-isothermal heating. Experiments and

analytical calculations were for a Bond number of 1.47 and a capillary number of

3.00×10^{-6}. Experimental data of the meniscus recession and advance agreed well with

a one-dimensional equation of motion accounting for the change in contact angle due to

thermocapillary effects.

Experimental

Acceleration Field

Transient acceleration fields were generated using a 2.4-m diameter centrifuge

table (Fig. 3.1) rotating with a time variant angular velocity. Angular velocity transients

were generated at a cyclic frequency, $f = 0.0015\,Hz$, using a signal or waveform

80

generator as a control input to the centrifuge. The angular velocity was increased linearly to a peak value at the midpoint of the cycle and subsequently decreased for two cycles. A tri-axis accelerometer (Columbia Research Laboratories, Inc.) was used to monitor the time variant acceleration components in a cartesian reference frame affixed to the centrifuge table. For this investigation, the peak angular velocity was specified such that a 4.2-g ± 0.1-g peak radial acceleration was generated (g_{pk} = 41.20 m/s²).

Capillary Test Cell

A sealed test cell was fabricated of delrin to contain an ethyl alcohol working fluid and a 1.0-mm diameter capillary tube as shown in Fig. 3.2a. The capillary tube was held in place using spring loaded positioning clamps. A transparent window allowed viewing of the capillary tube during experimental testing. A 1 cm long transparent gold film was vapor deposited on the top exterior surface of the capillary tube and served as a heater.[31] A Kepco precision dc power supply (Kepco, Inc.) was used to power the gold film heater.

Exposed junction copper-constantan type thermocouples were attached at a spacing of approximately 1 cm to the exterior surface of the capillary tube with a graphite slurry to maintain a thermal bond with an outside coating of high temperature ceramic to maintain strength integrity. Additional thermocouples were placed in the liquid reservoir and vapor space (properties of the ethyl alcohol were assumed to be that of the bulk reservoir fluid corresponding to an experimental temperature of 30°C). Thermocouple signals were linearized and amplified to a 0 - 5 volt signal on the centrifuge to eliminate slip ring noise and error due to dissimilar metal junctions. The data acquisition system (including signal conditioner, slip ring, A/D converter, etc.) and thermocouples were

81

calibrated over a temperature range of 25 - 70°C using a high precision temperature probe (Hart Scientific 5690) to within ±1°C.

The test cell and capillary tube were cleaned using potassium hydroxide and thoroughly rinsed with ethyl alcohol. The test cell was filled and subsequently sealed resulting in a fill that had a combination of air, fluid vapor, and liquid. The sealed test cell containing a glass capillary tube and reservoir was positioned on the centrifuge as shown in Fig. 3.2b. The test cell was mounted to a motorized optics rotation stage (Newport) such that the capillary tube was allowed to pivot about its center of mass. The dynamic response of the meniscus to the transient acceleration field was observed using an 8-mm format CCD camera (Sony, 30 frames/s) mounted adjacent to the test cell. Video images were used to provide a record of the meniscus height relative to the reservoir meniscus, η, as a function of time to within ±1.0 mm. An equivalent static contact angle, θ_s, (with and without the addition of heat) was calculated from the experimentally determined static wicking height, h_o, for conditions when the transverse acceleration component was zero ($h_o \rho g \approx (2\sigma/a) \cos\theta_s$).

Analytical Formulation

The goals of the analytical formulation were to expand the mathematical formulation described in chapters I and II to: (i) mathematically describe the dynamic behavior of a heated meniscus as a result of the temporal acceleration induced forces using a simplified one-dimensional model accounting for changes in the dynamic contact angle due to heat addition; (ii) address the altered dynamic behavior of the heated meniscus by accounting for thermocapillary effects through a change in the dynamic

contact angle; and (iii) compare experimental results and analytical calculations.

Acceleration Vector

Acceleration measurements were obtained with regard to a three-dimensional cartesian non-inertial reference frame affixed to the centrifuge as described in chapter one. The acceleration field was then referenced to fixed locations on the capillary tube and subsequently decomposed into transverse and axial acceleration components relative to the capillary tube as shown in Fig. 3.3.

The resulting transient acceleration vector decomposed into an axial component, b_z, and a transverse component, b_R, becomes

$$\bar{b} = \left[-\omega^2 \left(r_o' + (z_1 - z) \cos\phi\right) \cos\phi + (-g) \sin\phi\right] \hat{e}_z +$$
$$\left[\left[-\omega^2 \left(r_o' + (z_1 - z) \cos\phi\right) \sin\phi - (-g) \cos\phi\right]^2 + \left[\left(r_o' + (z_1 - z) \cos\phi\right) \frac{d\omega}{dt}\right]^2\right]^{1/2}$$

(1)

Here, the transverse component, b_R, is a magnitude with no reference to direction due to the axisymmetric nature of the capillary tube.

Equation of Motion

A simple analytical model taking into account changes in the dynamic contact angle upon recession and advance was used to predict the motion of the meniscus subjected to transient accelerations. The analytical formulation of the equation of motion was simplified assuming bulk flow only in the axial direction of the capillary tube. Effectively, the liquid column in the capillary tube was assumed to undergo a slug flow.

83

The contact line force is defined assuming a spherical meniscus and a constant receding or advancing contact angle, θ_d, differing from that of the static contact angle, θ_s.

The resulting dimensional form of the momentum equation is

$$\frac{2\sigma\cos\theta}{\rho a} = \left[\eta\frac{d^2\eta}{dt^2} + \left(\frac{d\eta}{dt}\right)^2\right] + \left[\frac{8\mu}{\rho a^2}\eta\frac{d\eta}{dt}\right]$$
$$+ \eta\left[\omega(t)^2\cos\phi\left((z_1 - \frac{\eta}{2})\cos\phi + r_o'\right) + g\sin\phi\right].$$

(2)

The transient angular velocity is of the form

$$\omega(t) = Bt, \qquad 0 \le t \le \frac{tf}{2}$$
$$= B(tf - t), \qquad \frac{tf}{2} \le t \le tf$$

(3)

where

$$B = \left(\frac{4\,g_{pk}}{(tf)^2 r_o'}\right)^{\frac{1}{2}}.$$

(4)

Using the following dimensionless parameters,

$$\zeta = \frac{\eta}{h_o}, \quad 0 \le \zeta \le 1$$
$$\Theta = \frac{t}{tf}, \quad 0 \le \Theta \le 1,$$

(5)

with the following initial conditions

$$\zeta = 1, \quad \frac{d\zeta}{d\Theta} = 0, \quad \Theta = 0,$$

the non-dimensional form of the momentum equation in terms of a transient dimensionless meniscus position becomes

$$\frac{g}{g_{pk}}\frac{\cos\theta_d}{\cos\theta_s}\sin\phi = \left[\frac{a}{h_o}\right]\left[\frac{Re\,Ca}{2Bo}\right]\left[\zeta\frac{d^2\zeta}{d\Theta^2}+\left(\frac{d\zeta}{d\Theta}\right)^2\right]+\left[\frac{16\,Ca}{Bo}\right]\left[\zeta\frac{d\zeta}{d\Theta}\right]$$
$$+\zeta\left[\Omega(\Theta)^2\cos\phi\left(\left(z_1-\frac{h_o\zeta}{2}\right)\cos\phi+r_o'\right)+\frac{g}{g_{pk}}\sin\phi\right].$$

(6)

where the angular velocity, Ω, is defined by

$$\Omega(\Theta) = \left(\frac{4}{r_o'}\right)^{\frac{1}{2}}\Theta, \qquad 0\le\Theta\le\frac{1}{2}$$
$$= \left(\frac{4}{r_o'}\right)^{\frac{1}{2}}(1-\Theta), \qquad \frac{1}{2}\le\Theta\le1.$$

(7)

The first and second terms of eq. (6) represent the inertial and viscous effects, respectively, with the coefficients formed as the products of the Reynolds number, capillary number, Bond number, and aspect ratio. The Reynolds and capillary numbers are referenced to a characteristic velocity, V_c, which is the maximum attainable velocity over one-half of the acceleration cycle period assuming $\eta = 0$ at g_{pk}. The Bond number is referenced to the peak radial acceleration component, g_{pk}.

Thermocapillary Effects

With addition of heat into the meniscus region, it has been speculated that thermocapillary stresses cause an increase in the apparent contact angle as discussed by Pratt and Hallinan.[26] The thermocapillary force defined by Pratt and Hallinan can be cast as a

85

function of the axial temperature gradient along the capillary tube and the gradient of surface tension to temperature such that

$$
\frac{d\sigma}{dz} z_o (2\pi a) = \frac{\partial\sigma}{\partial T}\frac{\partial T}{\partial z} z_o (2\pi a)
$$

$$
\sim \frac{\partial\sigma}{\partial T}\Delta T(2\pi a)
\tag{8}
$$

assuming a constant wall temperature gradient. Using this approximation, it follows that a change in static contact angle as a result of heat addition can be accounted for where

$$
\sigma(2\pi a)\cos\theta_{s,\ heat} = \sigma(2\pi a)\cos\theta_s - \frac{\partial\sigma}{\partial T}\frac{\partial T}{\partial z} z_o(2\pi a)
$$

$$
\sim \sigma(2\pi a)\cos\theta_s - \frac{\partial\sigma}{\partial T}\Delta T(2\pi a)
\tag{9}
$$

$$
\frac{\partial\sigma}{\partial T}\Delta T \sim \sigma(\cos\theta_s - \cos\theta_{s,\ heat})
$$

If it is further assumed that heat addition produces a change in contact angle from the static value to a constant dynamic contact angle such that $\theta_d = \theta_{s,\ heat}$, then the derived analytical form, eq. (6), can be solved to determine the meniscus dynamic response to an acceleration transient with the addition of heat provided that $\theta_{s,\ heat}$ is known. This analysis assumes negligible buoyancy effects as discussed by Pratt and Hallinan.[26]

Results

Equation (6) was solved for the dimensionless meniscus position, ζ, using a central-difference scheme. Numerical solutions were consistent with the experimental

86

parameters for $Bo = 1.47$ and $Ca = 3.00 \times 10^{-6}$ with two acceleration transient cycles. For the case with no heat addition and due to the slow acceleration transient, solutions were obtained by specifying the experimentally inferred static contact angle (see Appendix B) to be equivalent to the dynamic contact angle, $\theta_s = \theta_d = 16.7\,^{\circ}$. With the addition of heat to the capillary tube there was an immediate recession of the contact line to a new static wicking height corresponding to an altered contact angle, $\theta_{s,\ heat}$, accounting for heat addition. The value of this contact angle was calculated from the experimental results as was the static contact angle for the unheated case (also see Appendix B). Numerical solutions for the case with heat addition assumed the static contact angle, $\theta_s = 16.7\,^{\circ}$, and a constant dynamic contact angle equivalent to the experimentally inferred contact angle at the retarded wicking height due heat addition such that $\theta_d = \theta_{s,\ heat} = 35.6\,^{\circ}$. Fluid properties ($\sigma$, ρ, μ) were referenced to the bulk fluid in the reservoir, $T_{res} = 30\,^{\circ}C$. The temperature gradient, ΔT, along the capillary tube was determined using thermocouple data and was assumed to be representative of the ΔT between thermocouples tc2 and tc3 just below the heater.

Experiments were performed at a fixed angle of inclination of 30° while applying heat to the top exterior of the capillary tube. The acceleration transient was not applied until thermal equilibrium was obtained within the test cell. Three levels of heat inputs, including line losses, were 1.0 , 3.5 W, and 4.0 W ± 0.5 W. The dynamic response of the heated meniscus was compared with solutions to the analytical model. Uncertainty in the experimentally obtained dimensionless meniscus position, ζ, and time, Θ, was on

87

the order of ζ, Θ ± 0.02 based on the accuracy and resolution of the experimentally measured quantities.

Figure 3.4 shows the temperature profile along the capillary tube and within the test cell for each of the three heat inputs. Also shown are the transient axial, b_z, and transverse, b_R, components of the acceleration vector at the pivot point of the capillary tube for two transient cycles. For clarification in Fig. 3.4c, the arrows at the uppermost part of the graph show the dimensionless time for which the dimensionless meniscus position corresponds to the indicated thermocouple location. The temperature variations during the experimental cycles are due to movement of the meniscus in the capillary tube as well as the orientation of the reservoir surface with respect to the capillary tube. As the liquid column moves either out of or into the capillary tube, there is a corresponding increase or decrease in the rate of energy storage within the capillary tube. This change in energy storage results in a change in the temperature profile of the capillary tube. Also, as the acceleration vector varies in magnitude and direction, the reservoir surface remains in an orientation normal to the acceleration vector and therefore is continually in motion as is the liquid column. The location of the reservoir surface relative to the proximity of the thermocouples will influence the local capillary tube temperature.

The variation in the temperature profile of the capillary tube as a result of the motion of both the liquid column and reservoir is depicted in Fig. 3.5. Figure 3.5 shows photographs of the meniscus and reservoir position and the temperature history for selected times during the first cycle with a heat input of 4.0 W, Fig. 3.4c. The photographs were taken at times corresponding to Θ = 0.0735, 0.1605, 0.2535, 0.4320,

0.7065, 0.8280, 0.9090 or to the maximum non-dimensional time indicated on the Θ axis of the accompanying temperature graph. From Fig. 3.5b, as the meniscus passes between thermocouples tc2 (located just below the heater) and tc3 there is an increases in temperature in tc2 and tc3 and a decrease in the reservoir temperature. As the meniscus passes between thermocouples tc3 and tc4, Fig. 3.5c, the reservoir temperature stabilizes with continued increases in temperature of tc2 and tc3. It may be noted that thermocouple tc4, located in close proximity of the reservoir surface at the start of the cycle, increases slightly in temperature and stabilizes as the reservoir is reoriented below the thermocouple. There is also an inflection in the transient temperature response of tc2 and tc3 as the transverse acceleration component passes through a minimum. As the acceleration reaches a maximum and begins to decline, Fig 3.5d and 3.5e, the rate of change of tc2 and tc3 decreases toward a peak temperature and there is a sudden increase in vapor temperature. At this point in time the meniscus position is at a minimum and conduction of heat down the capillary tube is approaching steady state conditions with a reduction in the energy storage (due in part to the absence of the column of liquid in the capillary tube) in the capillary tube itself. As a result, the excess energy is going into the vapor causing a temperature rise. As the acceleration is decreased for the remainder of the cycle, the return path of the meniscus and reservoir surface motion, Figs. 3.5 e-g, result in the reversal in the transient temperature response.

Figure 3.6 compares experimental results and analytical calculations for each of the three heat inputs for two acceleration transient cycles. Also shown are the components of the acceleration vector. There was no significant difference in the

measured dimensionless meniscus position due to the heat inputs. Analytical solutions consisted of: (i) maintaining a constant contact angle such that $\theta_d = \theta_s = 16.7°$; (ii) assuming a change in contact angle due the thermocapillary effects such that $\theta_d = 35.6°$, $\theta_s = 16.7°$; (iii) assuming a change in contact angle due the thermocapillary effects such that $\theta_d = 40.0°$, $\theta_s = 16.7°$; and (iv) the dynamic contact angle, $\theta_d = \theta_{s, heat}$, was constant for the three heat inputs. Analytical solutions consistent with the assumption that there is a change in contact angle due to thermocapillary effects showed good correlation with the experimental results for the three heat inputs for the case where $\theta_d = 35.6°$. Solutions for $\theta_d = 40.0°$ resulted in a retarded meniscus height compared to the experimental results.

The results discussed so far have assumed that thermocapillary effects due to heating of the meniscus will result in a change in contact angle and that this contact angle can subsequently be used to predict the meniscus motion with heating. Equation (9) can be verified using experimental data to evaluate ΔT, $\theta_{s'}$, and $\theta_d = \theta_{s, heat}$ and standard property tables for σ and $\partial\sigma/\partial T$. An average ΔT was calculated from experimental data using the difference between the thermocouples tc2 and tc3. Table 3.1 summarizes, the information required to evaluate the terms in eq. (9) for the heat inputs of 1.0, 3.5, and 4.0 W. For a heat input of 4.0 W, the error between the two terms was within 5% while for a heat input of 1.0 W, the error was 76%. This discrepancy may be in part due to the assumption that the fluid properties were evaluated at the reservoir temperature as well as error in the experimentally inferred contact angle, $\theta_{s, heat}$. In

addition, the defined temperature gradient, ΔT, is a critical value for which thermocapillary stresses will result in an altered contact angle. In general, an increase in temperature will decrease the density and surface tension. The combined effects of a decrease in density and a reduced surface tension for a fixed contact angle, assuming negligible thermocapillary stresses, may result in a recession in the static wicking height due to heat input. If in fact density, surface tension, and contact angle change due to the combined effects of an increase in temperature and thermocapillary stresses (or a critical ΔT) as a result of an increased heat input, there may be situations for which the static wicking height may not be altered from the case where thermocapillary effects were assumed to be negligible. This may be why the combined assumptions of a constant $\theta_{s, \, heat}$ and evaluation of fluid properties at 30°C resulted in a good correlation between analytical calculations and experimental results.

Table 3.1
Summary of thermocapillary terms in eq. (9).

σ, (@30°C), (N/m)	0.02189		
$\dfrac{\partial \sigma}{\partial T}$, $(20° \leq T \leq 100°)$ (N/m-°C)	-9.15×10^{-5}		
θ_s (deg.)	16.7		
$\theta_d = \theta_{s, heat}$ (deg.)	35.6		
ΔT (°C)	-33.3 ± 3.3	-28.9 ± 2.7	-7.9 ± 0.5
$\dfrac{\partial \sigma}{\partial T} \Delta T$ (N/m)	3.02×10^{-3} $\pm 0.27 \times 10^{-3}$	2.64×10^{-3} $\pm 0.25 \times 10^{-3}$	7.2×10^{-4} $\pm 0.5 \times 10^{-4}$
$\sigma (\cos\theta_s - \cos\theta_{s, heat})$ (N/m)	3.17×10^{-3}		
Q (W)	4.0	3.5	1.0

Fig. 3.1 Schematic of centrifuge.

a)

$\bar{b}$

thermocouples

TC1

gold film
heater

spring
loaded
clamp

TC2

vapor
thermocouple

capillary
tube

TC3

TC4

reservoir
thermocouple

pivot
point

TC5

TC6

reservoir

b)

8mm CCD
camera

optics
rotation angular
stage position
transducer

test cell w/
capillary tube

accelerometer
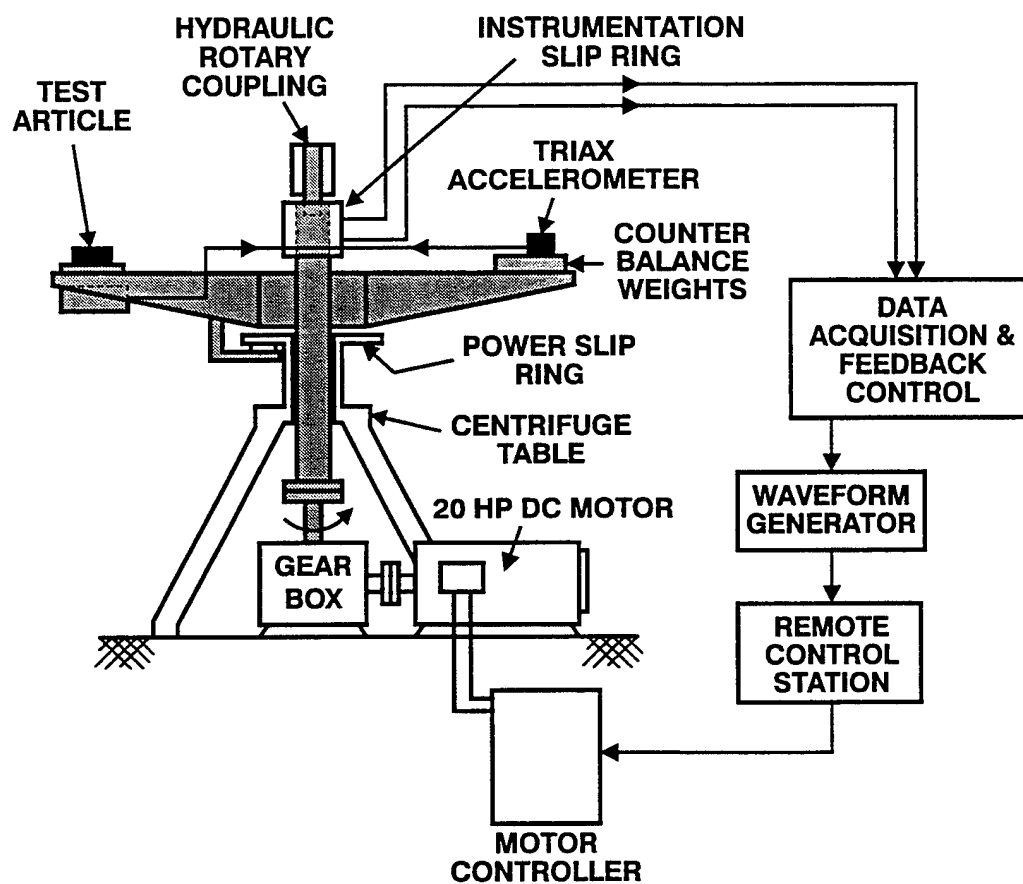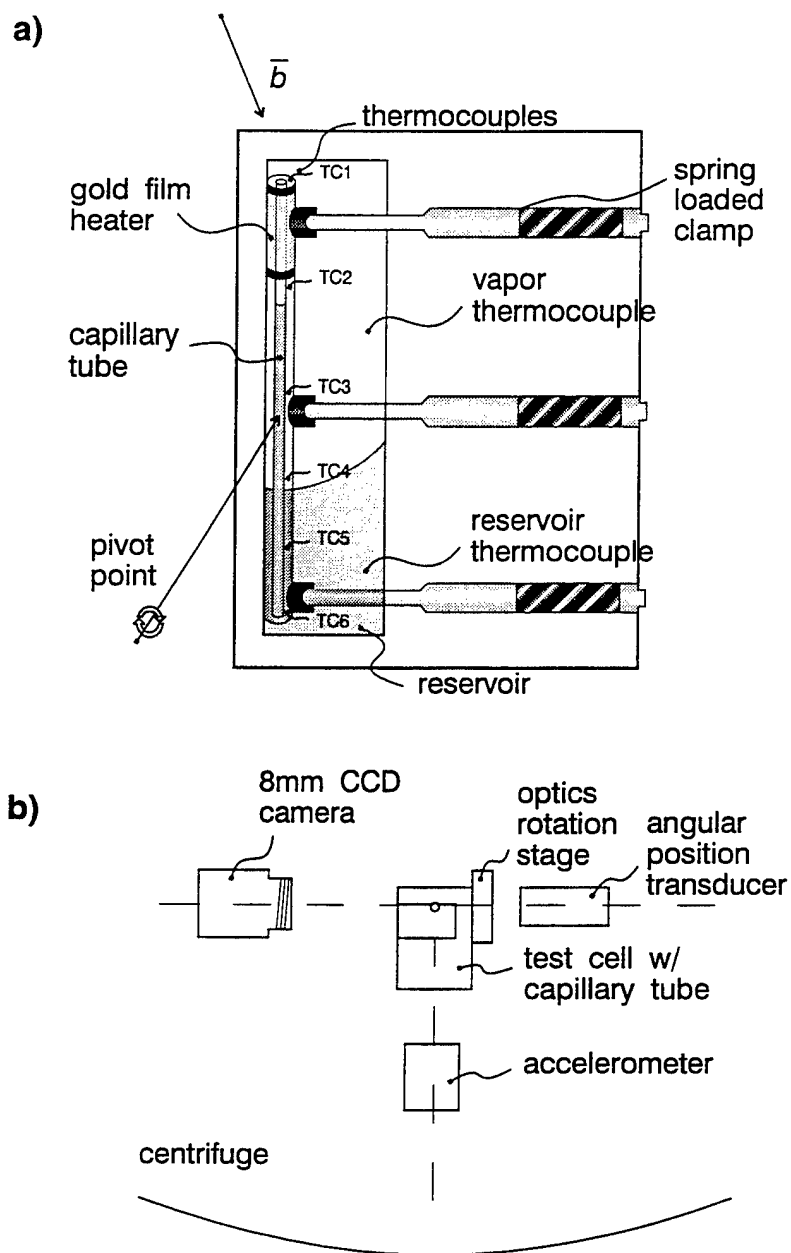
centrifuge

Fig. 3.2 Experimental apparatus: a) sealed test cell
and b) schematic of experimental apparatus as mounted on the centrifuge.

94
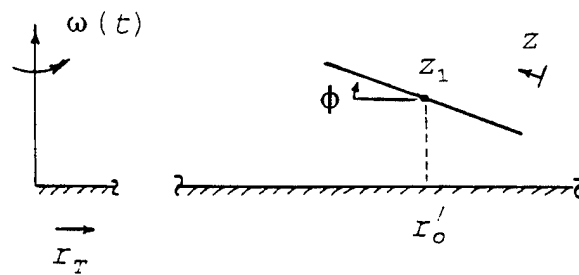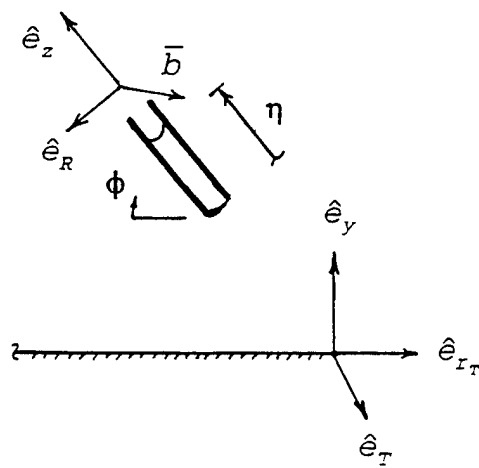
Fig. 3.3 Capillary tube orientation: a) pivot point location, directional coordinates and b) coordinate systems as referenced to the centrifuge accelerometer and capillary tube.

95
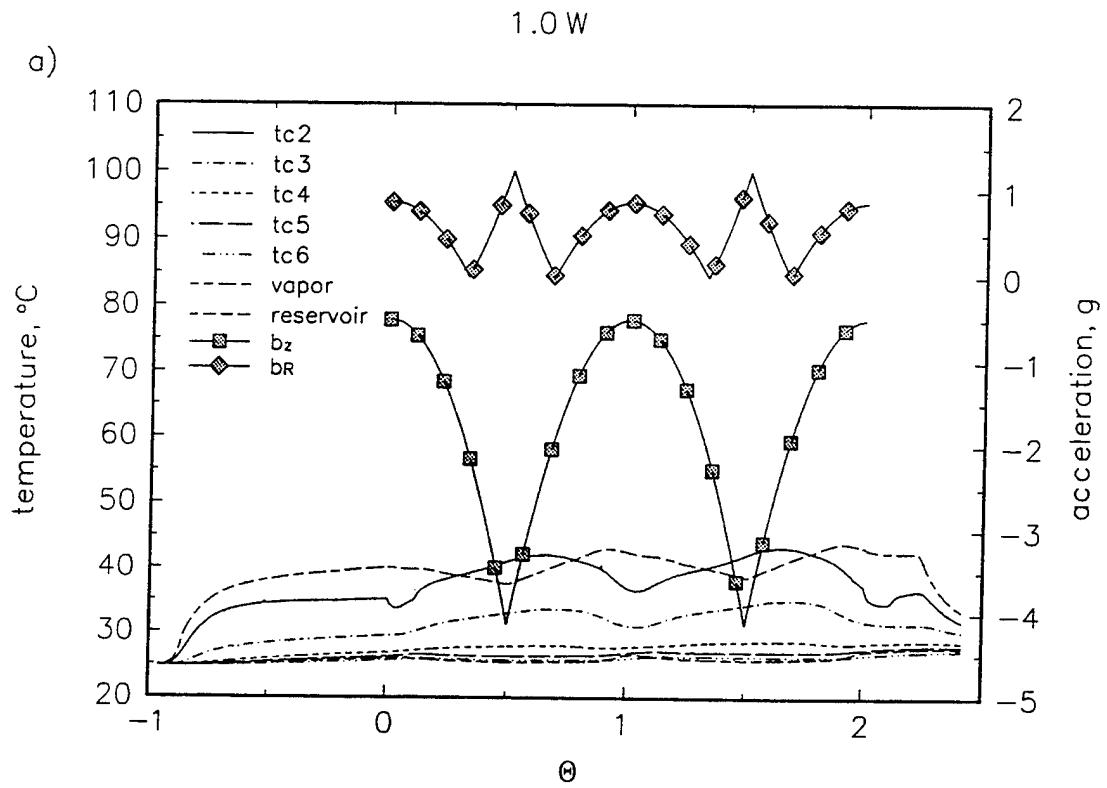
Fig. 3.4 Experimental temperature variation for: a) 1.0 W,

3.5 W

b)

Fig. 3.4(contd) b) 3.5 W,

97
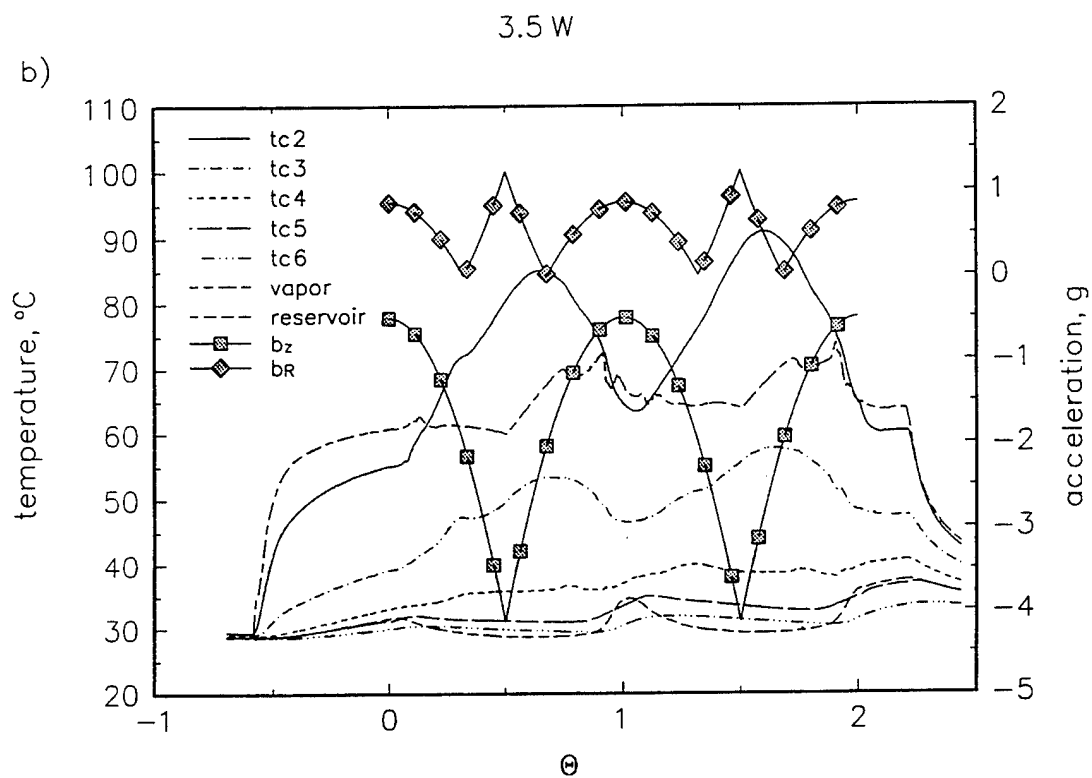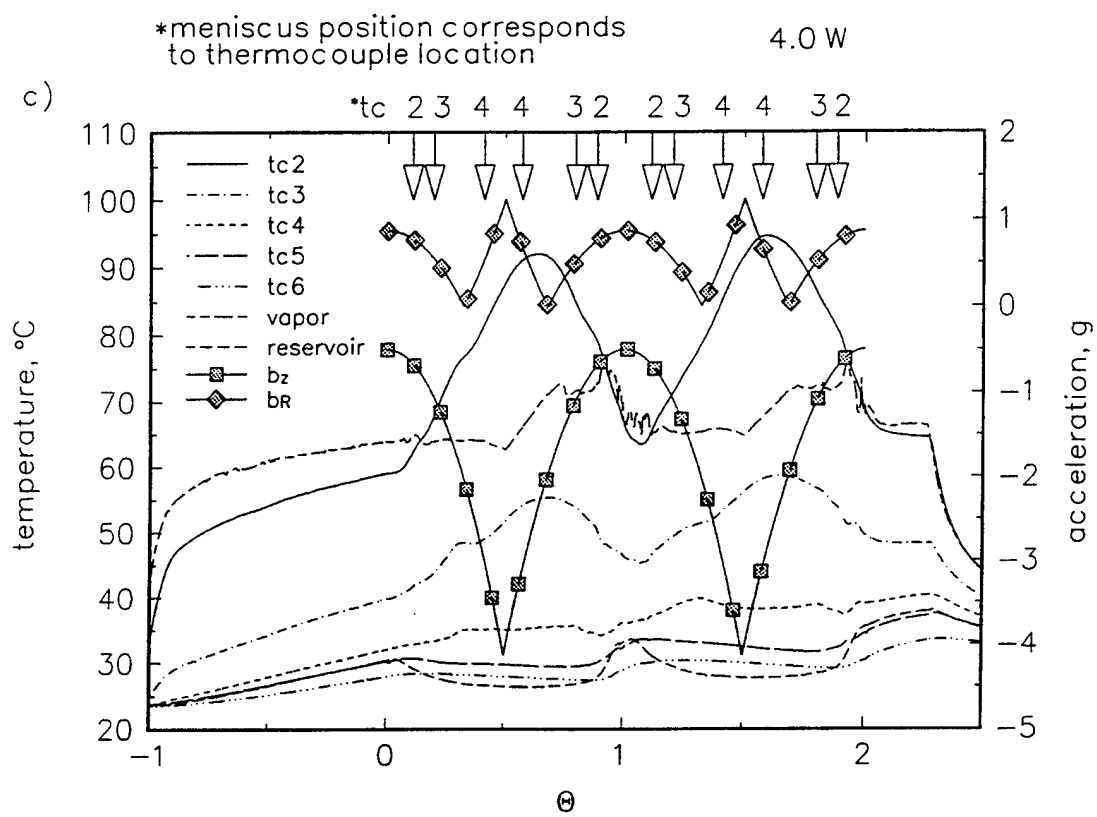
Fig. 3.4(contd) c) 4.0 W.
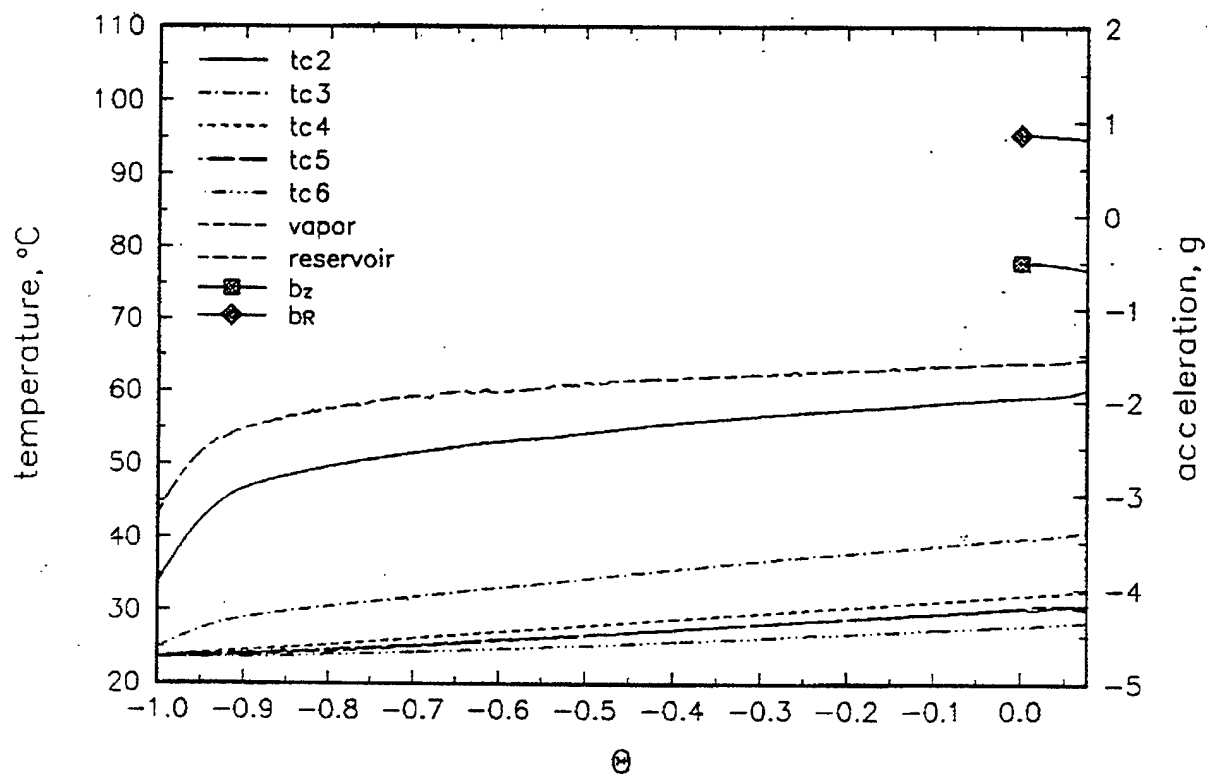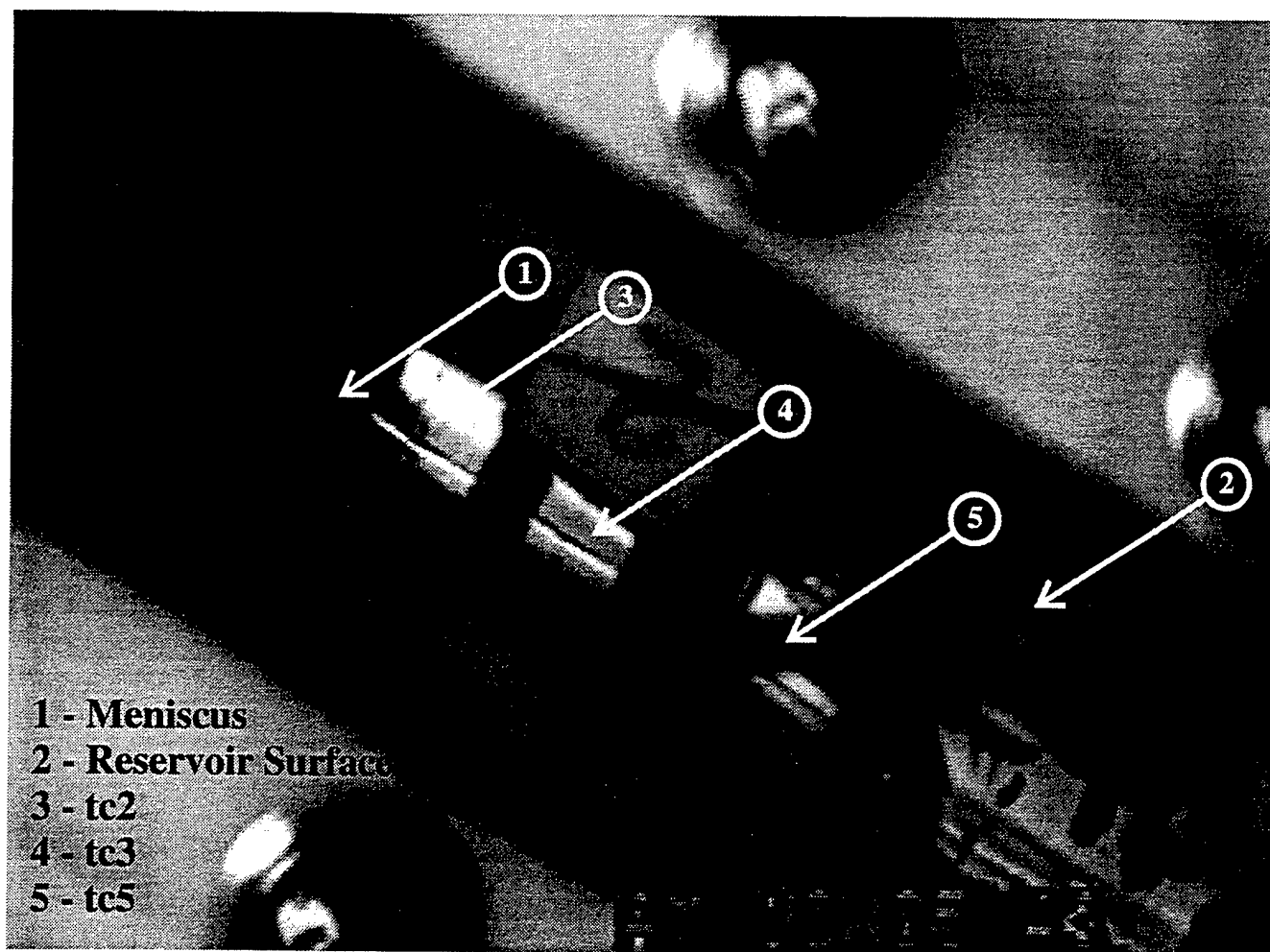
Fig. 3.5 Sequential photos of meniscus position with corresponding
plots showing temperature history: a) Θ = 0.0735,
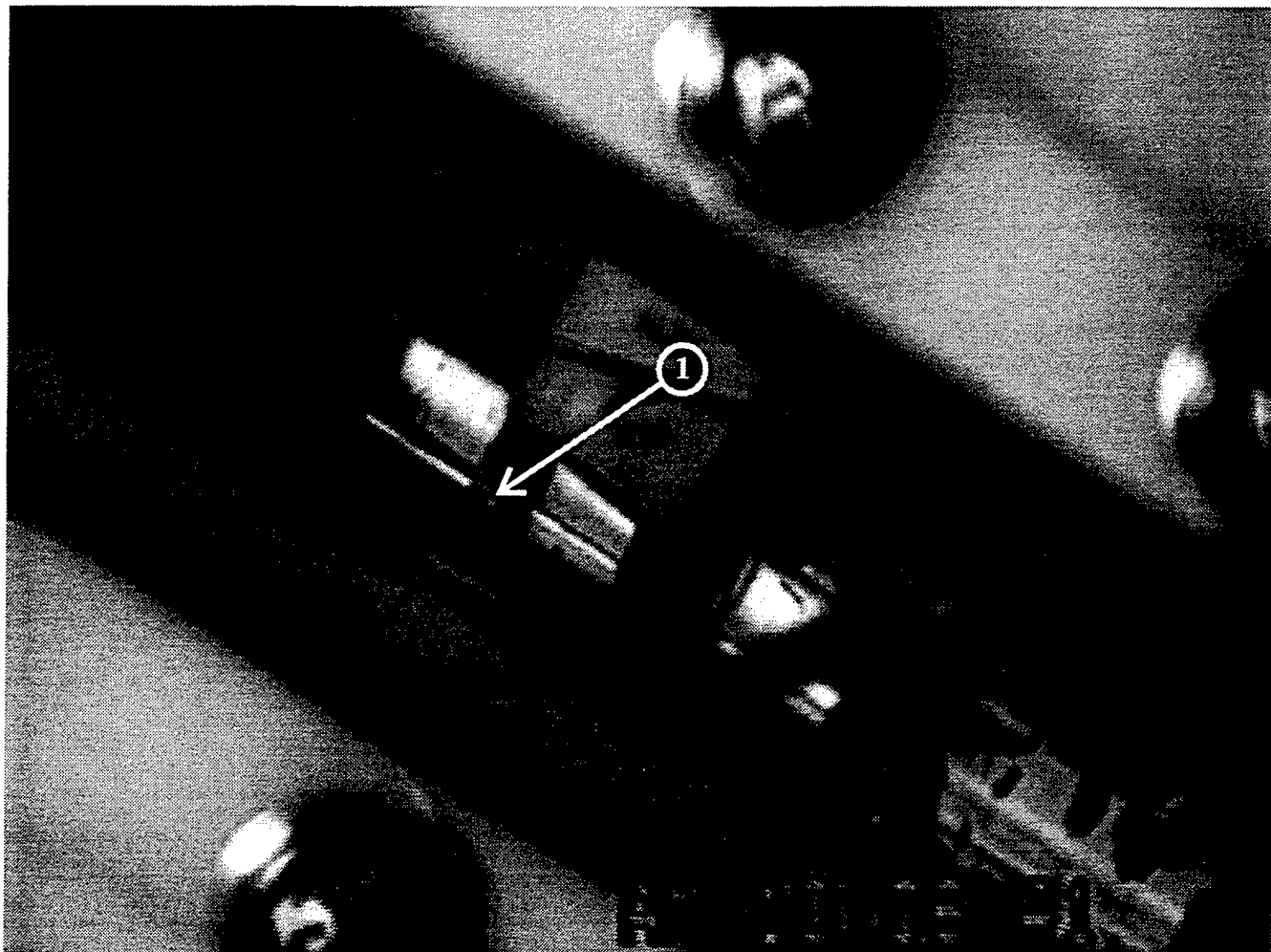
*meniscus position corresponds
to thermocouple location
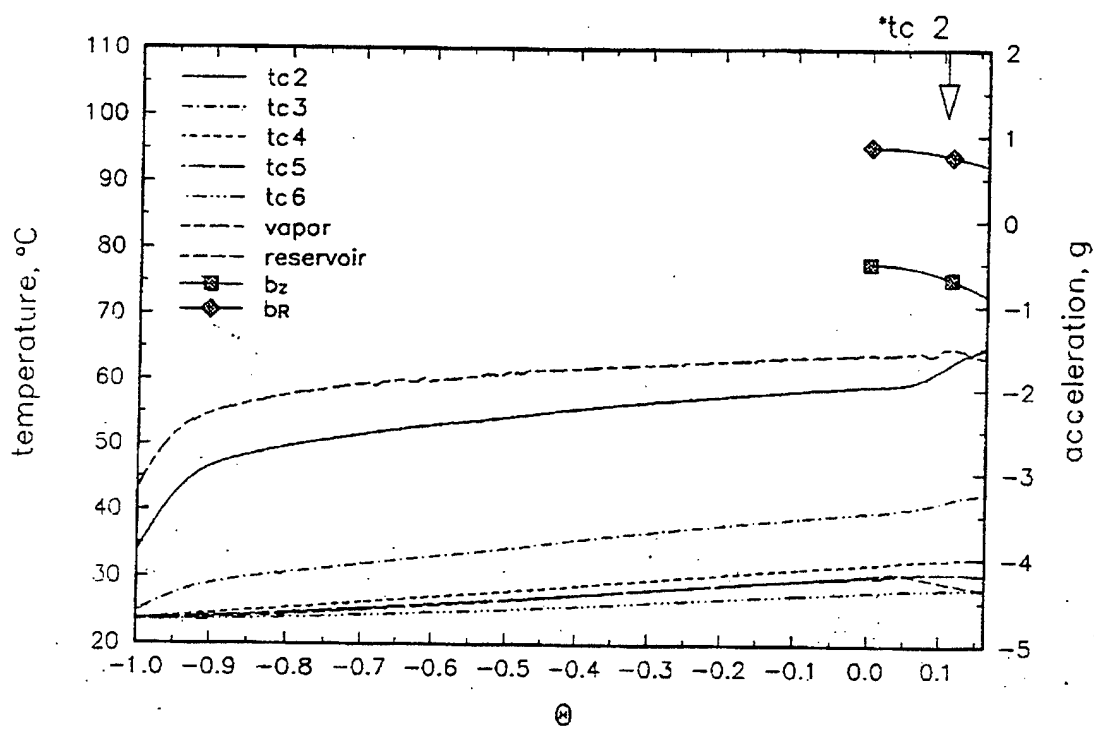
Fig. 3.5(contd) b) $\Theta = 0.1605,$

100
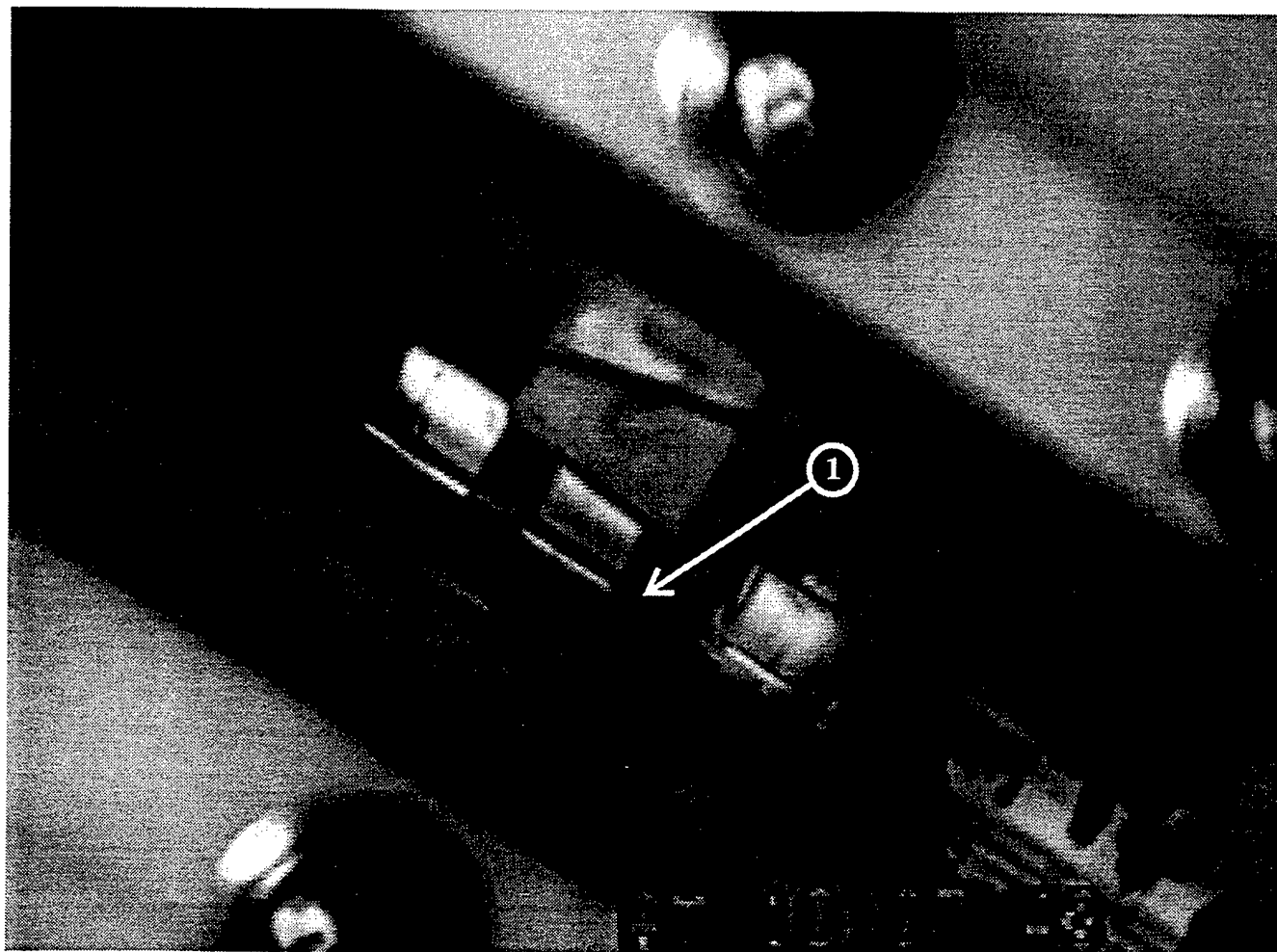
*meniscus position corresponds
to thermocouple location

Fig. 3.5(contd) c) Θ = 0.2535,

101
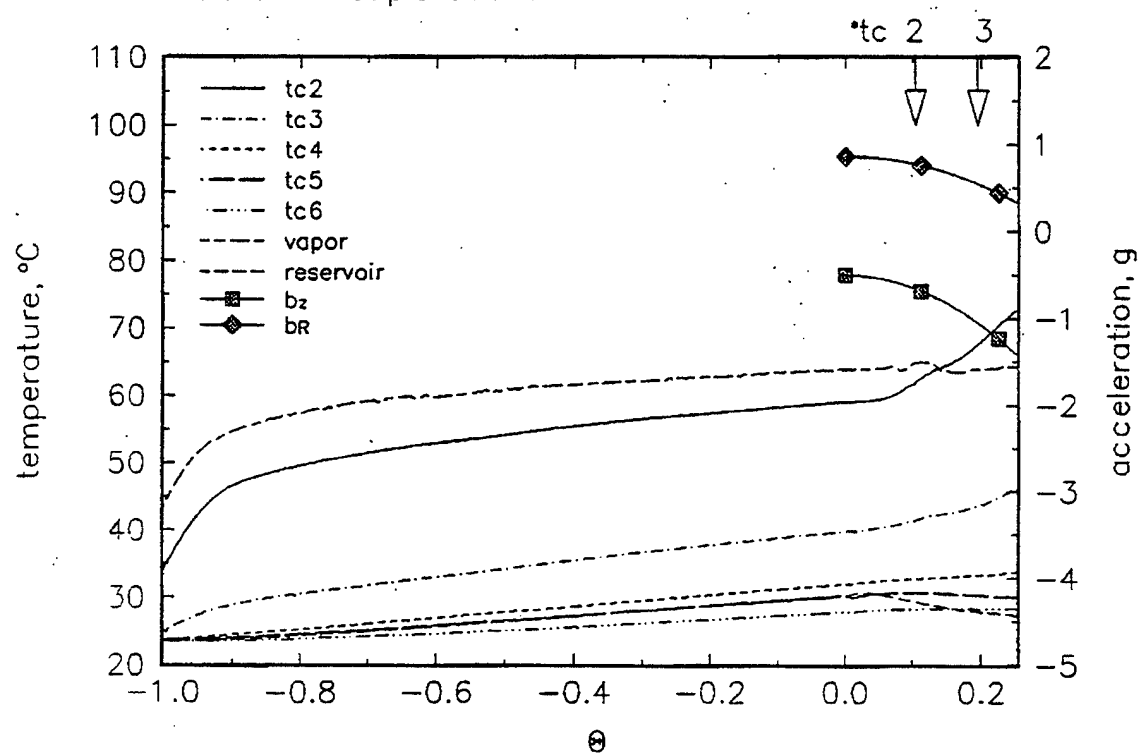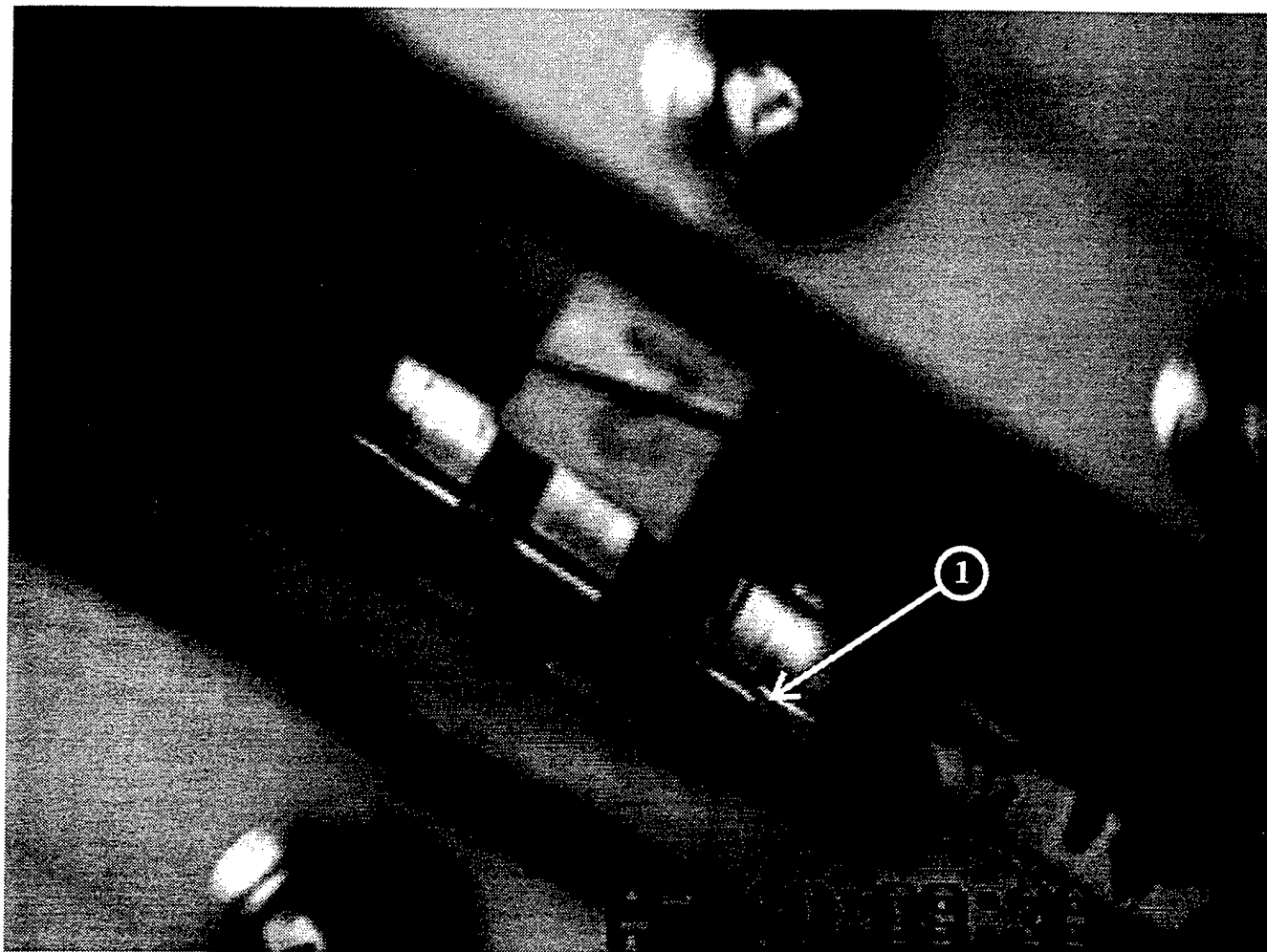
*meniscus position corresponds
to thermocouple location
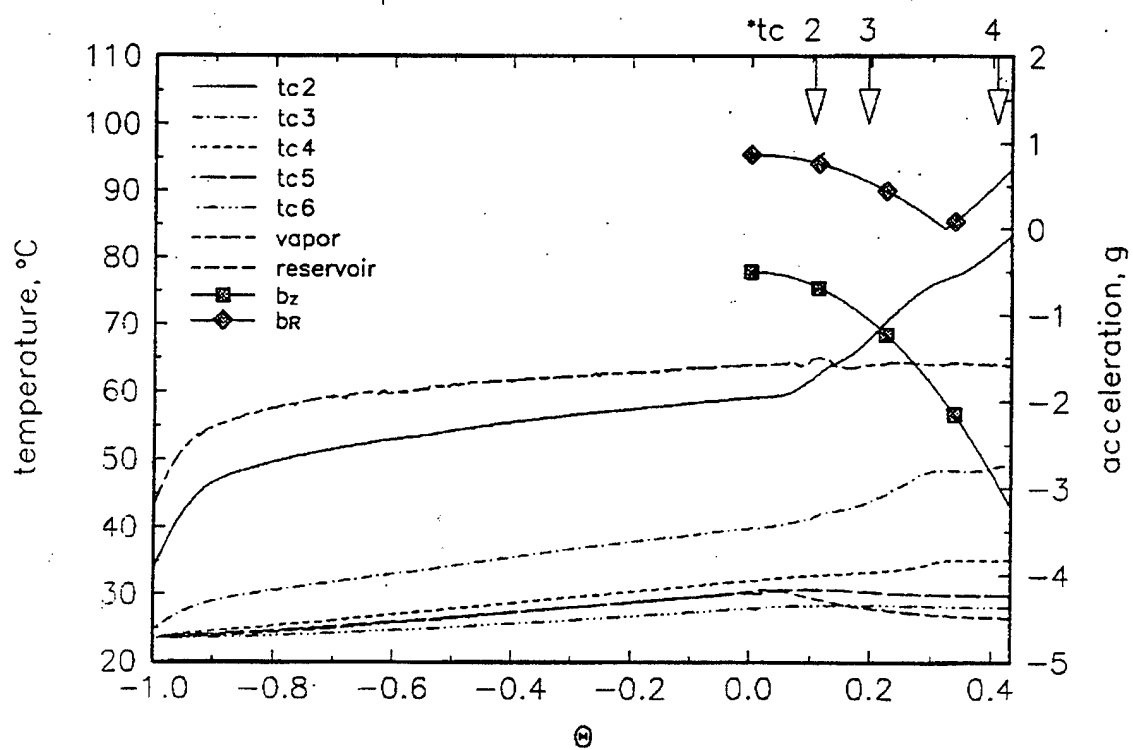
Fig. 3.5(contd) d) $\Theta = 0.4320$,
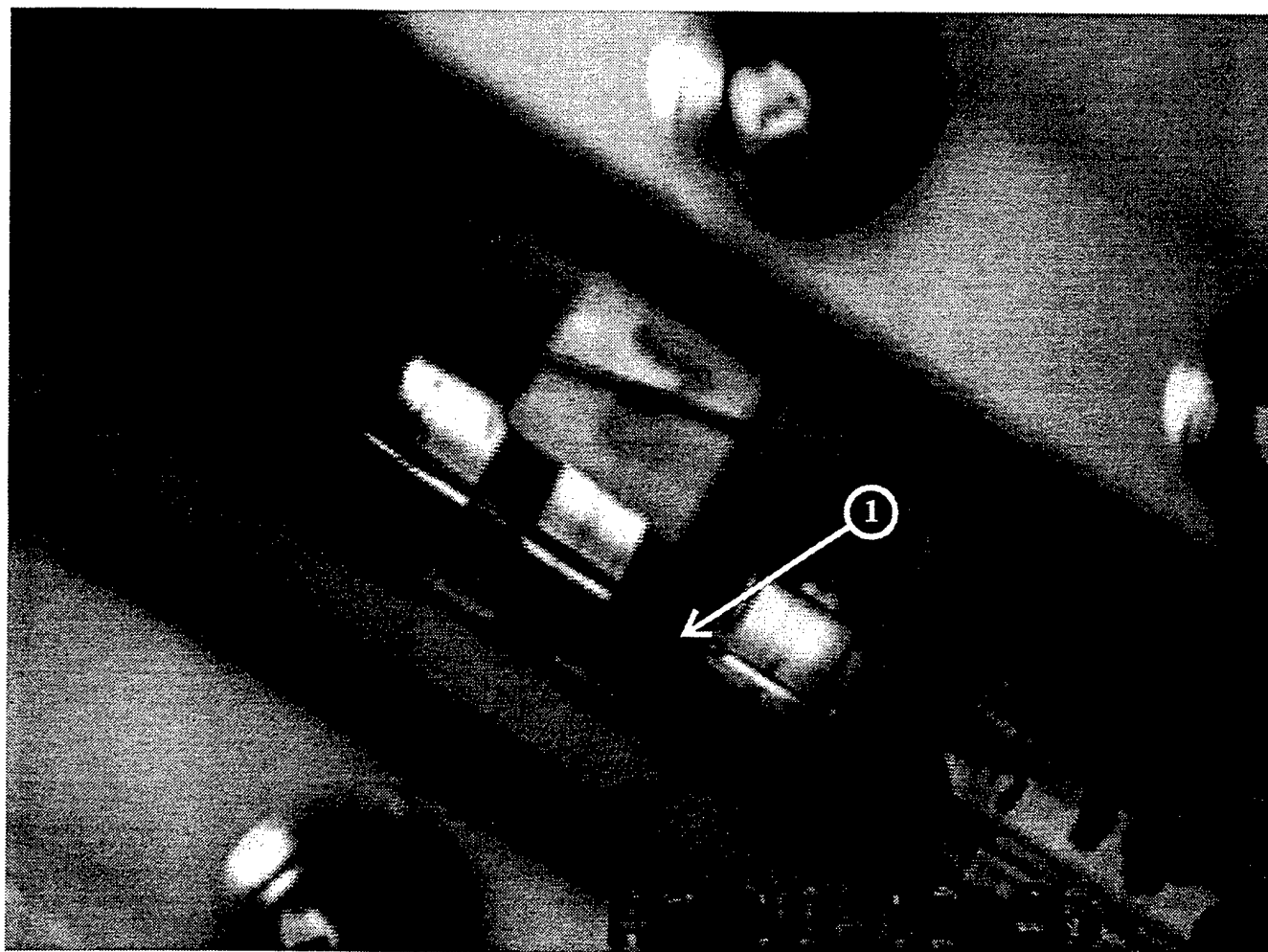
*meniscus position corresponds
to thermocouple location

Fig. 3.5(contd) e) Θ = 0.7065,

103
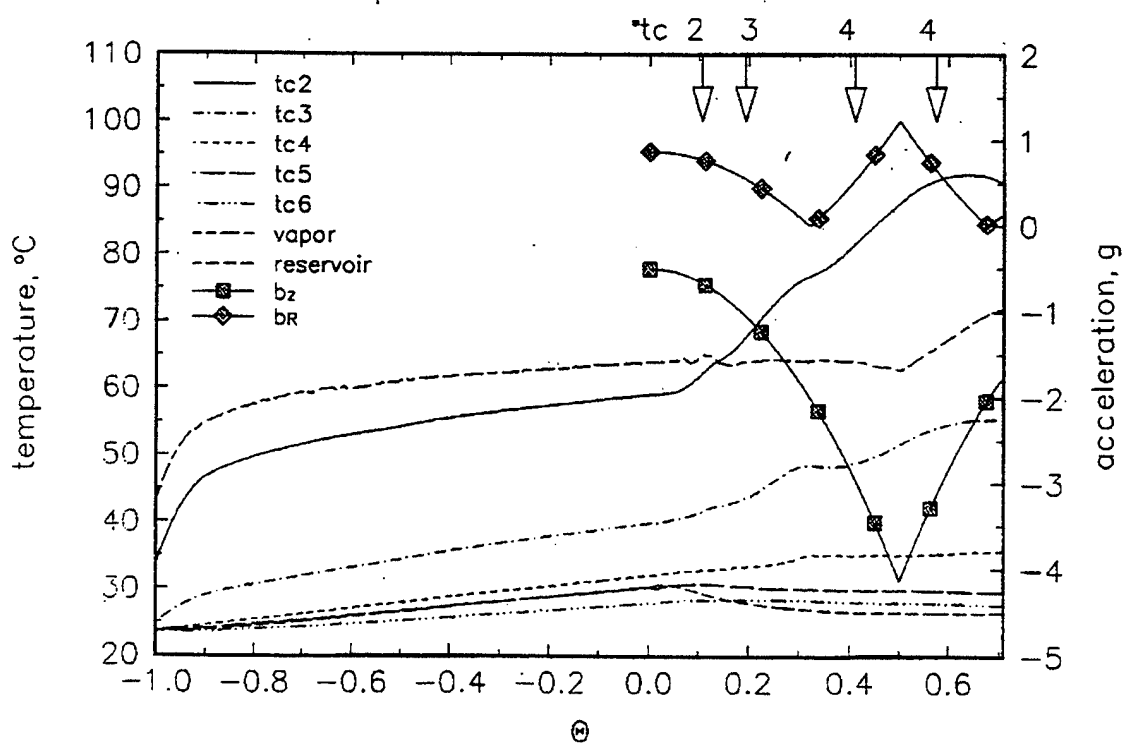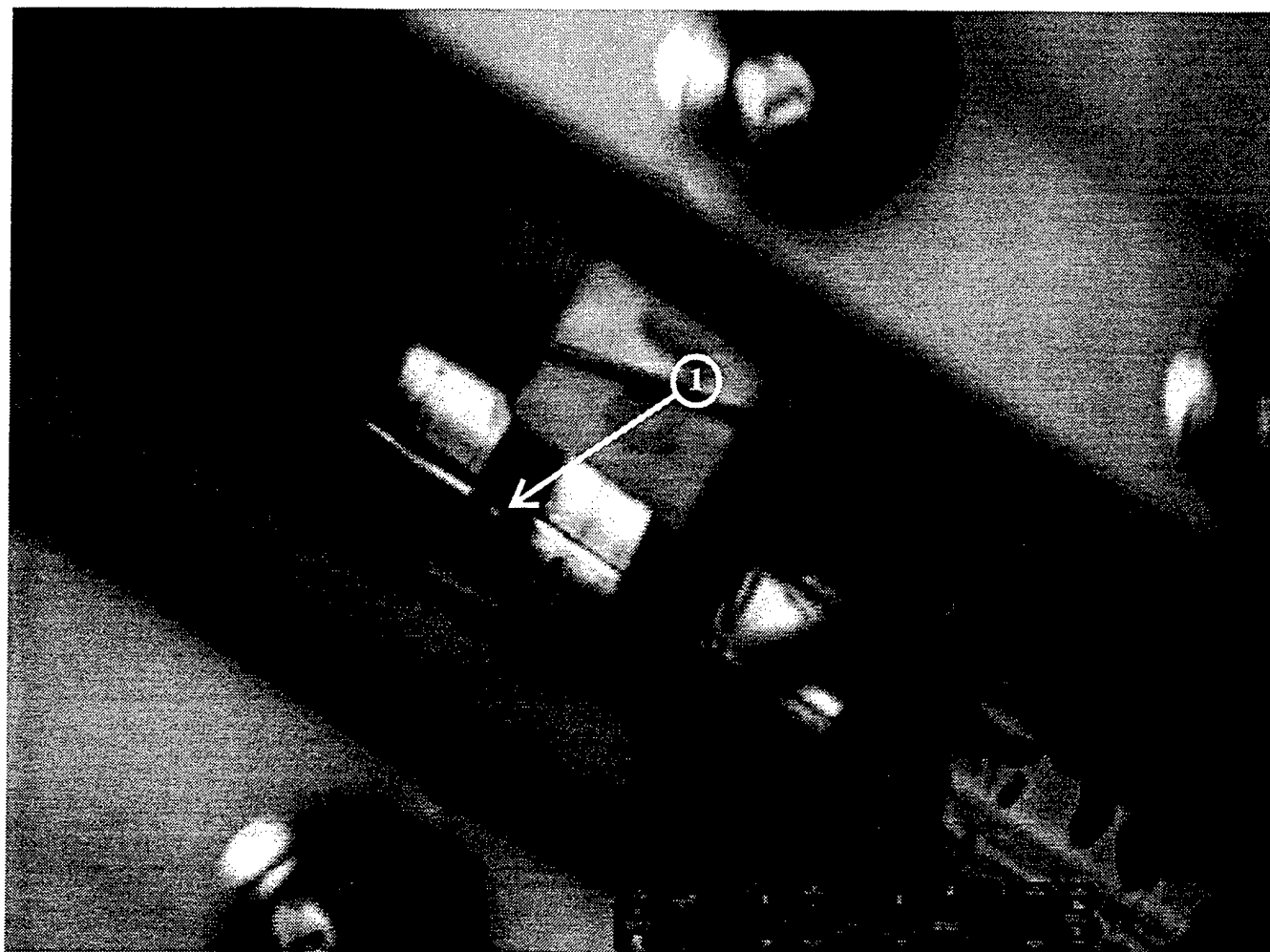
*meniscus position corresponds
to thermocouple location

Fig. 3.5(contd) f) Θ = 0.8280,

104
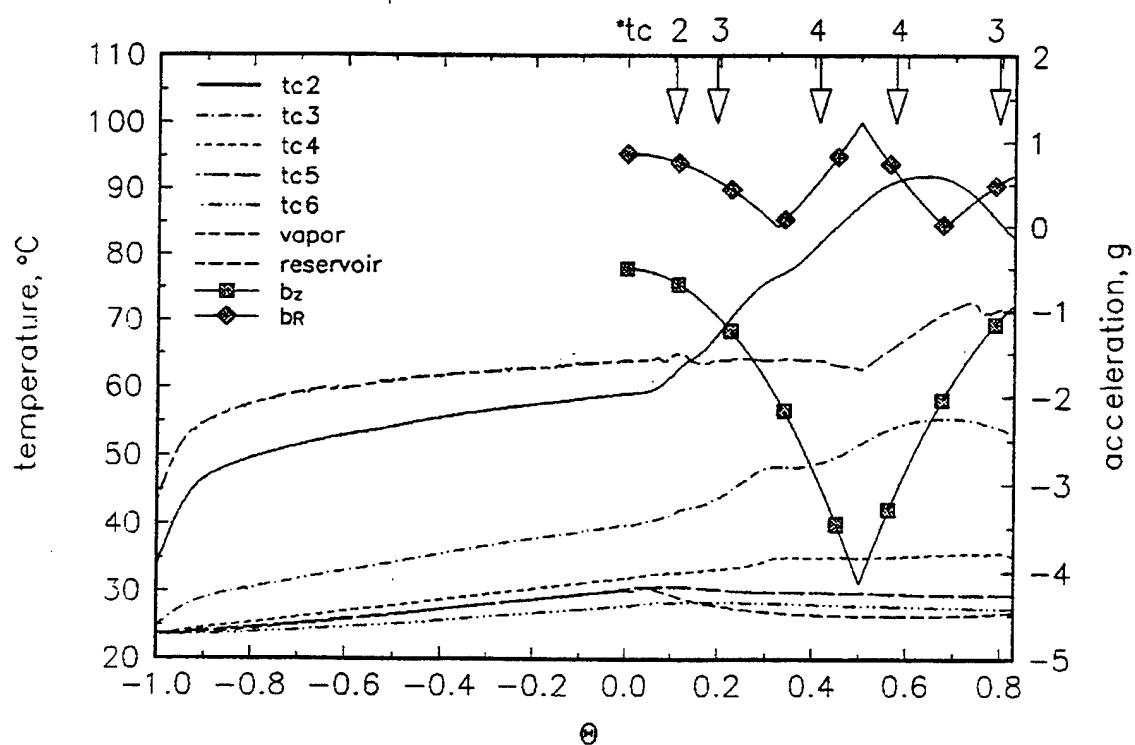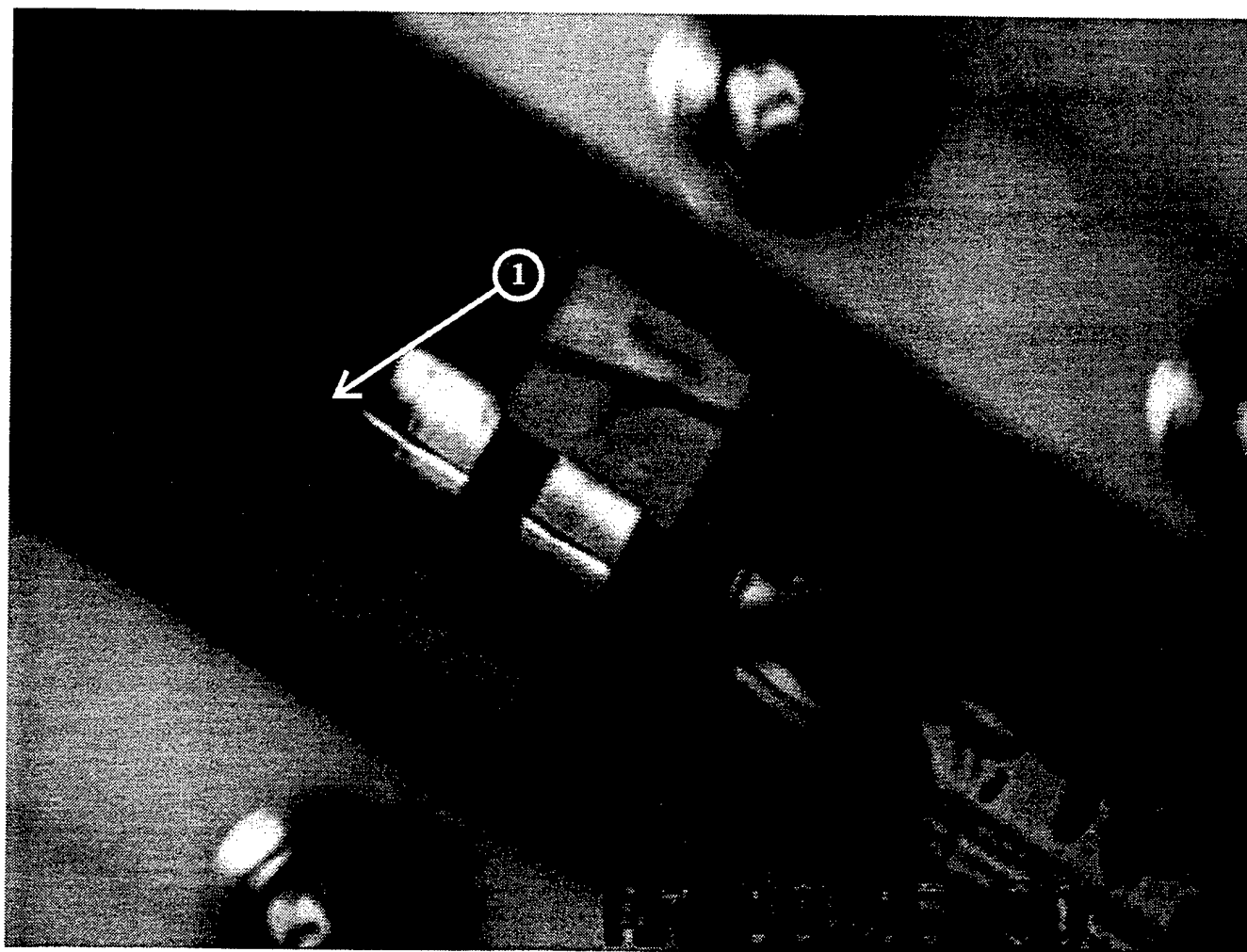
*meniscus position corresponds
to thermocouple location
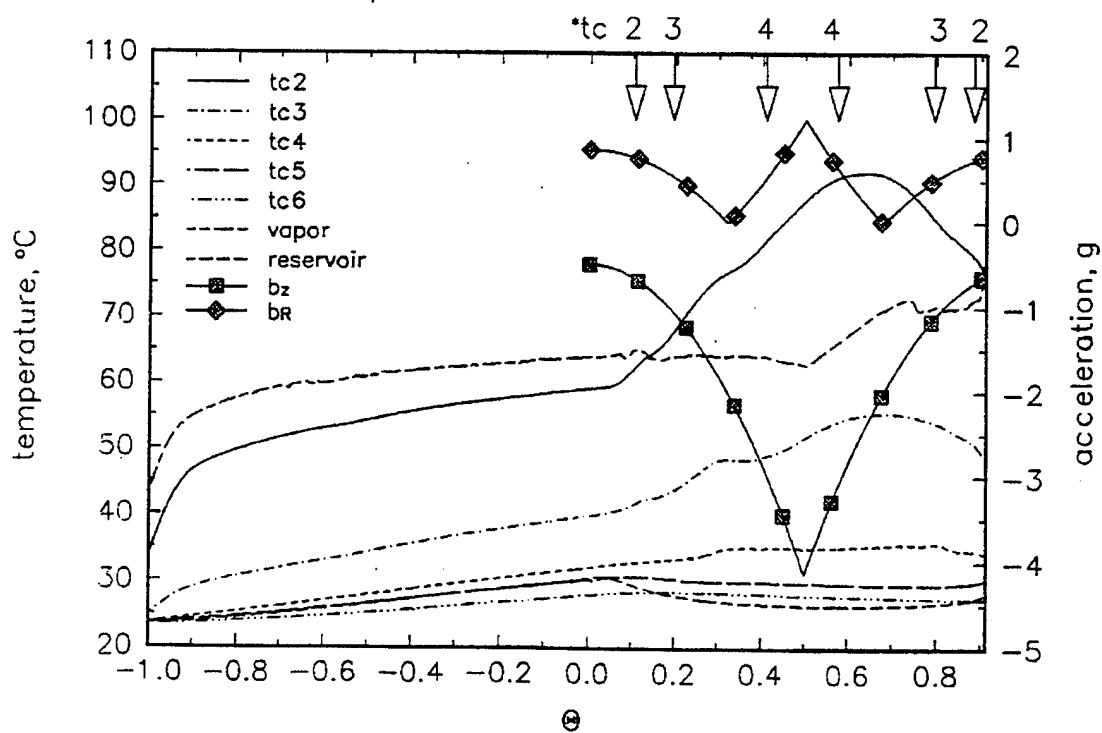
Fig. 3.5(contd) g) Θ = 0.9090,

105
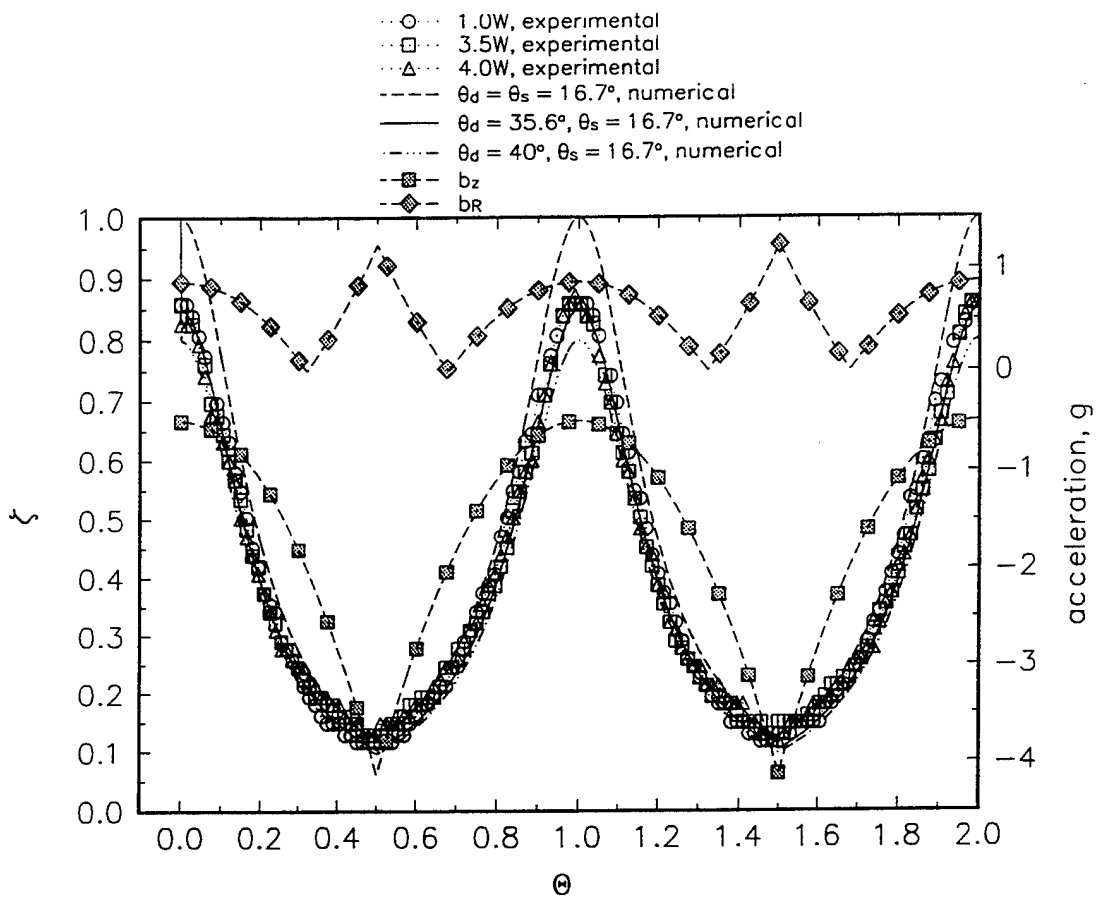
Fig. 3.6 Experimental data compared to analytical results.

CHAPTER IV

SUMMARY AND CONCLUSIONS

In summary, the dynamic response of an unheated and heated meniscus within a capillary tube subjected to single and multiple cycle transient acceleration induced forces was studied experimentally and analytically. A capillary tube, contained within a test cell, was partially filled with either water or ethyl alcohol and mounted on a centrifuge for visual observation of the dynamic response of the meniscus subjected to the transient acceleration field. Experimental parameters were specified such that the capillary and Bond numbers were of sufficient magnitude to account for viscous, inertial, and combined axial and transverse acceleration effects on the unheated and heated meniscus. A one-dimensional mathematical model, assuming a spherically shaped meniscus, was formulated to predict the dynamic response of the meniscus to an acceleration transient and compared with experimental results. For the case in which the meniscus was heated, thermocapillary effects were modeled by accounting a change in contact angle due to heating and incorporated in the one-dimensional equation of motion.

Comparison of the experimental results and analytical calculations for the case of an unheated meniscus showed that a combined axial and elevated transverse acceleration significantly altered the dynamic response of the meniscus and resulting in an increased meniscus velocity and subsequently lower meniscus position. Systems characterized by

large Bond numbers, greater than 1.5, as distinguished by the larger capillary tube diameters were particularly sensitive to an elevated transverse acceleration component greater than 2g. It is speculated that this dynamic response in meniscus position is due to a reduced overall contact line force in the near contact line region resulting from the meniscus being moved in a transverse direction and distended in the axial direction. Systems typified by a low Bond number, less than 1.5, tended to be insensitive to a transverse acceleration component due to the small capillary tube diameter.

For systems typified by the combination of a low Bond number, less than 1.5, and high capillary number, greater than 10^{-5}, there was a significant change in the dynamic response of the meniscus. There was a significant amount of retardation in the meniscus position, when compared to an inviscid solution, due to a combination of viscous forces, acceleration induced inertial forces, and interfacial forces. It may be noted that variations in either the receding contact angle or the advancing contact angle are indicative of changes in any or all of these forces described.

Hysteresis and "sticking" of the advancing meniscus exhibited with water may be attributed to such phenomena as: (i) surface roughness; (ii) contamination; or (iii) draining or evaporating of the thin film left from the receding contact line resulting in the meniscus advancing onto a dry surface.

When the meniscus was heated, without an induced acceleration, there was an initial recession of the meniscus that was accounted through thermocapillary stresses bringing about a change in the contact angle. Experimental results and analytical calculations for a Bond number of 1.47 and a capillary number of 3.00×10^{-6} agreed

well when accounting for the change in contact angle, due to thermocapillary effects, in the dynamic contact angle term in the equation of motion.

Experiments and analytical calculations were not performed for cases in which viscous, inertial, and combined axial and transverse acceleration effects all contribute to the dynamic response of the heated meniscus. The combined effects of heating, viscous, inertial, and combined axial and transverse accelerations may result in a meniscus dynamic response differing significantly from observations noted in this investigation. In addition, the extent that the near contact line region affects the transient behavior of the meniscus was not addressed in this investigation except through changes in the dynamic contact angle.

Some suggested areas of future research as a direct result of this investigation include the: (i) meniscus dynamic response to steady state heating with a combination of low Bond number and high capillary number; (ii) meniscus dynamic response to increased heat fluxes and the consideration of additional fluids; (iii) use of microscopy techniques to verify contact angles inferred from experimental data; (iv) meniscus dynamic response to cyclic heat inputs coupled to acceleration transients; and (v) meniscus dynamic response to variations in the transient form of acceleration.

The practical significance of these results, as related to heat transfer devices utilizing contact lines and capillarity to enhance heat and mass transfer, will be to provide information helpful in defining transient performance parameters and operational limits. It has long been assumed that the operating performance of such devices subjected to transverse acceleration components would not be altered significantly. However, as

demonstrated in this study, the combined axial and transverse acceleration components may result in an increased depriming rate leading to a dry out condition sooner than typically predicted by conventional approaches. Also with the addition of heat, the deprime and reprime dynamics may be significantly altered due to thermocapillary effects and result in either a degraded or possibly improved performance such as with the arterial heat pipe discussed by Yerkes et al.[32].

APPENDIX A

MATHEMATICAL DERIVATIONS

Acceleration Field

The acceleration field was derived using the geometry shown in Fig. A.1a.

For $0 \le \phi \le \dfrac{\pi}{2}$,

$$
\begin{aligned}
r_o - r_T &= z\cos\phi \\
r_T &= r_o - z\cos\phi \\
r_T &= r_o' + (z_1 - z)\cos\phi
\end{aligned}
\tag{1}
$$

and

$$
y = y_o - (z_1 - z)\sin\phi
\tag{2}
$$

The position vector from the non-inertial reference frame

$$
\overline{r}' = r_T \hat{e}_{r_T} + y\,\hat{e}_y
\tag{3}
$$

now becomes

$$\bar{r}' = \left(r_o' + (z_1 - z)\cos\phi\right)\hat{e}_{r_T} + \left(y_o - (z_1 - z)\sin\phi\right)\hat{e}_y \tag{4}$$

and its derivative

$$\frac{d\bar{r}'}{dt} = \left[\left(-\frac{d\phi}{dt}(z_1 - z)\sin\phi\right) - \frac{dz}{dt}\cos\phi\right]\hat{e}_{r_T} + \left[\left(-\frac{d\phi}{dt}(z_1 - z)\cos\phi\right) + \frac{dz}{dt}\sin\phi\right] \tag{5}$$

with the angular velocity vector

$$\bar{\omega} = \omega\,\hat{e}_y. \tag{6}$$

Referencing an inertial reference frame

$$\frac{d^2\bar{r}}{dt^2} = \frac{d^2\bar{r}'}{dt^2} + 2\bar{\omega}\times\frac{d\bar{r}'}{dt} + \frac{d\bar{\omega}}{dt}\times\bar{r}' + \bar{\omega}\times(\bar{\omega}\times\bar{r}') \tag{7}$$

and rearranging for the non-inertial frame as reference, the effective forces experienced by an observer on the centrifuge becomes

$$\overline{F}_{eff} = m\frac{d^2\overline{r}'}{dt^2} = m\frac{d^2\overline{r}}{dt^2} + m\left[-2\overline{\omega}\times\frac{d\overline{r}'}{dt} - \frac{d\overline{\omega}}{dt}\times\overline{r}' - \overline{\omega}\times(\overline{\omega}\times\overline{r}')\right] \tag{8}$$

$$= \overline{F}_{ext} + m\left[-2\overline{\omega}\times\frac{d\overline{r}'}{dt} - \frac{d\overline{\omega}}{dt}\times\overline{r}' - \overline{\omega}\times(\overline{\omega}\times\overline{r})\right]$$

$$= \overline{F}_{ext} + m\left[-2\omega\left(\frac{d\phi}{dt}(z_1-z)\sin\phi + \frac{dz}{dt}\cos\phi\right) + \frac{d\omega}{dt}(r_o' + (z_1-z)\cos\phi)\right]\hat{e}_T$$
$$+ m\left[\omega^2(r_o' + (z_1-z)\cos\phi)\right]\hat{e}_{r_T}. \tag{9}$$

If the capillary tube is at a fixed angle of inclination such that $d\phi/dt = 0$ and assuming the only external force is due to gravity ($\overline{F}_{ext} = m(-g)\hat{e}_y$) the effective force becomes

$$\overline{F}_{eff} = m\left[\omega^2(r_o' + (z_1-z)\cos\phi)\right]\hat{e}_{r_T}$$
$$+ m(-g)\hat{e}_y + m\left[\frac{d\omega}{dt}(r_o' + (z_1-z)\cos\phi) - 2\omega\frac{dz}{dt}\cos\phi\right]\hat{e}_T \tag{10}$$
$$= m\overline{b}$$

Now the acceleration vector is cast into a form referenced to a non-inertial reference frame affixed to the centrifuge where

$$\overline{b} = b_{r_T}\hat{e}_{r_T} + b_y\hat{e}_y + b_T\hat{e}_T. \tag{11}$$

Rotating the non-inertial reference frame $(180 - \phi)^\circ$ about $\hat{e}_T$, as shown in Fig. A.1b, the transformed acceleration vector referenced to the capillary tube can be determined where

$$\overline{b}' = \tilde{A}\overline{b} \tag{12}$$

113

with

$$\tilde{A} = \begin{bmatrix} \hat{e}'_{r_T} \cdot \hat{e}_{r_T} & \hat{e}'_{r_T} \cdot \hat{e}_y & \hat{e}'_{r_T} \cdot \hat{e}_T \\ \hat{e}'_y \cdot \hat{e}_{r_T} & \hat{e}'_y \cdot \hat{e}_y & \hat{e}'_y \cdot \hat{e}_T \\ \hat{e}'_T \cdot \hat{e}_{r_T} & \hat{e}'_T \cdot \hat{e}_y & \hat{e}'_T \cdot \hat{e}_T \end{bmatrix} \quad (13)$$

$$\tilde{A} = \begin{bmatrix} \cos(180-\phi) & \cos(90-\phi) & \cos(90) \\ \cos(90+\phi) & \cos(180-\phi) & \cos(90) \\ \cos(90) & \cos(90) & \cos(0) \end{bmatrix} \quad (14)$$

$$\tilde{A} = \begin{bmatrix} -\cos\phi & \sin\phi & 0 \\ -\sin\phi & -\cos\phi & 0 \\ 0 & 0 & 1 \end{bmatrix} \quad (15)$$

now

$$\bar{b}' = \begin{bmatrix} -\cos\phi & \sin\phi & 0 \\ -\sin\phi & -\cos\phi & 0 \\ 0 & 0 & 1 \end{bmatrix} \begin{bmatrix} b_{r_T} \\ b_y \\ b_T \end{bmatrix} \quad (16)$$

where

$$\overline{b}' = \left(b_{r_T}(-\cos\phi) + b_y \sin\phi\right) \hat{e}'_{r_T}$$
$$+ \left(b_{r_T}(-\sin\phi) + b_y(-\cos\phi)\right) \hat{e}'_y \qquad (17)$$
$$+ \left(b_T\right) \hat{e}'_T$$

Assuming a fixed axial location, $dz/dt = 0$, and eliminating the prime notation letting $\hat{e}'_{r_T} = \hat{e}_z$

and combining the $\hat{e}'_y$ and $\hat{e}'_T$ components to form a magnitude of the transverse

component $\hat{e}_R$

$$\overline{b} = \left[-\omega^2 (r'_o + (z_1 - z)\cos\phi)\cos\phi + (-g)\sin\phi\right] \hat{e}_z +$$
$$\left[\left[-\omega^2 (r'_o + (z_1 - z)\cos\phi)\sin\phi - (-g)\cos\phi\right]^2 + \left[(r'_o + (z_1 - z)\cos\phi)\frac{d\omega}{dt}\right]^2\right]^{1/2}$$
$$(18)$$

(Note, the assumption of a fixed axial location, $dz/dt = 0$, implies negligible effects
due to the Coriolis acceleration which is embodied in the transverse acceleration
component. The Coriolis acceleration is induced from the motion of the fluid column or
meniscus. Therefore prior knowledge of the meniscus dynamics, specifically the velocity,
is required to evaluate the Coriolis acceleration. The one-dimensional equation of motion
for the meniscus formulated for this investigation assumes that the transverse acceleration
component has a negligible effect on the dynamic behavior of the meniscus and therefore
does not account for tangential and Coriolis acceleration effects.)

If the angular velocity is assumed to be linear as a function of time where the

115

transient angular velocity is of the form

$$\omega(t) = Bt, \qquad 0 \le t \le \frac{tf}{2}$$
$$= B(tf - t), \qquad \frac{tf}{2} \le t \le tf \qquad \textbf{(19)}$$

where

$$B = \left(\frac{4\, g_{pk}}{(tf)^2\, r_o'} \right)^{\frac{1}{2}}. \qquad \textbf{(20)}$$

The coefficient B can be determined as a function of the desired peak radial acceleration at $t = tf/2$, cycle time, and radial position at the pivot point. Using the angular velocity at $t = \frac{tf}{2}$, g_{pk} can be found in terms of the coefficient B where

$$\omega = B\frac{tf}{2}$$
$$g_{pk} = \omega^2 r_o'$$
$$= B^2 \left(\frac{tf}{2} \right)^2 r_o' \qquad \textbf{(21)}$$

Solving for B results in

$$B = \left(\frac{4\, g_{pk}}{(tf)^2\, r_o'} \right)^{\frac{1}{2}}. \qquad \textbf{(22)}$$

A typical angular velocity profile with a cycle frequency of $0.0015\, Hz$ is shown

116

in Fig. A.2 with a 4.2-g peak radial acceleration. The resulting acceleration fields referenced to the capillary tube with the inclination angle ranging from 0° to 60° are shown in Fig. A.3.

Equation of Motion

A simple analytical model was derived to predict the motion of the meniscus subjected to transient accelerations. The analytical formulation of the equation of motion was simplified assuming bulk flow only in the axial direction of the capillary tube. Effectively the liquid column in the capillary tube is assumed to undergo a slug flow. From the conservation of momentum,

$$\Sigma \overline{F} = \overline{F}_s + \overline{F}_b = \frac{d(m\overline{V})}{dt} , \qquad (23)$$

the surface and body forces in the axial direction combine resulting in the axial force

$$F_z = F_{s_z} + F_{b_z} . \qquad (24)$$

Consider a control volume, depicted in Fig. A.4, bordered by the walls of the capillary tube, meniscus surface, and a level of the surface of the reservoir. The surface force, F_{s_z}, is formulated by accounting for the net pressure force on the meniscus surface and at the level of the reservoir, cumulative effect of solid-liquid intermolecular forces in the near contact line region, and the wall shear stress associated with Poiseuille flow in the liquid column. The contact line force is defined assuming a spherical meniscus and

117

a constant equivalent or apparent contact angle such that

$$F_{s_z} = \sigma (2\pi a) \cos\theta + \tau_w (2\pi a) \eta + (P_o \pi a^2 - P_1 \pi a^2) . \qquad (25)$$

Since the lower control volume surface is at the level of the reservoir surface, the net pressure force is zero, $P_1 = P_o$. The shear stress at the wall is defined using the Darcy friction factor assuming laminar tube flow where

$$\lambda = \frac{64}{Re}$$

$$= \frac{4\tau_w}{\frac{1}{2}\rho V_{ave}^2} ,$$

$$\tau_w = \frac{64}{Re}\left(\frac{\rho V_{ave}^2}{8}\right) \qquad (26)$$

$$= \frac{4\mu V_{ave}}{a}$$

$$= \frac{4\mu}{a}\frac{d\eta}{dt} .$$

This results in the following surface force formulation while using a slug flow approximation to describe the flow of liquid in the column, i.e., $V_{ave} = d\eta/dt$.

$$F_{s_z} = \sigma (2\pi a) \cos\theta - 8\pi\mu\eta\frac{d\eta}{dt} \qquad (27)$$

118

The total body force,

$$F_{b_z} = \int_0^\eta \int_0^a b_z \rho \, (2\pi) \, r dr dz$$
$$= \int_0^\eta b_z \rho \, (\pi a^2) \, dz, \qquad\qquad (28)$$

is formulated by integrating over the volume of the liquid column the axial acceleration component, b_z, from eq. (18) as defined by

$$b_z = -\omega(t)^2 \cos\phi \left(r_o' + (z_1 - z) \cos\phi\right) - g \sin\phi. \qquad (29)$$

The transient angular velocity is of the form

$$\omega(t) = Bt, \qquad\qquad 0 \le t \le \frac{tf}{2}$$
$$= B(tf - t), \qquad \frac{tf}{2} \le t \le tf \qquad (30)$$

where

$$B = \left(\frac{4 \, g_{pk}}{(tf)^2 \, r_o'}\right)^{\frac{1}{2}}. \qquad\qquad (31)$$

Assuming that the axial fluid velocity is also defined by $v_z = d\eta/dt$ (due to the slug flow assumption) and the mass in the capillary tube as $m = \rho \, (\pi a^2) \, \eta$, the relation for the time rate of change in momentum is defined as

119

$$\frac{d(mv_z)}{dt} = \rho (\pi a^2) \left[\eta \frac{d^2\eta}{dt^2} + \left(\frac{d\eta}{dt}\right)^2 \right]. \tag{32}$$

Combining eqs. (27), (28), and (32), the momentum equation becomes

$$\left[\frac{2\sigma\cos\theta}{\rho a} \right] - \left[\frac{8\mu}{\rho a^2}\eta \frac{d\eta}{dt} \right] + \left[\int_0^\eta b_z dz \right] = \left[\eta \frac{d^2\eta}{dt^2} + \left(\frac{d\eta}{dt}\right)^2 \right]. \tag{33}$$

Integrating the axial acceleration term, b_z,

$$\int_0^\eta b_z dz = \int_0^\eta \left[-\omega(t)^2 \cos\phi(r_o' + (z_1 - z)\cos\phi) - g\sin\phi \right] dz$$
$$= \eta \left[\omega(t)^2 \cos\phi \left((\frac{\eta}{2} - z_1)\cos\phi - r_o' \right) - g\sin\phi \right] \tag{34}$$

rearranging, the momentum equation becomes

$$\frac{2\sigma\cos\theta}{\rho a} = \left[\eta \frac{d^2\eta}{dt^2} + \left(\frac{d\eta}{dt}\right)^2 \right] + \left[\frac{8\mu}{\rho a^2}\eta \frac{d\eta}{dt} \right]$$
$$+ \eta \left[\omega(t)^2 \cos\phi \left((z_1 - \frac{\eta}{2})\cos\phi + r_o' \right) + g\sin\phi \right]. \tag{35}$$

with initial conditions

$$\eta = h_o, \quad \frac{d\eta}{dt} = 0, \quad t = 0 \tag{36}$$

A non-dimensional form of the momentum equation can now be derived using the following dimensionless parameters

120

$$\zeta = \frac{\eta}{h_o}, \quad 0 \le \zeta \le 1$$

$$\Theta = \frac{t}{tf}, \quad 0 \le \Theta \le 1. \tag{37}$$

The static wicking height, h_o, is defined using the static contact angle, θ_s, where

$$h_o = \frac{2\sigma\cos\theta_s}{\rho a g \sin\phi}. \tag{38}$$

A new angular velocity, Ω, is formed by factoring g_{pk} out of the coefficient B (defined by eq. (31)) in eq. (30) and casting it in terms of the non-dimensional time, Θ, where

$$\Omega(\Theta) = \left(\frac{4}{r'_o}\right)^{\frac{1}{2}} \Theta, \quad 0 \le \Theta \le \frac{1}{2}$$

$$= \left(\frac{4}{r'_o}\right)^{\frac{1}{2}} (1-\Theta), \quad \frac{1}{2} \le \Theta \le 1. \tag{39}$$

The non-dimensional form of the momentum equation in terms of a transient dimensionless meniscus position becomes

$$\frac{2\sigma\cos\theta}{\rho a} = \left[\zeta\frac{h_o^2}{tf^2}\frac{d^2\zeta}{d\Theta^2} + \frac{h_o^2}{tf^2}\left(\frac{d\zeta}{d\Theta}\right)^2\right] + \left[\zeta\frac{8\mu h_o^2}{\rho a^2 tf}\frac{d\zeta}{d\Theta}\right]$$

$$+ \zeta h_o\left[\Omega(\Theta)^2 g_{pk}\cos\phi\left(\left(z_1 - \frac{h_o\zeta}{2}\right)\cos\phi + r'_o\right) + g\sin\phi\right]. \tag{40}$$

dividing through by $h_o g_{pk}$

121

$$\frac{2\sigma\cos\theta}{\rho a h_o g_{pk}} = \frac{h_o}{t f^2 g_{pk}}\left[\zeta\frac{d^2\zeta}{d\Theta^2} + \left(\frac{d\zeta}{d\Theta}\right)^2\right] + \frac{8\mu h_o}{\rho a^2 t f g_{pk}}\left[\zeta\frac{d\zeta}{d\Theta}\right]$$

$$+ \zeta\left[\Omega\left(\Theta\right)^2\cos\phi\left(\left(z_1 - \frac{h_o\zeta}{2}\right)\cos\phi + r_o'\right) + \frac{g}{g_{pk}}\sin\phi\right].$$

(41)

The momentum equation can be modified to include a constant receding or advancing contact angle, θ_d, differing from that of the static contact angle, θ_s. It may be noted that the general form of the dynamic contact angle is known to be functionally dependent on the contact line receding and advancing velocity, $\theta_d = \theta_d(d\zeta/d\Theta)$. Substituting the static wicking height, h_o, into the left hand side of eq. (41) and realizing that the contact angle, θ, is equivalent to the dynamic contact angle where , $\theta = \theta_d$, results in

$$\frac{2\sigma\cos\theta}{\rho a h_o g_{pk}} = \frac{2\sigma\cos\theta_d}{\rho a g_{pk}\left(\dfrac{2\sigma\cos\theta_s}{\rho a g\sin\phi}\right)}$$

(42)

$$= \frac{g}{g_{pk}}\frac{\cos\theta_d}{\cos\theta_s}\sin\phi.$$

Defining the following dimensionless numbers

122

$$\left[\frac{acceleration}{surface\ tension}\right],\ Bo = \frac{(2a)^2 g_{pk}\rho}{\sigma},$$

$$\left[\frac{viscous}{surface\ tension}\right],\ Ca = \frac{\mu V_c}{\sigma},\ V_c = \frac{2h_o}{tf}, \tag{43}$$

$$\left[\frac{inertia}{viscous}\right],\ Re = \frac{(2a)\rho V_c}{\mu},$$

the non-dimensional form of the momentum equation becomes

$$\frac{g}{g_{pk}}\frac{\cos\theta_d}{\cos\theta_s}\sin\phi = \left[\frac{a}{h_o}\right]\left[\frac{Re\,Ca}{2Bo}\right]\left[\zeta\frac{d^2\zeta}{d\Theta^2} + \left(\frac{d\zeta}{d\Theta}\right)^2\right] + \left[\frac{16\,Ca}{Bo}\right]\left[\zeta\frac{d\zeta}{d\Theta}\right]$$
$$+ \zeta\left[\Omega(\Theta)^2\cos\phi\left(\left(z_1 - \frac{h_o\zeta}{2}\right)\cos\phi + r_o'\right) + \frac{g}{g_{pk}}\sin\phi\right]. \tag{44}$$

with initial conditions

$$\zeta = 1,\ \frac{d\zeta}{d\Theta} = 0,\ \Theta = 0 \tag{45}$$

The first and second terms of eq. (44) represent the inertial and viscous effects, respectively, with the coefficients formed as the products of the dimensionless parameters of aspect ratio, Reynolds, capillary, and Bond numbers. The Reynolds and capillary numbers are referenced to a characteristic velocity, V_c, which is the maximum attainable velocity over one-half of the acceleration cycle period assuming $\eta = 0$ at g_{pk}. The Bond number is referenced to the peak radial acceleration component, g_{pk}.

For small inertial and viscous effects, the momentum equation can be reduced to

123

the following quadratic form for the transient dimensionless meniscus position.

$$\zeta^2 - \left(\frac{\Omega(\Theta)^2\cos\phi\,(z_1\cos\phi + r_o') + \dfrac{g}{g_{pk}}\sin\phi}{\Omega(\Theta)^2\,\dfrac{h_o}{2}\cos^2\phi}\right)\zeta + \left(\frac{\dfrac{g}{g_{pk}}\dfrac{\cos\theta_d}{\cos\theta_s}\sin\phi}{\Omega(\Theta)^2\,\dfrac{h_o}{2}\cos^2\phi}\right) = ($$

(46)

Discretization was done using a central difference scheme in time only where

$$\frac{d\zeta}{d\Theta} = \frac{\zeta_{i+2} - \zeta_i}{2\Delta\Theta} + O(\Delta\Theta)^2$$

(47)

$$\frac{d^2\zeta}{d\Theta^2} = \frac{\zeta_{i+2} - 2\zeta_{i+1} + \zeta_i}{\Delta\Theta^2} + O(\Delta\Theta)^2$$

(48)

and substituting into the non-dimensional equation of motion, eq. (43), results in

$$\frac{g}{g_{pk}}\frac{\cos\theta_d}{\cos\theta_s}\sin\phi = \left[\frac{a}{h_o}\right]\left[\frac{ReCa}{2Bo}\right]\left[\zeta_{i+1}\left(\frac{\zeta_{i+2} - 2\zeta_{i+1} + \zeta_i}{\Delta\Theta^2}\right) + \left(\frac{\zeta_{i+2} - \zeta_i}{2\Delta\Theta}\right)^2\right]$$
$$+ \left[\frac{16Ca}{Bo}\right]\left[\zeta_{i+1}\left(\frac{\zeta_{i+2} - \zeta_i}{2\Delta\Theta}\right)\right]$$
$$+ \zeta_{i+1}\left[\Omega(\Theta)^2\cos\phi\left(\left(z_1 - \frac{h_o\zeta_{i+1}}{2}\right)\cos\phi - r_o'\right) + \frac{g}{g_{pk}}\sin\phi\right]$$

(49)

Combining like terms and expanding results in

124

$$\left[\frac{aRe}{8h_o}\right]\zeta_{i+2}^2 + \left[\frac{aRe}{2h_o}\zeta_{i+1} + 8\Delta\Theta\zeta_{i+1} - \frac{aRe}{4h_o}\zeta_i\right]\zeta_{i+2}$$

$$= \frac{\Delta\Theta^2 Bo}{Ca}\frac{g}{g_{pk}}\frac{\cos\theta_d}{\cos\theta_s}\sin\phi$$

$$- \frac{\Delta\Theta^2 Bo}{Ca}\zeta_{i+1}\left[\Omega(\Theta)^2\cos\phi\left(\left(z_1 - \frac{h_o\zeta_{i+1}}{2}\right)\cos\phi + r_o'\right) + \frac{g}{g_{pk}}\sin\phi\right] \qquad (50)$$

$$- \left[\frac{aRe}{2h_o} - 8\Delta\Theta\right]\zeta_i\zeta_{i+1}$$

$$+ \left[\frac{aRe}{h_o}\right]\zeta_{i+1}^2$$

$$- \left[\frac{aRe}{8h_o}\right]\zeta_i^2$$

with initial conditions

$$\zeta = 1, \quad \frac{d\zeta}{d\Theta} = 0, \quad \Theta = 0 \qquad (51)$$

or

$$\zeta_i = \zeta_{i+1} = 1, \quad \Theta = 0 \qquad (52)$$

Now ζ_{i+2} can be determined at each time step, $\Delta\Theta$, by solving in the quadratic using the root consistent for a converging solution over the cycle time, $0 \le \Theta \le 1$.

Solutions to eq. (50) were calculated by varying the Bond and capillary numbers. Numerical error due to time step size is on the order of $(\Delta\Theta)^2$ and was minimized by obtaining solutions at varying time step size and selecting a time step appropriate to have

125

negligible effects on the resulting solution ($\Delta\Theta \leq 0.0001$). These solutions were compared to the inviscid solution and the percent deviation or retardation from the inviscid solution determined. In these solutions the static contact angle of 16.7° was assumed to be equivalent to the dynamic contact angle. It is interesting to note that the requirement that the static contact angle be specified is for the calculation of the aspect ratio and capillary and Reynolds numbers. For fixed Bond and capillary numbers and for a dynamic contact angle equivalent to the static contact angle, solutions are insensitive to the changes in the static contact angle since the cosine of the static contact angle cancels out in the inertial grouping of the aspect ratio and Reynolds number. This is not the case, however, when the dynamic contact angle differs from the static contact angle. By comparing the inertial and viscous terms, the relative magnitude and functional relationship to each other was ascertained. Tables A.1a-A.3a show the conditions for the numerical solutions for a capillary angle of inclination of 25°, 30°, and 50°. Tables A.1b-A.3b show the relevant statistical information for logarithmic linear regressions as the functional relation between the inertial and viscous terms for each angle of inclination. Figures A.5-A.7 graphically present the functional relationships between the inertial and viscous terms as well as showing the magnitude of the viscous term contributing to the dynamic response of the meniscus resulting in a retardation of the meniscus height from the inviscid solution.

Tables A.4-A.7 are the computer programs, written in C, to calculate acceleration fields and dimensionless meniscus position used for this investigation.

126

a)

$\omega(t)$

$\bar{r}$

$\bar{r}'$

ϕ

z_1

z

y_o

$\overrightarrow{r_T}$

r_o'

r_o

b)

$\hat{e}_z$

$\bar{b}$

η

$\hat{e}_R$

ϕ

$\hat{e}_y$

$\hat{e}_{r_T}'$

$\hat{e}_{r_T}$

$\hat{e}_y'$

$\hat{e}_{T'}$

$\hat{e}_T'$
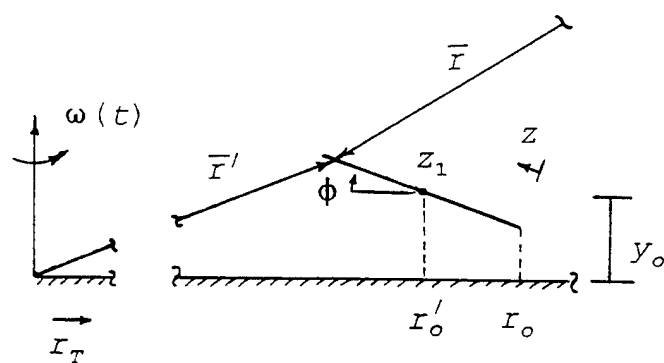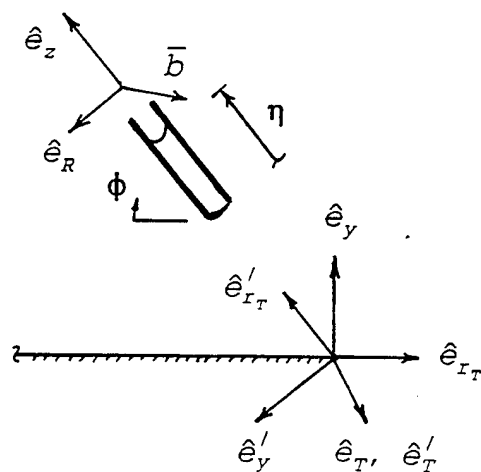
Fig. A.1 Capillary tube orientation: a) pivot point location, directional coordinates and b) coordinate systems as referenced to the centrifuge accelerometer and capillary tube.

Fig. A.2 Plot of the centrifuge angular velocity test cycle (f = 0.0015 Hz).
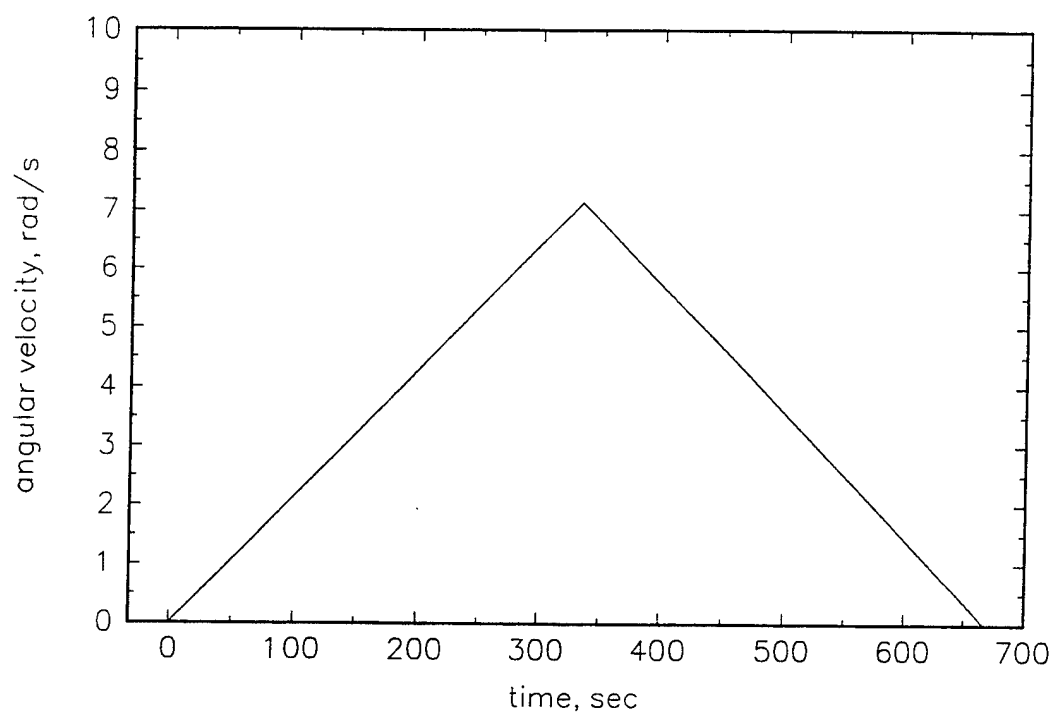
Axial and Transverse Acceleration Components
0° inclination, f = 0.0015 Hz, g_{pk} = 4.2 g
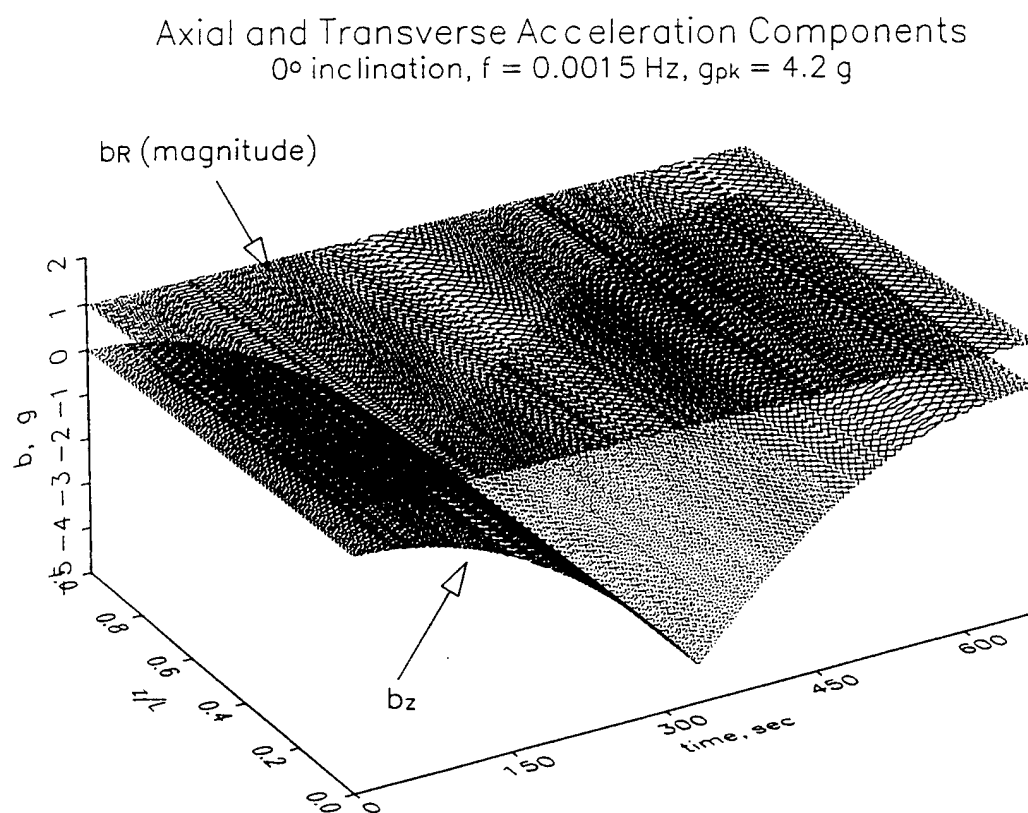
Fig. A.3 Acceleration field referenced to the capillary tube ($f = 0.0015\ Hz$):
a) $\phi = 0°$,

Axial and Transverse Acceleration Components
20° inclination, f = 0.0015 Hz, gpk = 4.2 g

bR (magnitude)

bz

Fig. A.3(contd) b) ϕ = 20°,

130
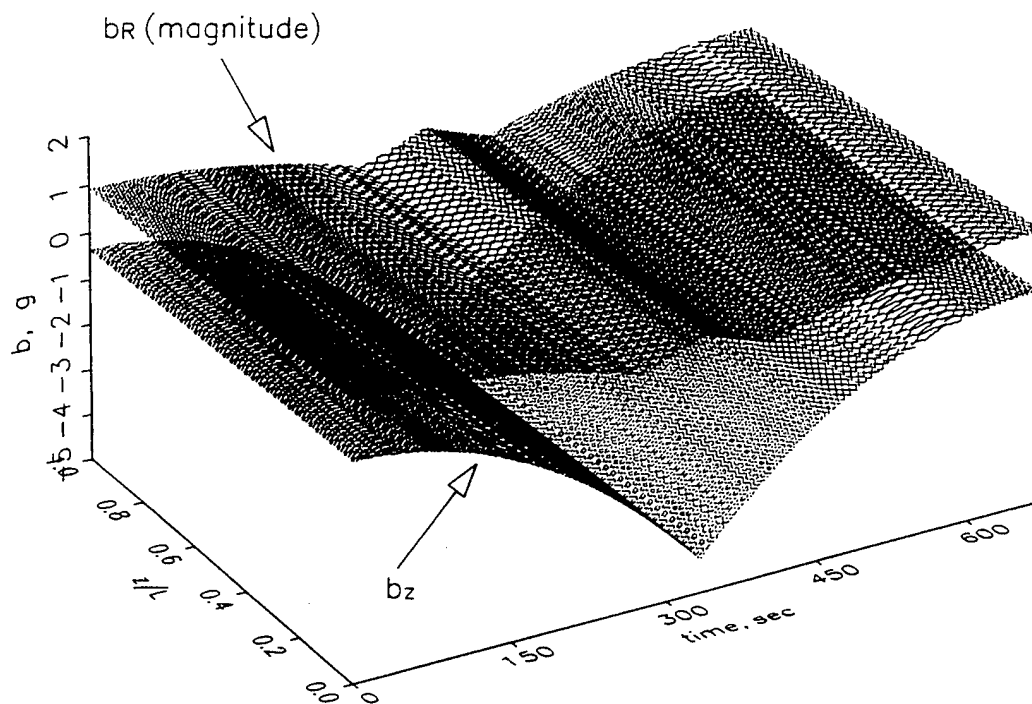
Axial and Transverse Acceleration Components
40° inclination, f = 0.0015 Hz, g_{pk} = 4.2 g

bR (magnitude)

bz
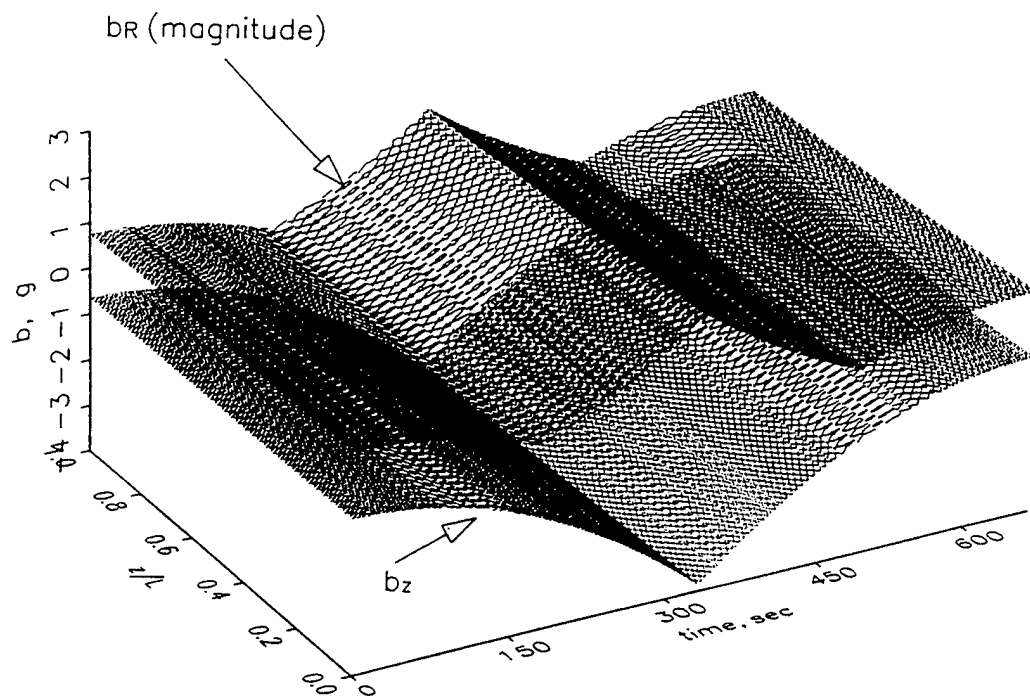
Fig. A.3(contd) c) ϕ = 40°,

Axial and Transverse Acceleration Components
60° inclination, f = 0.0015 Hz, g$_{pk}$ = 4.2 g
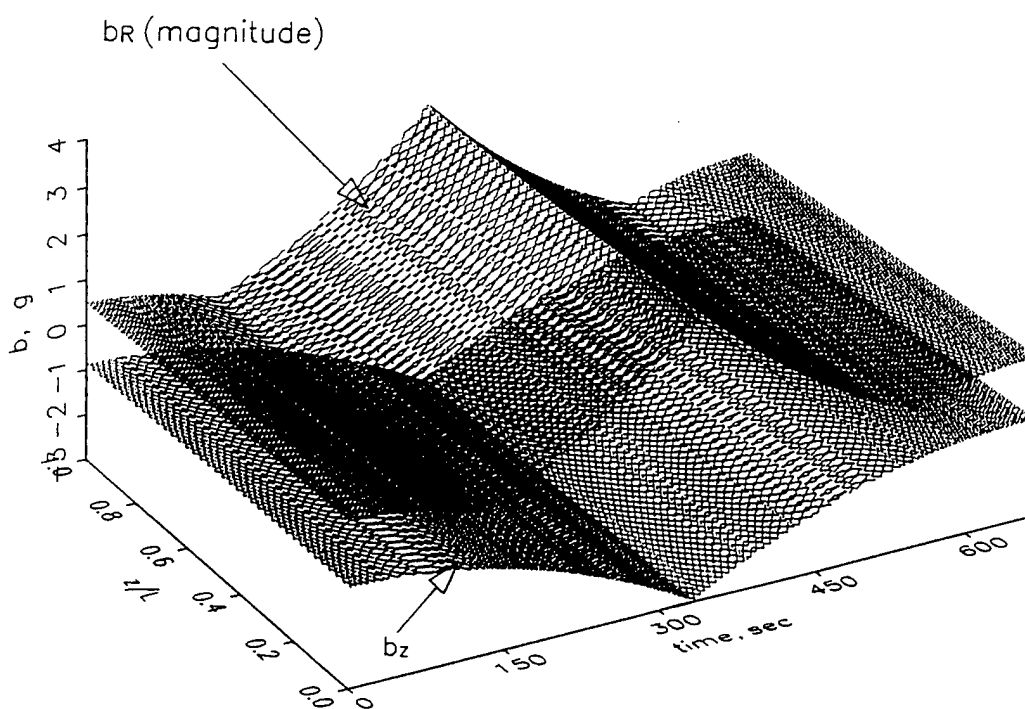
Fig. A.3(contd) d) ϕ = 60°,
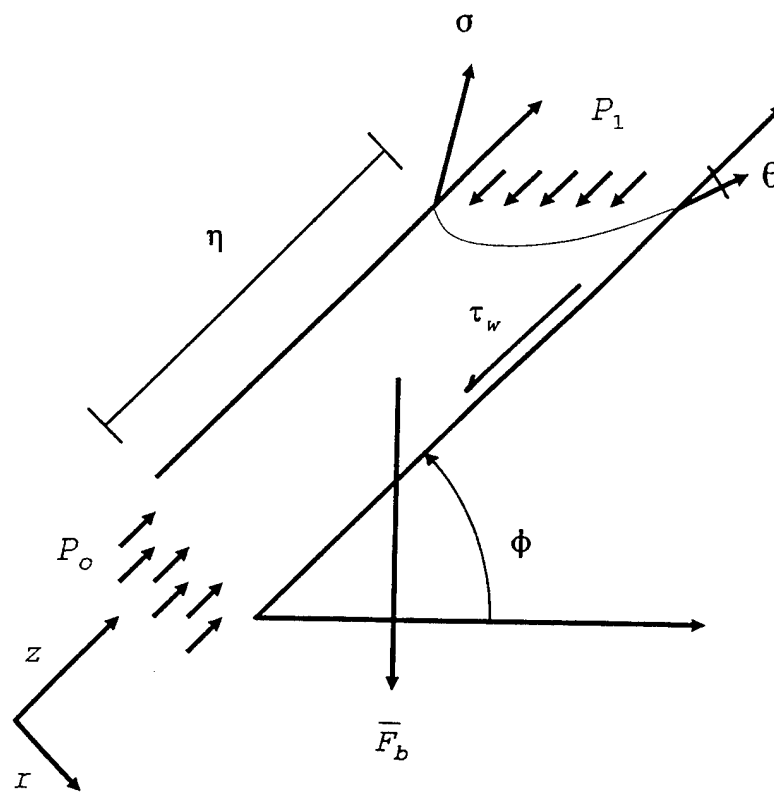
Fig. A.4 Free body diagram of forces acting on the control volume.

Table A.1a
Dimensionless parameters and % deviation
from the inviscid solution ($\phi = 25^\circ$).

Bo	Ca	ϕ	$\dfrac{a}{h_o}\dfrac{Re\,Ca}{Bo}$	$\dfrac{Ca}{Bo}$	% deviation
0.2	1.0e-3	25°	8.281e-5	5.0e-3	45.7
	1.0e-4		8.281e-7	5.0e-4	11.7
	1.0e-5		8.281e-9	5.0e-5	0.41
	1.0e-6		8.281e-11	5.0e-6	0
0.4	1.0e-3		1.171e-4	2.5e-3	34.9
	1.0e-4		1.171e-6	2.5e-4	5.5
	1.0e-5		1.171e-8	2.5e-5	0.11
	1.0e-6		1.171e-10	2.5e-6	0
1.0	1.0e-3		1.852e-4	1.0e-3	20.8
	1.0e-4		1.852e-6	1.0e-4	1.4
	1.0e-5		1.852e-8	1.0e-5	0.02
	1.0e-6		1.852e-10	1.0e-6	0
1.5	1.0e-3		2.268e-4	6.7e-4	15.1
	1.0e-4		2.268e-6	6.7e-5	0.65
	1.0e-5		2.268e-8	6.7e-6	0.01
	1.0e-6		2.268e-10	6.7e-7	0

134

Table A.1b
Statistical information showing the functional relationship
between inertial and viscous terms ($\phi = 25°$).

Bo	ϕ	ind. var.	dep. var.	R-sqd.	slope	intercept
0.2	25°	$\log\left(\dfrac{a}{h_o}\dfrac{Re\,Ca}{Bo}\right)$	$\log\left(\dfrac{Ca}{Bo}\right)$	1.0	0.50	-0.26007
0.4				1.0		-0.63634
1.0				1.0		-1.1338
1.5				1.0		-1.3539
all	25°	intercepts	$\log(Bo)$	1.0	-1.25	-1.1338

135
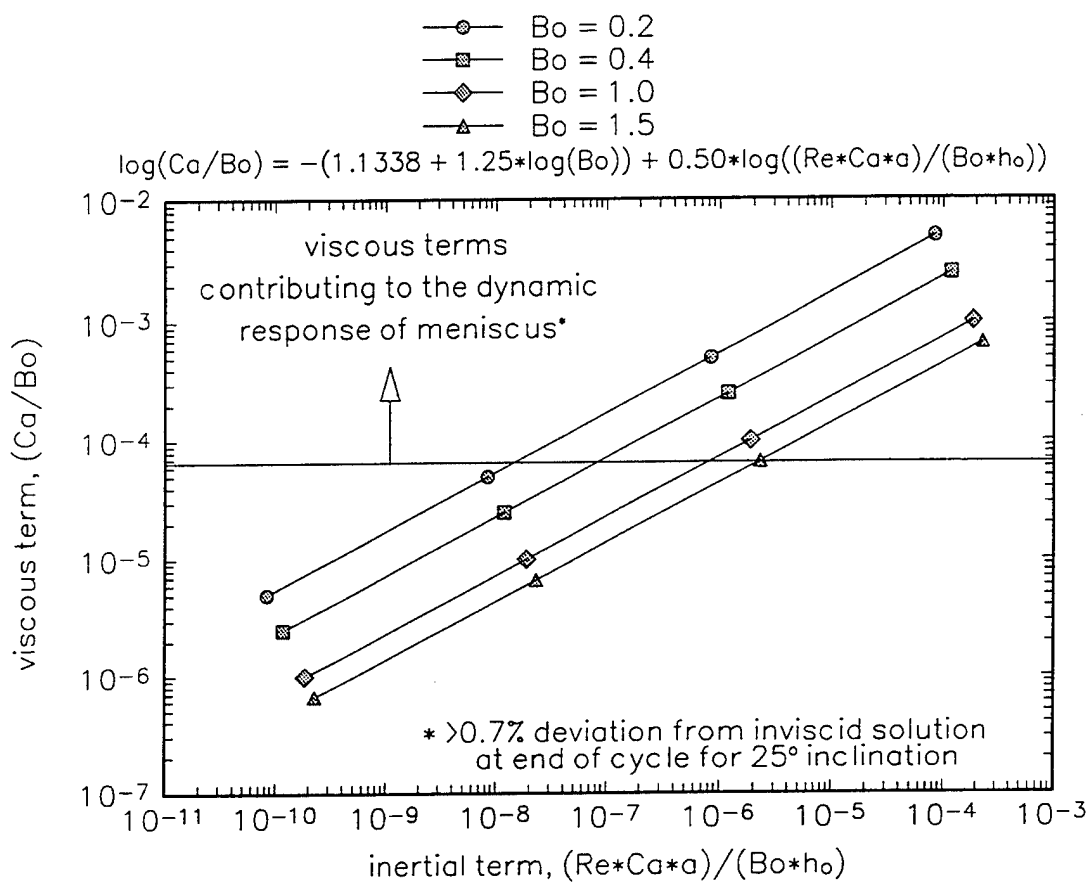
Fig. A.5 Functional relationship between viscous and inertial terms (ϕ = 25°).

Table A.2a

Dimensionless parameters and % deviation
from the inviscid solution ($\phi = 30°$).

Bo	Ca	ϕ	$\dfrac{a}{h_o}\dfrac{Re\,Ca}{Bo}$	$\dfrac{Ca}{Bo}$	% deviation
0.2	1.0e-3	30°	9.797e-5	5.0e-3	41.4
	1.0e-4		9.797e-7	5.0e-4	8.9
	1.0e-5		9.797e-9	5.0e-5	0.24
	1.0e-6		9.797e-11	5.0e-6	0
0.4	1.0e-3		1.386e-4	2.5e-3	30.5
	1.0e-4		1.386e-6	2.5e-4	3.8
	1.0e-5		1.386e-8	2.5e-5	0.06
	1.0e-6		1.386e-10	2.5e-6	0
1.0	1.0e-3		2.191e-4	1.0e-3	16.9
	1.0e-4		2.191e-6	1.0e-4	0.86
	1.0e-5		2.191e-8	1.0e-5	0.01
	1.0e-6		2.191e-10	1.0e-6	0
1.5	1.0e-3		2.683e-4	6.7e-4	11.7
	1.0e-4		2.683e-6	6.7e-5	0.37
	1.0e-5		2.683e-8	6.7e-6	0
	1.0e-6		2.683e-10	6.7e-7	0

Table A.2b
Statistical information showing the functional relationship
between inertial and viscous terms ($\phi = 30°$).

Bo	ϕ	ind. var.	dep. var.	R-sqd.	slope	intercept
0.2	30°	$\log\left(\dfrac{a}{h_o}\dfrac{Re\,Ca}{Bo}\right)$	$\log\left(\dfrac{Ca}{Bo}\right)$	1.0	0.50	-0.29658
0.4				1.0		-0.67294
1.0				1.0		-1.1703
1.5				1.0		-1.3904
all	30°	intercepts	$\log(Bo)$	1.0	-1.25	-1.1703

138
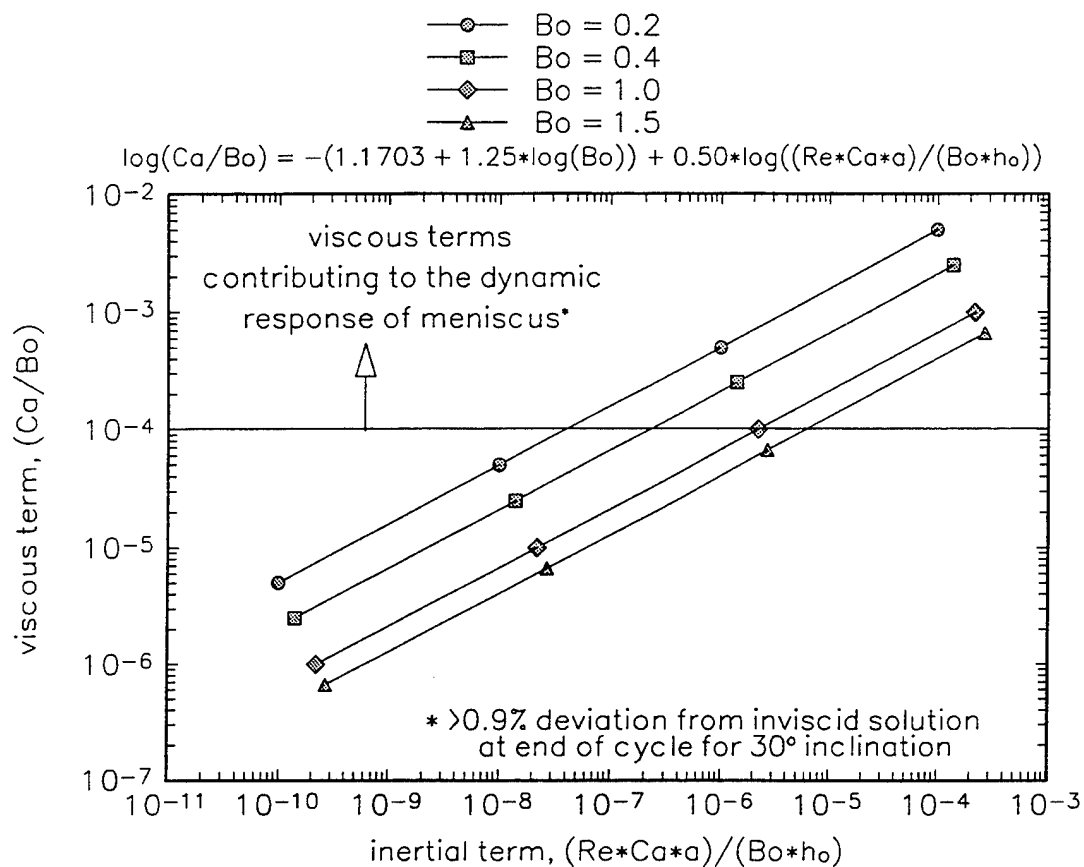
Fig. A.6 Functional relationship between viscous and inertial terms ($\phi = 30\,^{\circ}$).

139

Table A.3a
Dimensionless parameters and % deviation
from the inviscid solution (ϕ = 50 °).

Bo	Ca	ϕ	$\dfrac{a}{h_o}\dfrac{Re\,Ca}{Bo}$	$\dfrac{Ca}{Bo}$	% deviation
0.2	1.0e-3	50°	1.501e-4	5.0e-3	29.0
	1.0e-4		1.501e-6	5.0e-4	3.3
	1.0e-5		1.501e-8	5.0e-5	0.05
	1.0e-6		1.501e-10	5.0e-6	0
0.4	1.0e-3		2.123e-4	2.5e-3	18.7
	1.0e-4		2.123e-6	2.5e-4	1.1
	1.0e-5		2.123e-8	2.5e-5	0.01
	1.0e-6		2.123e-10	2.5e-6	0
1.0	1.0e-3		3.356e-4	1.0e-3	7.8
	1.0e-4		3.356e-6	1.0e-4	0.18
	1.0e-5		3.356e-8	1.0e-5	0
	1.0e-6		3.356e-10	1.0e-6	0
1.5	1.0e-3		4.111e-4	6.7e-4	4.3
	1.0e-4		4.111e-6	6.7e-5	0.06
	1.0e-5		4.111e-8	6.7e-6	0
	1.0e-6		4.111e-10	6.7e-7	0

140

Table A.3b
Statistical information showing the functional relationship
between inertial and viscous terms (ϕ = 50°).

Bo	ϕ	ind. var.	dep. var.	R-sqd.	slope	intercept
0.2	50°	$\log\left(\dfrac{a}{h_o}\dfrac{Re\,Ca}{Bo}\right)$	$\log\left(\dfrac{Ca}{Bo}\right)$	1.0	0.50	-0.38922
0.4				1.0		-0.76553
1.0				1.0		-1.2629
1.5				1.0		-1.4830
all	50°	intercepts	$\log(Bo)$	1.0	-1.25	-1.2629

141
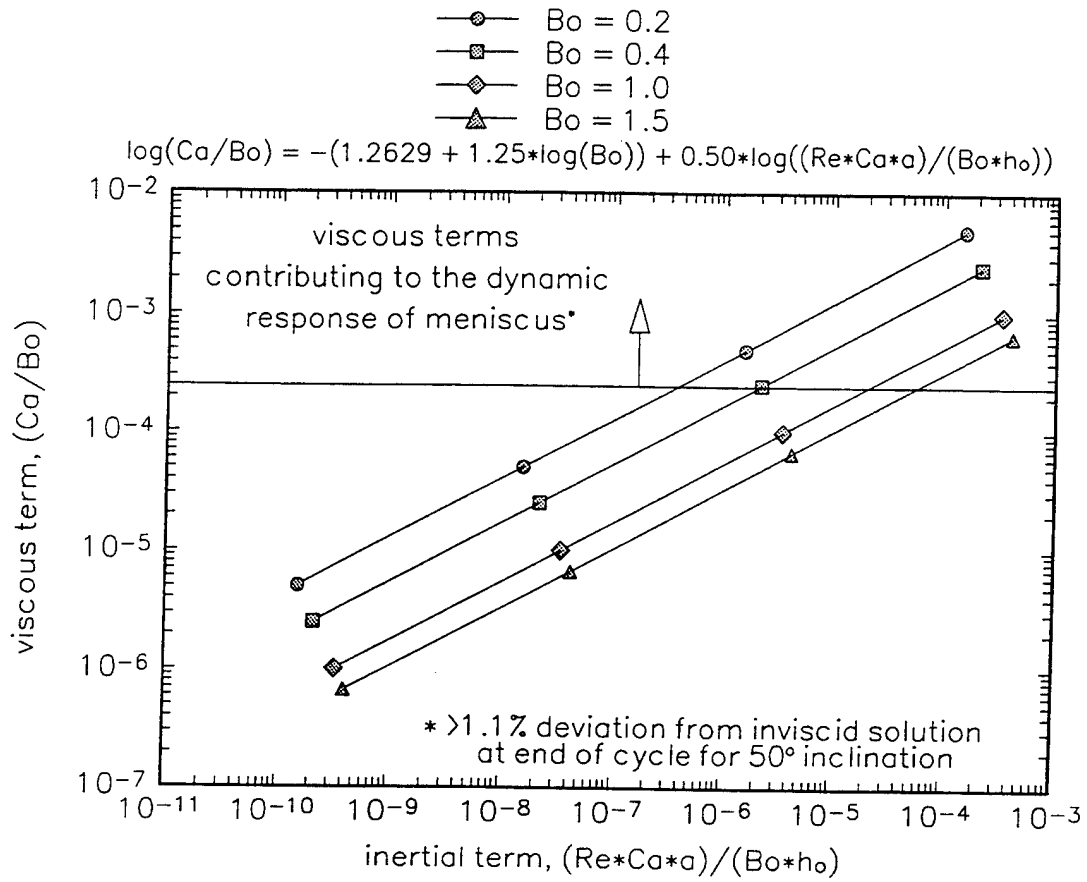
Fig. A.7 Functional relationship between viscous and inertial terms ($\phi = 50°$).

Computer program to calculate the acceleration field in space and time.

```c
#include <stdio.h>
#include <math.h>




main()


{


        float angularfreq;      /*angular velocity frequency, Hz*/
        float tf;               /*time period for angular velocity cycle, sec*/
        float accelpk;          /*peak acceleration at tf/2, "g"*/
        float ro;               /*radial location of cap tube pivot point, m*/
        float rt;               /*radial table coordinate*/
        float angularvel1;      /*angular velocity for t = 0-tf/2*/
        float angularvel2;      /*angular velocity for t = tf/2-tf*/
        float t;                /*time, sec*/
        float B;                /*positive slope of angular velocity*/
        float z1;               /*z1 = z/L = 0.5*/
        float z;                /*z*L = axial cap tube coordinate, m*/
        float angle;            /*inclination angle of cap tube, radians*/
        float L;                /*cap tube length, m*/
        float bz;               /*axial acceleration component, "g"*/
        float bR;               /*transverse acceleration component, "g"*/
        float k,i;

        char filenm[20];
        FILE *fp;

        printf ("\nThis program will calculate the axial and transverse\n");
        printf ("acceleration components as a function of space and time\n");
        printf ("\nenter inclination angle, deg.\n");
        scanf ("%f",&angle);
        angle = angle*3.141592/180;
        printf ("\nenter cycle frequency for angular velocity, Hz\n");
        scanf ("%f",&angularfreq);
        printf ("\nenter peak acceleration (half period), g's\n");
        scanf ("%f",&accelpk);
        printf ("\nenter filename for your data\n");
        scanf ("%s",filenm);
```

```
        fp = fopen (filenm,"w");
        ro = 0.8073;
        L = 10/100;
        tf = 1/angularfreq;
        B = sqrt(accelpk/(ro*pow(tf/2,2)));
        z1 = 0.5;

    t = 0;
    for (i=0; i<=tf; i++)
    {
        z = 0;


        for (k=0; k<=10; k++)
        {

        rt = ro + (z1-z)*L*cos(angle);

        /*(t = 0-tf/2)*/
        if (t <= tf/2)
        {
        angularvel1 = B*t;
        bz = - pow(angularvel1,2)*rt*cos(angle) + (-9.81)*sin(angle)/9.81;
        Br = pow(pow(- pow(angularvel1,2)*rt*sin(angle) - (-9.81)*cos(angle)/9.81,2)
            + pow(rt*B,2),0.5);
        }



        /*(t = tf/2-tf)*/
        if (t > tf/2)
        {
        angularvel2 = B*(tf-t);
        bz = - pow(angularvel2,2)*rt*cos(angle) + (-9.81)*sin(angle)/9.81;
        Br = pow(pow(- pow(angularvel2,2)*rt*sin(angle) - (-9.81)*cos(angle)/9.81,2)
            + pow(rt*(-B),2),0.5);
        }
        fprintf (fp,"%4.3e\t%4.3e\t%4.3e\t%4.3e\n",t,z,bz,Br);
        z = z + 0.1;
        }
    t = t + 1;
    }
fclose (fp);
}
```

Table A.5
Computer program to calculate the acceleration at the capillary
tube pivot point in time.

```c
#include <stdio.h>
#include <math.h>




main()


{

        float angularfreq;     /*angular velocity frequency, Hz*/
        float tf;              /*time period for angular velocity cycle, sec*/
        float accelpk;         /*peak acceleration at tf/2, "g"*/
        float ro;              /*radial location of cap tube pivot point, m*/
        float rt;              /*radial table coordinate*/
        float angularvel1;     /*angular velocity for t = 0-tf/2*/
        float angularvel2;     /*angular velocity for t = tf/2-tf*/
        float t;               /*time, sec*/
        float B;               /*positive slope of angular velocity*/
        float z1;              /*z1 = z/L = 0.5*/
        float z;               /*z*L = axial cap tube coordinate, m*/
        float angle;           /*inclination angle of cap tube, radians*/
        float L;               /*cap tube length, m*/
        float bz;              /*axial acceleration component, "g"*/
        float Br;              /*transverse acceleration component, "g"*/
        float dt;              /*time step*/
        float k,i;

        char filenm[20];
        FILE *fp;

        printf ("\Nthis program will calculate the axial and transverse\n");
        printf ("acceleration components as a function of space and time\n");
        printf ("\nenter inclination angle, deg.\n");
        scanf ("%f",&angle);
        angle = angle*3.141592/180;
        printf ("\nenter cycle frequency for angular velocity, Hz\n");
        scanf ("%f",&angularfreq);
        printf ("\nenter peak acceleration (half period), g's\n");
        scanf ("%f",&accelpk);
```

145

```c
        printf ("\nenter time step\n");
        scanf ("%f",&dt);
        printf ("\nenter filename for your data\n");
        scanf ("%s",filenm);
        fp = fopen (filenm,"w");
        ro = 0.8073;
        L = 10/100;
        tf = 1/angularfreq;
        B = sqrt(accelpk/(ro*pow(tf/2,2)));
        z1 = 0.5;

t = 0;
do
{
        z = z1;



        rt = ro + (z1-z)*L*cos(angle);

        /*(t = 0-tf/2)*/
        if (t <= tf/2)
        {
        angularvel1 = B*t;
        bz = - pow(angularvel1,2)*rt*cos(angle) + (-9.81)*sin(angle)/9.81;
        Br = pow(pow(- pow(angularvel1,2)*rt*sin(angle) - (-9.81)*cos(angle)/9.81,2)
            + pow(rt*B,2),0.5);
        }



        /*(t = tf/2-tf)*/
        if (t > tf/2)
        {
        angularvel2 = B*(tf-t);
        bz = - pow(angularvel2,2)*rt*cos(angle) + (-9.81)*sin(angle)/9.81;
        Br = pow(pow(- pow(angularvel2,2)*rt*sin(angle) - (-9.81)*cos(angle)/9.81,2)
            + pow(rt*(-B),2),0.5);
        }
        fprintf (fp,"%4.3e\t%4.3e\t%4.3e\t%4.3e\n",t,z,bz,Br);
```

```
      t = t + dt;
      }
      while (t<=tf);
fclose (fp);
}
```

Table A.6
Computer program to calculate the transient
dimensionless meniscus position for ethyl alcohol.

```c
#include <stdio.h>
#include <math.h>




main()


{


        double angularfreq;    /*angular velocity frequency, Hz*/
        double tf;             /*time period for angular velocity cycle, sec*/
        double accelpk;            /*peak acceleration at tf/2, "g"*/
        double ro;             /*radial location of cap tube pivot point, m*/
        double rt,rtv;         /*radial table coordinate*/
        double t;              /*time, sec*/
        double B;              /*positive slope of angular velocity*/
        double z1;             /*z1 = z/L = 0.5*/
        double z;              /*z*L = axial cap tube coordinate, m*/
        double angle;          /*inclination angle of cap tube, radians*/
        double dangle;             /*inclination angle increment*/
        double thetas;             /*static contact angle, radians*/
        double theta;          /*apparent recession contact angle
                                  (assumed constant), radians*/
        double thetaa;             /*apparent advancing contact angle
                                  (assumed constant), radians*/
        double L;              /*cap tube length, m*/
        double a;              /*cap tube radius, m*/
        double d;              /*cap tube diameter, m*/
        double gamma;              /*surface tension, N/m*/
        double rho;            /*fluid density, kg/cu.m*/
        double visc;           /*fluid viscosity, kg/m-s*/
        double ho;             /*static wicking height, m*/
        double Vc;             /*characteristic velocity, m/s*/
        double Bo;             /*Bond number*/
        double Ca;             /*Capillary number*/
        double Re;             /*Reynolds number*/
        double H0,H1,H0v,H1v;  /*dimensionaless height, h/ho*/
        double Hinert;             /*dimensionaless height inviscid
                                  with inertia term, h/ho*/
```

148

```c
double Hvisc;                /*dimensionaless height with
                             viscous and inertia terms, h/ho*/
double Happrx;               /*dimensionaless height approximated
                             for small inertia and viscous terms, h/ho*/
double acoef,bcoef,ccoef;/*coefficients*/
double a1,b1,c1;         /*coefficients*/
double a1v,b1v,c1v;      /*coefficients*/
double T;                /*dimensionaless time, t/tf*/
double time;             /*dimensionaless time, t/tf (mulitple cycles)*/
double Dt;               /*incremental dimensionaless time*/
double omega1;               /*dimensionaless angular
                             velocity, T = 0-0.5*/
double omega2;               /*dimensionaless angular
                             velocity, T = 0.5-1.0*/
float cyclenum;              /*number of cycles*/

float k,i,j,n;

char filenm[20];
FILE *fp;

printf ("\Nthis program will calculate the \n");
printf ("meniscus height as a function of time\n");
printf ("\nBond number (eg. 0.1-2.0) = ");
scanf ("%lf",&Bo);
printf ("\nCapillary number (eg. 1e-4 - 1e-8) = ");
scanf ("%lf",&Ca);
printf ("\nenter peak acceleration (half period), g's\n");
scanf ("%lf",&accelpk);
Bo = Bo/accelpk;
printf ("\enter number of cycles\n");
scanf ("%1f",&cyclenum);
printf ("\nenter dimensionaless incremental time step, Dt < 0.001\n");
scanf ("%lf",&Dt);
printf ("\nenter inclination angle, deg.\n");
scanf ("%lf",&angle);
angle = angle*3.141592/180;
printf ("\nenter static contact angle, deg.\n");
scanf ("%lf",&thetas);
printf ("\nenter recession contact angle, deg.\n");
scanf ("%lf",&theta);
printf ("\nenter advancing contact angle, deg.\n");
scanf ("%lf",&thetaa);
thetas = thetas*3.141592/180;
```

```c
theta = theta*3.141592/180;
thetaa = thetaa*3.141592/180;
printf ("\nenter filename for your data\n");
scanf ("%s",filenm);
fp = fopen (filenm,"w");
ro = 0.8073;
L = 10/100;
z1 = 0.5;
rho = 781.0;        /*Ethyl alcohol at 30C*/
gamma = .02189;     /*Ethyl alcohol at 30C*/
visc = 0.001;       /*Ethyl alcohol at 30C*/
a = sqrt(Bo*gamma/(4*rho*9.81));
d = 2*a;
Vc = gamma*Ca/visc;
ho = 2*gamma*cos(thetas)/(rho*a*9.81*sin(angle));
tf = 2*ho/Vc;
Re = rho*Vc*d/visc;




B = sqrt(accelpk/(ro*pow(tf/2,2)));




fprintf
(fp,"\ntime\tHvisc\tHinert\tHapprx\tBo\tCa\tRe\ta/ho\tangle\tinertia\tviscous\n");




/*initial conditions*/
H0v = 1.0;
H1v = H0v;
H0 = 1.0;
H1 = H0;
Happrx = H0;
T = 0;
time = 0;
k = 0;
n = cyclenum;




fprintf
```

150

```
(fp,"%4.3e\t%4.3e\t%4.3e\t%4.3e\t%4.3e\t%4.3e\t%4.3e\t%4.3e\t%4.3e\t%4.3e\n",

time,H0v,H0,Happrx,Bo*accelpk,Ca,Re,a/ho,angle/3.141592*180,Re*Ca*a/Bo/accelpk/
ho,Ca/Bo/accelpk);

  do
  {


  for (i=0; i<=1/Dt; i++)
  {



        T = T + Dt;
        k = k + Dt;
        time = time + Dt;

        rt = ro + (z1*L - ho*H1/2)*cos(angle);
        rtv = ro + (z1*L - ho*H1v/2)*cos(angle);

        /*(T = 0-0.5)*/
        if (T <= 0.5)
        {
        omega1 = B*tf*T;

        /*viscous formulation with inertia term*/

        alv = a*Re/(8*ho);

        blv = (a*Re*H1v/(2*ho)) + (8*Dt*H1v) - (a*Re*H0v/(4*ho));

        clv = -(Dt*Dt*Bo/Ca * (sin(angle)*cos(theta)/cos(thetas)
                - H1v*(pow(omega1,2)*cos(angle)*rtv + sin(angle)))
                - (a*Re/(2*ho) - 8*Dt) * H0v * H1v
                - (a*Re/(8*ho)) * H0v * H0v
                + (a*Re/(ho)) * H1v * H1v);


        Hvisc = (-blv + sqrt(pow(blv,2)-4*alv*clv))/(2*alv);
```

151

```c
/*inviscid formulation with inertia term

b1 = 4*H1 - 2*H0;

c1 = -(8*Dt*Dt*ho*Bo/(a*Re*Ca)*(sin(angle)*cos(theta)/cos(thetas)
     - H1*(pow(omega1,2)*rt*cos(angle) + sin(angle)))
     +(8*H1*H1 - 4*H1*H0 - H0*H0));



Hinert = (-b1 + sqrt(pow(b1,2)-4*c1))/2;  */




/*approximation without viscous and inertia terms*/

bcoef = - (2*z1*L/ho + 2*ro/(ho*cos(angle))
          + 2*sin(angle)/(pow(omega1,2)*pow(cos(angle),2)*ho));
ccoef = 2*sin(angle)*cos(theta)/cos(thetas)/(pow(omega1,2)*pow(cos(angle),2)*ho);

Happrx = (-bcoef - sqrt(pow(bcoef,2)-4*ccoef))/2;
}



/*(T = 0.5-1.0)*/
if (T > 0.5)
{
omega2 = B*tf*(1-T);

/*viscous formulation with inertia term*/

alv = a*Re/(8*ho);

blv = (a*Re*H1v/(2*ho)) + (8*Dt*H1v) - (a*Re*H0v/(4*ho));

clv = -(Dt*Dt*Bo/Ca * (sin(angle)*cos(thetaa)/cos(thetas)
      - H1v*(pow(omega2,2)*cos(angle)*rtv + sin(angle)))
      - (a*Re/(2*ho) - 8*Dt) * H0v * H1v
      - (a*Re/(8*ho)) * H0v * H0v
      + (a*Re/(ho)) * H1v * H1v);
```

152

```
Hvisc = (-b1v + sqrt(pow(b1v,2)-4*a1v*c1v))/(2*a1v);



/*inviscid formulation with inertia term

b1 = 4*H1 - 2*H0;

c1 = -(8*Dt*Dt*ho*Bo/(a*Re*Ca)*(sin(angle)*cos(thetaa)/cos(thetas)
     - H1*(pow(omega2,2)*rt*cos(angle) + sin(angle)))
     +(8*H1*H1 - 4*H1*H0 - H0*H0));




Hinert = (-b1 + sqrt(pow(b1,2)-4*c1))/2;  */



/*approximation without viscous and inertia terms*/

bcoef = - (2*z1*L/ho + 2*ro/(ho*cos(angle))
              + 2*sin(angle)/(pow(omega2,2)*pow(cos(angle),2)*ho));
ccoef =
2*sin(angle)*cos(thetaa)/cos(thetas)/(pow(omega2,2)*pow(cos(angle),2)*ho);

Happrx = (-bcoef - sqrt(pow(bcoef,2)-4*ccoef))/2;
}

if (k >= 0.001)
{
fprintf
(fp,"%4.3e\t%4.3e\t%4.3e\t%4.3e\t%4.3e\t%4.3e\t%4.3e\t%4.3e\t%4.3e\t%4.3e\t%4.3e\n",

time,Hvisc,Hinert,Happrx,Bo*accelpk,Ca,Re,a/ho,angle/3.141592*180,Re*Ca*a/ho/Bo/a
ccelpk,Ca/Bo/accelpk);
        k = 0;
        }
        H0v = H1v;
        H1v = Hvisc;
        H0 = H1;
        H1 = Hinert;
```

```
        }

    T = 0;
    k = 0;
    n = n-1;
    }
    while (n>0);

fclose (fp);
}
```

Computer program to calculate the transient
dimensionless meniscus position for water.

```c
#include <stdio.h>
#include <math.h>




main()


{


        double angularfreq;    /*angular velocity frequency, Hz*/
        double tf;             /*time period for angular velocity cycle, sec*/
        double accelpk;              /*peak acceleration at tf/2, "g"*/
        double ro;             /*radial location of cap tube pivot point, m*/
        double rt,rtv;         /*radial table coordinate*/
        double t;              /*time, sec*/
        double B;              /*positive slope of angular velocity*/
        double z1;             /*z1 = z/L = 0.5*/
        double z;              /*z*L = axial cap tube coordinate, m*/
        double angle;          /*inclination angle of cap tube, radians*/
        double dangle;               /*inclination angle increment*/
        double thetas;               /*static contact angle, radians*/
        double theta;          /*apparent recession contact angle
                                 (assumed constant), radians*/
        double thetaa;               /*apparent advancing contact angle
                                 (assumed constant), radians*/
        double L;              /*cap tube length, m*/
        double a;              /*cap tube radius, m*/
        double d;              /*cap tube diameter, m*/
        double gamma;                /*surface tension, N/m*/
        double rho;            /*fluid density, kg/cu.m*/
        double visc;           /*fluid viscosity, kg/m-s*/
        double ho;             /*static wicking height, m*/
        double Vc;             /*characteristic velocity, m/s*/
        double Bo;             /*Bond number*/
        double Ca;             /*Capillary number*/
        double Re;             /*Reynolds number*/
        double H0,H1,H0v,H1v;      /*dimensionaless height, h/ho*/
        double Hinert;               /*dimensionaless height inviscid
                                 with inertia term, h/ho*/
```

```c
    double Hvisc;                 /*dimensionaless height with
                                  viscous and inertia terms, h/ho*/
    double Happrx;                /*dimensionaless height approximated
                                  for small inertia and viscous terms, h/ho*/
    double acoef,bcoef,ccoef;/*coefficients*/
    double a1,b1,c1;        /*coefficients*/
    double a1v,b1v,c1v;     /*coefficients*/
    double T;               /*dimensionaless time, t/tf*/
    double time;            /*dimensionaless time, t/tf (mulitple cycles)*/
    double Dt;              /*incremental dimensionaless time*/
    double omega1;                /*dimensionaless angular
                                  velocity, T = 0-0.5*/
    double omega2;                /*dimensionaless angular
                                  velocity, T = 0.5-1.0*/
    float cyclenum;               /*number of cycles*/

    float k,i,j,n;

    char filenm[20];
    FILE *fp;

    printf ("\Nthis program will calculate the \n");
    printf ("meniscus height as a function of time\n");
    printf ("\Nbond number (eg. 0.1-2.0) = ");
    scanf ("%lf",&Bo);
    printf ("\Ncapillary number (eg. 1e-4 - 1e-8) = ");
    scanf ("%lf",&Ca);
    printf ("\nenter peak acceleration (half period), g's\n");
    scanf ("%lf",&accelpk);
    Bo = Bo/accelpk;
    printf ("\enter number of cycles\n");
    scanf ("%1f",&cyclenum);
    printf ("\nenter dimensionaless incremental time step, Dt < 0.001\n");
    scanf ("%lf",&Dt);
    printf ("\nenter inclination angle, deg.\n");
    scanf ("%lf",&angle);
    angle = angle*3.141592/180;
    printf ("\nenter static contact angle, deg.\n");
    scanf ("%lf",&thetas);
    printf ("\nenter recession contact angle, deg.\n");
    scanf ("%lf",&theta);
    printf ("\nenter advancing contact angle, deg.\n");
    scanf ("%lf",&thetaa);
    thetas = thetas*3.141592/180;
```

156

```c
theta = theta*3.141592/180;
thetaa = thetaa*3.141592/180;
printf ("\nenter filename for your data\n");
scanf ("%s",filenm);
fp = fopen (filenm,"w");
ro = 0.8073;
L = 10/100;
z1 = 0.5;
rho = 997.0;        /*water at 300K*/
gamma = .0717;      /*water at 300K*/
visc = 855e-6;      /*water at 300K*/
a = sqrt(Bo*gamma/(4*rho*9.81));
d = 2*a;
Vc = gamma*Ca/visc;
ho = 2*gamma*cos(thetas)/(rho*a*9.81*sin(angle));
tf = 2*ho/Vc;
Re = rho*Vc*d/visc;



B = sqrt(accelpk/(ro*pow(tf/2,2)));



fprintf
(fp,"\ntime\Thvisc\Thinert\Thapprx\Tbo\Tca\Tre\ta/ho\tangle\tinertia\tviscous\n");



/*initial conditions*/
H0v = 1.0;
H1v = H0v;
H0 = 1.0;
H1 = H0;
Happrx = H0;
T = 0;
time = 0;
k = 0;
n = cyclenum;



fprintf
```

```c
(fp,"%4.3e\t%4.3e\t%4.3e\t%4.3e\t%4.3e\t%4.3e\t%4.3e\t%4.3e\t%4.3e\t%4.3e\n",

time,H0v,H0,Happrx,Bo*accelpk,Ca,Re,a/ho,angle/3.141592*180,Re*Ca*a/Bo/accelpk/
ho,Ca/Bo/accelpk);

   do
   {


   for (i=0; i<=1/Dt; i++)
   {



         T = T + Dt;
         k = k + Dt;
         time = time + Dt;

         rt = ro + (z1*L - ho*H1/2)*cos(angle);
         rtv = ro + (z1*L - ho*H1v/2)*cos(angle);

         /*(T = 0-0.5)*/
         if (T <= 0.5)
         {
         omega1 = B*tf*T;

         /*viscous formulation with inertia term*/

         alv = a*Re/(8*ho);

         blv = (a*Re*H1v/(2*ho)) + (8*Dt*H1v) - (a*Re*H0v/(4*ho));

         clv = -(Dt*Dt*Bo/Ca * (sin(angle)*cos(theta)/cos(thetas)
                  - H1v*(pow(omega1,2)*cos(angle)*rtv + sin(angle)))
                  - (a*Re/(2*ho) - 8*Dt) * H0v * H1v
                  - (a*Re/(8*ho)) * H0v * H0v
                  + (a*Re/(ho)) * H1v * H1v);


         Hvisc = (-blv + sqrt(pow(blv,2)-4*alv*clv))/(2*alv);
```

```
/*inviscid formulation with inertia term

b1 = 4*H1 - 2*H0;

c1 = -(8*Dt*Dt*ho*Bo/(a*Re*Ca)*(sin(angle)*cos(theta)/cos(thetas)
     - H1*(pow(omega1,2)*rt*cos(angle) + sin(angle)))
     +(8*H1*H1 - 4*H1*H0 - H0*H0));


Hinert = (-b1 + sqrt(pow(b1,2)-4*c1))/2;   */




/*approximation without viscous and inertia terms*/

bcoef = - (2*z1*L/ho + 2*ro/(ho*cos(angle))
          + 2*sin(angle)/(pow(omega1,2)*pow(cos(angle),2)*ho));
ccoef = 2*sin(angle)*cos(theta)/cos(thetas)/(pow(omega1,2)*pow(cos(angle),2)*ho);

Happrx = (-bcoef - sqrt(pow(bcoef,2)-4*ccoef))/2;
}




/*(T = 0.5-1.0)*/
if (T > 0.5)
{
omega2 = B*tf*(1-T);

/*viscous formulation with inertia term*/

alv = a*Re/(8*ho);

b1v = (a*Re*H1v/(2*ho)) + (8*Dt*H1v) - (a*Re*H0v/(4*ho));

c1v = -(Dt*Dt*Bo/Ca * (sin(angle)*cos(thetaa)/cos(thetas)
      - H1v*(pow(omega2,2)*cos(angle)*rtv + sin(angle)))
      - (a*Re/(2*ho) - 8*Dt) * H0v * H1v
      - (a*Re/(8*ho)) * H0v * H0v
      + (a*Re/(ho)) * H1v * H1v);
```

```c
Hvisc = (-b1v + sqrt(pow(b1v,2)-4*a1v*c1v))/(2*a1v);



/*inviscid formulation with inertia term

b1 = 4*H1 - 2*H0;

c1 = -(8*Dt*Dt*ho*Bo/(a*Re*Ca)*(sin(angle)*cos(thetaa)/cos(thetas)
     - H1*(pow(omega2,2)*rt*cos(angle) + sin(angle)))
     +(8*H1*H1 - 4*H1*H0 - H0*H0));




Hinert = (-b1 + sqrt(pow(b1,2)-4*c1))/2;   */



/*approximation without viscous and inertia terms*/

bcoef = - (2*z1*L/ho + 2*ro/(ho*cos(angle))
           + 2*sin(angle)/(pow(omega2,2)*pow(cos(angle),2)*ho));
ccoef =
2*sin(angle)*cos(thetaa)/cos(thetas)/(pow(omega2,2)*pow(cos(angle),2)*ho);

Happrx = (-bcoef - sqrt(pow(bcoef,2)-4*ccoef))/2;
}

if (k >= 0.001)
{
fprintf
(fp,"%4.3e\t%4.3e\t%4.3e\t%4.3e\t%4.3e\t%4.3e\t%4.3e\t%4.3e\t%4.3e\t%4.3e\t%4.3e\n",

time,Hvisc,Hinert,Happrx,Bo*accelpk,Ca,Re,a/ho,angle/3.141592*180,Re*Ca*a/ho/Bo/a
ccelpk,Ca/Bo/accelpk);
        k = 0;
        }
        H0v = H1v;
        H1v = Hvisc;
        H0 = H1;
        H1 = Hinert;
```

```
      }

      T = 0;
      k = 0;
      n = n-1;
      }
      while (n>0);

fclose (fp);
}
```

APPENDIX B

EXPERIMENTAL SETUP AND INSTRUMENTATION

Centrifuge Test Bed

Transient acceleration fields were generated using a 2.4-m diameter centrifuge table (as discussed in chapters I-III) rotating with a time variant angular velocity. Single and multiple cycle angular velocity transients were generated using a signal or waveform generator as a control input to the centrifuge. Using the signal generator as the centrifuge control input allowed the peak to peak values and frequency of the periodic angular velocity transient to be specified for experimental purposes. For all experiments, the angular velocity was increased linearly to a peak value at the midpoint of the cycle and subsequently decreased as discussed in chapters I-III.

A tri-axis accelerometer (Columbia Research Laboratories, Inc.) was used to monitor the time variant acceleration components, in a cartesian reference frame affixed to the centrifuge table, in response to the angular velocity transient. The accelerometer output reflects the acceleration components as referenced to the mounting location of the accelerometer on the centrifuge. A transformation of the accelerometer output from the accelerometer mounting location to the capillary pivot point was performed using the relations ($r_o' = r_{T,\ pivot} = 0.8072\,m$)

(i)

$$b_{y,pivot} \approx b_{y,accel},$$

(ii)

$$b_{r_T, pivot} = \omega^2 r_{T, pivot}$$
$$b_{r_T, accel} = \omega^2 r_{r_T, accel}$$
$$b_{r_T, pivot} = \frac{r_{T, pivot}}{r_{T, accel}} b_{r_T, accel}$$
, $r_{T, accel} = 0.9390\,m$

(iii)

$$b_{T, pivot} = \frac{d\omega}{dt} r_{T, pivot}$$
$$b_{T, accel} = \frac{d\omega}{dt} r_{r_T, accel}$$
, $r_{T, accel} = 0.9819\,m.$
$$b_{T, pivot} = \frac{r_{T, pivot}}{r_{T, accel}} b_{r_T, accel}$$

Capillary Test Cell

A sealed test cell was fabricated of either acrylic or delrin to contain the working fluid and capillary tube as shown schematically in Figs. 1.3, 2.4, and 3.2 or as a detailed drawing in Fig. B.1. The photographs in Figs. B.2 and B.3 show the test cell as fabricated of delrin. The capillary tube was held in place using spring loaded positioning clamps. A transparent window allowed viewing of the capillary tube during experimental testing. The sealed test cell containing a glass capillary tube and reservoir was positioned on the centrifuge as discussed in chapters I-III. The test cell was mounted to a motorized optics rotation stage (Newport), as shown in Fig. B.4, such that the capillary tube was allowed to pivot about its center of mass. This pivot point was displaced vertically from

163

the centrifuge surface at a fixed radial location, r_o', as discussed in chapters I-III. Angles of inclination of the capillary tube were determined from the output of a calibrated angular displacement transducer (Trans-Tek, Inc.) accurate to within ±0.2 degrees.

Figure B.5 shows the test cell mounted on the centrifuge along with the video camera to monitor the dynamic response of the meniscus. Experiments were conducted by fixing various size diameters of capillary tubes at a specified inclination angle while subjecting it to the transient acceleration field. Increasing the inclination angle elevates the transverse acceleration component referenced to the capillary tube. This allowed the dynamic response of the meniscus subjected to an increasing transverse acceleration component to be observed experimentally. The dynamic response of the meniscus to the transient acceleration field was observed using an 8-mm format CCD camera (Sony, 30 frames/s) mounted adjacent to the test cell. The meniscus height relative to the reservoir meniscus, η, was measured as a function of time to within ±1.0 mm using the magnified video image with a calibrated reference contained within the test cell. An equivalent contact angle, θ, was calculated from the experimentally determined static wicking height, h_o, for conditions when the transverse acceleration component was zero ($h_o \rho g \approx (2\sigma/a)\cos\theta$).

Water (reverse osmosis) and ethyl alcohol were used as the test fluids to demonstrate the importance of the equilibrium contact angle on the advance and recession of the meniscus due to a transient acceleration field. Properties of these fluids were assumed to be that of the bulk fluid corresponding to a experimental temperature of 30°C.

The test cell and capillary tube were cleaned using potassium hydroxide and rinsed

with distilled water. The test cell was filled and subsequently sealed resulting in a fill that had a combination of air, fluid vapor, and liquid.

<u>Experimental Instrumentation</u>

Experimental instrumentation including, calibration instrumentation, used for this investigation are as follows:

Calibration Devices (secondary standards)

(1) CLINOMETER: High Resolution (P/N 02543-01),
                        Anglestar Protractor(Schaevitz),
                        Lucas Sensing Systems, Inc.
     LINEAR RANGE: $\pm$19.99 deg.
     RESOLUTION: 0.01 deg.
     CALIBRATION: USAF Calibration Laboratory
                        Traceable to NIST

(2) TEMPERATURE
     PROBE: Hart Scientific 5690
     SENSOR
     ELEMENT: High Precision 4-Wire Platinum Sensor
     RESOLUTION: 0.001°C
     TEMPERATURE
     RANGE: -183 - 500°C
     CALIBRATION: Factory Calibration
                        5 mK Uncertainty, Traceable to NIST

Instrumentation Devices

(1) ACCELEROMETER: High Precision (SA-307-HPTX),
                        Columbia Research Laboratories, Inc.
     RANGE: $\hat{e}_T$, $\pm$1.5 g
                        $\hat{e}_{r_r}$, $\pm$10 g
                        $\hat{e}_y$, $\pm$1.0 g
     OUTPUT: $\pm$7.5 Volts into 100K Load
     RESOLUTION: 0.001% F.R.
     NON-LINEARITY: $\pm$0.03% F.R.
     NATURAL

165

	FREQUENCY:	75 to 300 Hz Dependent Upon Range
	CALIBRATION:	Factory Calibration, Verification Using Digital Tachometer

(2) ANGULAR
DISPLACEMENT

	TRANSDUCER:	Model 0605-S41020202, Trans-Tek, Inc.
	RANGE:	0 - 90 deg.
	SENSITIVITY:	0.0074 VDC / deg. / Volt Input
	CALIBRATION:	Factory Calibration, Calibration With Assembled Test Cell Performed Using Clinometer

(3) THERMOCOUPLES: Type-T
SIGNAL
CONDITIONER

	OUTPUT:	±5 Volts
	RANGE:	0 - 199°C
	CALIBRATION:	Calibration With High Precision Temperature Probe Using a Constant Temperature Oil Bath

Calibration Procedures

Calibrations were performed on the angular displacement transducer and thermocouples using the high resolution clinometer and the high precision temperature probe respectively. Measurements of the capillary tube diameters were verified using pin gauges to within 0.001 inch.

Angular displacement transducer use and calibration. The angular displacement transducer was used to position the capillary tube at a specified inclination angle with respect to the centrifuge surface. Since the angular displacement transducer was calibrated prior to receipt, it was only necessary to zero the transducer with respect to the capillary tube and spot verify the factory calibration. Figure B.6 shows the results of zeroing the angular position transducer and subsequent calibration fitted to a linear

166

regression.

Thermocouple use and calibration. Thermocouples are a first order response temperature measurement device for which dissimilar metals generate a voltage (Seebeck voltage). To measure temperature accurately, a reference junction must be used in conjunction with the thermocouple. For most applications, reference junctions are incorporated within the electronics used for linearization and amplification of the thermocouple output. Using thermocouples on rotating devices, such as with the centrifuge, requires either the routing of the thermocouple wires through a rotating slip ring or conditioning the thermocouple signal prior to the slip ring. The former can result in significant error in temperature measurements due to the creation of additional dissimilar metal junctions with the slip ring materials. For these experiments, the thermocouple signals were electronically conditioned on the centrifuge resulting in a ±5 volt output signal.

Exposed junction copper-constantan type thermocouples were attached to the exterior surface of the capillary tube with a graphite slurry to maintain a thermal bond with an outside coating of high temperature ceramic to maintain strength integrity. The capillary tube was mounted into the test cell and the entire test cell immersed in a constant temperature oil bath for calibration. The data acquisition system (including signal conditioner, slip ring, A/D converter, etc.) and thermocouples were calibrated over a temperature range of 25 - 70°C using the high precision temperature probe as a reference. Calibration data for each thermocouple were obtained and fit to a linear regression for experimental use, Fig. B.7.

Uncertainty Analysis

Each of the above mentioned instrumentation devices and experimental measurements have some error associated with their use. This error must be considered either during the calibration procedure or when using instrumentation to determine the overall calibration and operational error due to the instrumentation. Instrument precision, accuracy, and resolution must all be considered when evaluating instrument error.

If a function, Φ, is considered in which $\Phi = \Phi(\alpha, \beta, \gamma)$, the absolute error for Φ can be determined[34] by,

$$E_\Phi = \left| \left(\frac{\partial \Phi}{\partial \alpha} \right) \Delta \alpha \right| + \left| \left(\frac{\partial \Phi}{\partial \beta} \right) \Delta \beta \right| + \left| \left(\frac{\partial \Phi}{\partial \gamma} \right) \Delta \gamma \right|$$

where $\Delta(\ )$ is the error associated with the measurement of the appropriate independent variable. When the $\Delta(\ )$'s are considered not as absolute limits of error, but rather as statistical bounds such as $\pm 3s$ limits, probable errors, or uncertainties, the proper method of combining the errors is to use the root-sum square so that the absolute error becomes

$$E_\Phi = \left[\left(\left(\frac{\partial \Phi}{\partial \alpha} \right) \Delta \alpha \right)^2 + \left(\left(\frac{\partial \Phi}{\partial \beta} \right) \Delta \beta \right)^2 + \left(\left(\frac{\partial \Phi}{\partial \gamma} \right) \Delta \gamma \right)^2 \right]^{\frac{1}{2}}$$

Error in inclination angle measurement. Sources of error in measurement of the inclination angle include error due to centrifuge table runout and voltage measurement resolution. The error associated with the centrifuge table runout was determined to be $\pm 0.05°$ and was added to the absolute error associated with uncertainties due to

168

measurement resolution. From the calibration linear regression and assuming a sensitivity of 9 deg./volt and the voltage measurement resolution of ±0.01 volts, the absolute error in inclination angle (using either error equation) due to measurement resolution was E_ϕ = ±0.09°. When this error is added to the variation of inclination angle due to the centrifuge table runout, the total absolute error becomes $E_{\phi, tot} < ± 0.2°$.

Error in temperature measurement. Thermocouple outputs are signal conditioned using a signal conditioner with a sensitivity of 40°C/volt. The thermocouple signal was digitized using a 16 bit A/D converter over a ±5 volt signal. This translates to a digital voltage resolution of

$$\frac{±5\,volt}{2^{16}} = \frac{10\,volt}{2^{16}}$$
$$= 1.53 \times 10^{-4}\,volt$$

Multiplying this digital voltage resolution times the sensitivity will result in a measurement resolution of 6.12×10^{-3}°C. The absolute error in temperature measurement is result of the variability observed during calibration due to variations in ice point drift and thermocouple thermal equilibrium with the high precision temperature probe during the temperature bath transients. The predicted temperature using the linear regression fit from the calibration data showed a deviation of less than 1°C from the actual temperature indicated by the high precision temperature probe.

Error in acceleration measurement. Accelerometer outputs for the three axis have the following sensitivities

169

$$b_y, \quad K_y = 0.1333 \frac{g}{volt}$$

$$b_{r_T}, \quad K_{r_T} = 1.146 \frac{g}{volt}$$

$$b_T, \quad K_T = 0.1644 \frac{g}{volt}.$$

Each accelerometer signal in digitized using a 32 bit A/D converter over a ± 10 volt signal. This translates to a digital voltage resolution of

$$\frac{\pm 10 \; volt}{2^{16}} = \frac{20 \; volt}{2^{32}}$$
$$= 4.66 \times 10^{-9} \; volt.$$

The absolute error due to the measurement voltage resolution is determined by multiplying the sensitivity for each axis by the digital voltage resolution. It follows that the measurement resolution for each axis becomes

$$b_y, \quad E_y = 6.2 \times 10^{-10} g,$$
$$b_{r_T}, \quad E_{r_T} = 5.3 \times 10^{-9} g,$$
$$b_T, \quad E_T = 7.7 \times 10^{-10} g.$$

The factory calibration showed an absolute error in sensitivity would result in a less than ± 0.013 g error in accuracy. Additional errors due to case alignment and radial position on the centrifuge also contribute to the accelerometer error. Gear train backlash and centrifuge runout contribute to transient accelerations during the experiments. Combining all of these potential sources of error showed a total absolute error and acceleration variation during the experiments to be on the order of ± 0.1 g.

Error in capillary tube diameter. Three sizes of capillary tube diameters were used during the course of this investigation. Pin gauges were used to determine the capillary tube diameter for each capillary tube;

(i)

$$2a = 1.892 \pm 0.038\,mm,$$

(ii)

$$2a = 1.016 \pm 0.025\,mm,$$

(iii)

$$2a = 0.483 \pm 0.025\,mm.$$

Error in video and time measurement. The non-dimensional meniscus position and time were extracted from video images recorded on an 8-mm, 30 frames/sec formatted tape. Meniscus height measurements were made at specific time intervals during the course of the acceleration transient. Time intervals for meniscus height measurements were specified to be less than 2% of the cycle period for accurate resolution of the transient variation in meniscus height. Meniscus height measurements were referenced to a tangent line to the bottom of the reservoir meniscus as shown in Figure B.8. The absolute error in the non-dimensional meniscus position is defined by

$$E_\zeta = \sqrt{\left(\left(\frac{\partial \frac{\eta}{h_o}}{\partial \eta}\right)\Delta\eta\right)^2 + \left(\left(\frac{\partial \frac{\eta}{h_o}}{\partial h_o}\right)\Delta h_o\right)^2}$$

$$= \sqrt{\left(\frac{1}{h_o}\Delta\eta\right)^2 + \left(-\frac{\eta}{h_o^2}\Delta h_o\right)^2}$$

$\Delta \eta$, $\Delta h_o \sim 0.3\, cm$

$h_o \sim 20\, cm$

consider two cases;

(i)

$$\eta \rightarrow h_o, \quad E_\zeta = \sqrt{\left(\frac{1}{h_o}\Delta \eta\right)^2 + \left(\frac{1}{h_o}\Delta h_o\right)^2}$$

$$E_\zeta = 0.021$$

(ii)

$$\eta \rightarrow 0, \quad E_\zeta = \sqrt{\left(\frac{1}{h_o}\Delta \eta\right)^2}$$

$$E_\zeta = 0.015$$

Experimental Procedures

Experimental parameters were specified such that the capillary and Bond numbers were of an order of magnitude sufficient to investigate viscous, inertial, and transverse acceleration effects on the dynamic response of the meniscus subject to a transient acceleration field. These experimental parameters consisted of the radial location of the capillary tube pivot point, $r_o' = 0.8072\, m$, static contact angle, θ_s, fluid properties of water and ethyl alcohol, ρ, μ, σ, inclination angle, ϕ, capillary tube radius, a, and acceleration transient frequency, f. Table B.1 summarizes the experimental tests

conducted during the course of this investigation and shows the dimensional experimental parameters and appropriate groupings of dimensionless numbers.

The static contact angle was inferred from experimental data using the relation

$$h_o \rho g \sin\phi \approx \frac{2\sigma}{a} \cos\theta_s$$

Experimental data were obtained when the transverse acceleration component was at a minimum as well as the static case when only the gravitational acceleration was acting on the fluid column inclined at angle, ϕ. All meniscus height measurements used to evaluate the static contact angle, θ_s, were referenced to the center support block of the test cell in order to obtain the dimensional meniscus height. Prior to assembling the test cell, the center support block was measured using a micrometer to within ± 0.03 mm. The apparent static wicking height and the acceleration term were used to calculate the contact angle. Error in the contact angle was determined statistically between multiple samples. Table B.2 summarizes the experimental tests and the appropriate dimension of the center support block and static contact angle.

As discussed in Appendix A, analytical solutions are insensitive to changes in the static contact angle but are sensitive to changes in the dynamic contact angle differing from the static contact angle.

Fluid properties for water and ethyl alcohol used for this investigation are shown in Table B.3. For experimental tests with the addition of heat to the capillary tube, the fluid properties were taken to be that of the bulk reservoir also at 30°C.

173

Table B.2

Summary of experimental reference dimensions for analysis of
video information and experimentally inferred static contact angle.

exp#'s	fluid	reference, mm	θ_s, deg.	$\theta_{s, heat}$, deg.
1-5	H_2O	6.88 ± 0.01	22.2 ± 6.6	-----
6-10	C_2H_6O	6.248 ± 0.025	16.7 ± 4.4	-----
11-21		6.713 ± 0.015		-----
22-24		6.573 ± 0.025		35.6 ± 2.0

Table B.3

Summary of fluid properties used for this investigation.

fluid	ρ, kg/m^3	μ, kg/m-s	σ, N/m
H_2O, 30°C	997.0	855e-6	0.0717
C_2H_6O, 30°C	781.0	0.001	0.02189

Experimental tests were conducted with and without the addition of heat to the capillary tube. In general, even for tests in which heat was not added to the capillary tube, the acceleration transient was not applied until thermal equilibrium was obtained. A simple string and weight mounted on the test cell allowed for visualization of the acceleration vector direction and peak magnitude in order to correlate the video time to the acceleration cycle generated by the waveform generator.

174

Fig. B.1 Detailed drawing of test cell.
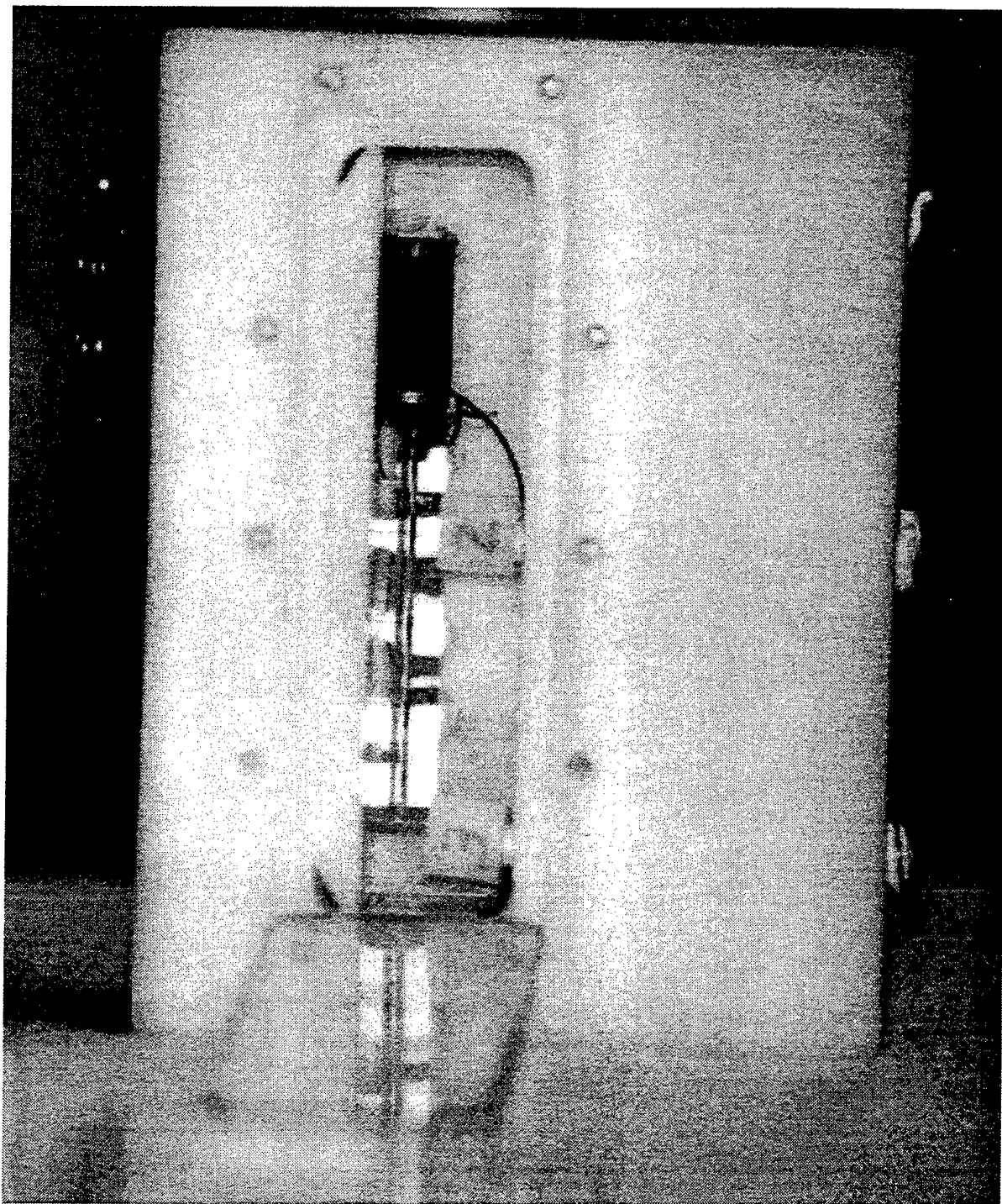
Fig. B.2 Photograph of test cell with capillary tube (front).
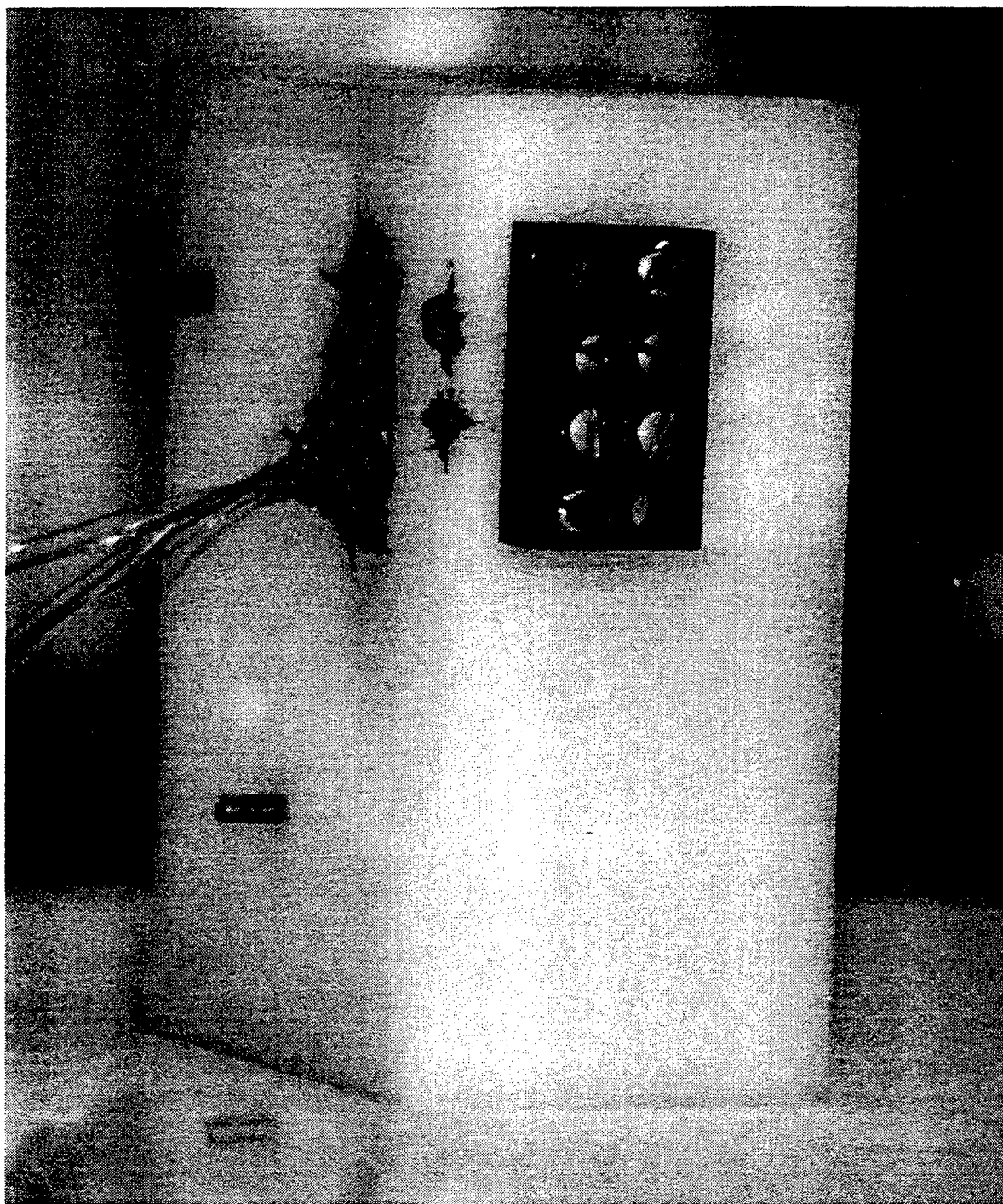
Fig. B.3 Photograph of test cell (rear).

177
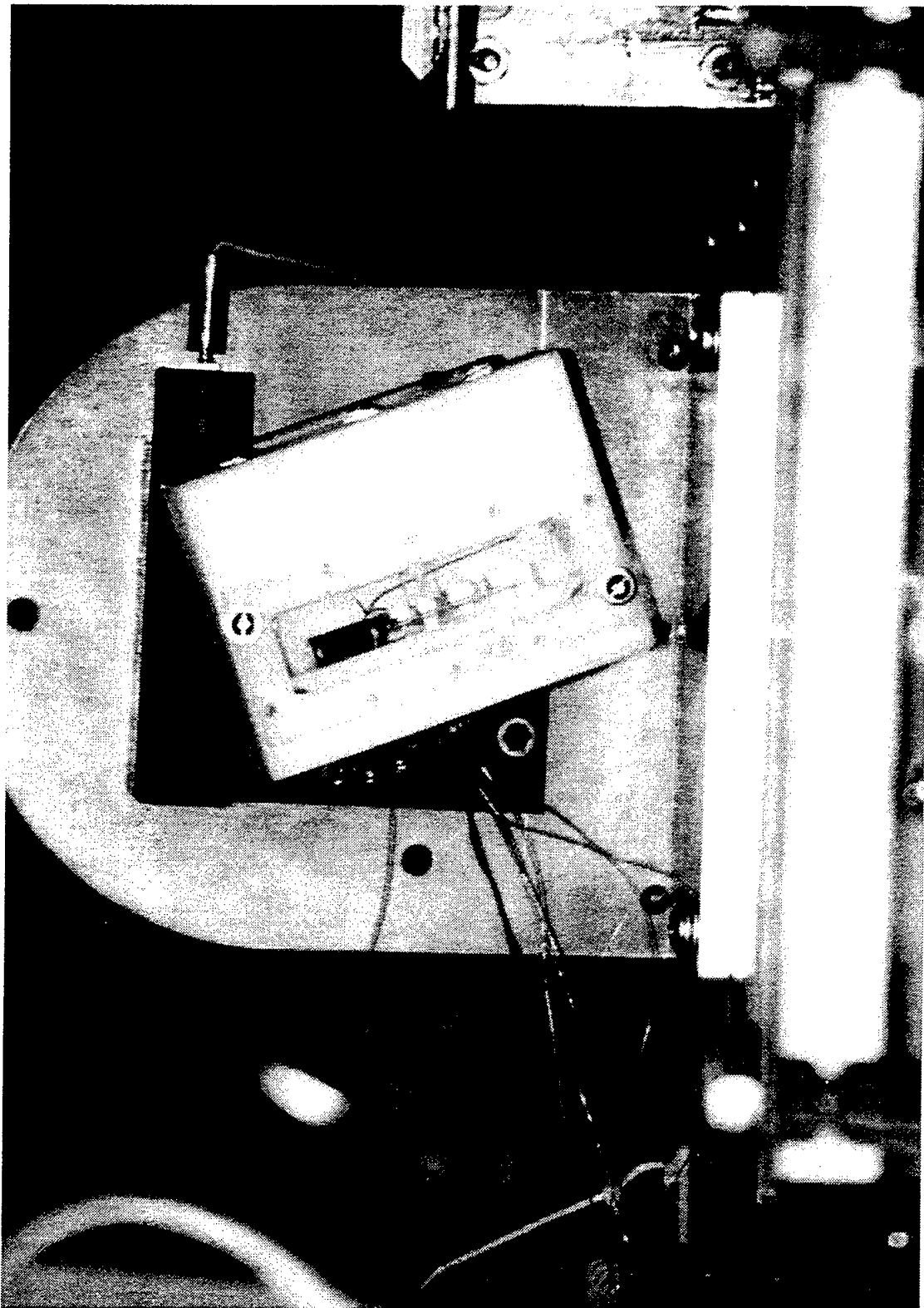
Fig. B.4 Photograph of test cell mounted on motorized optics rotation stage.
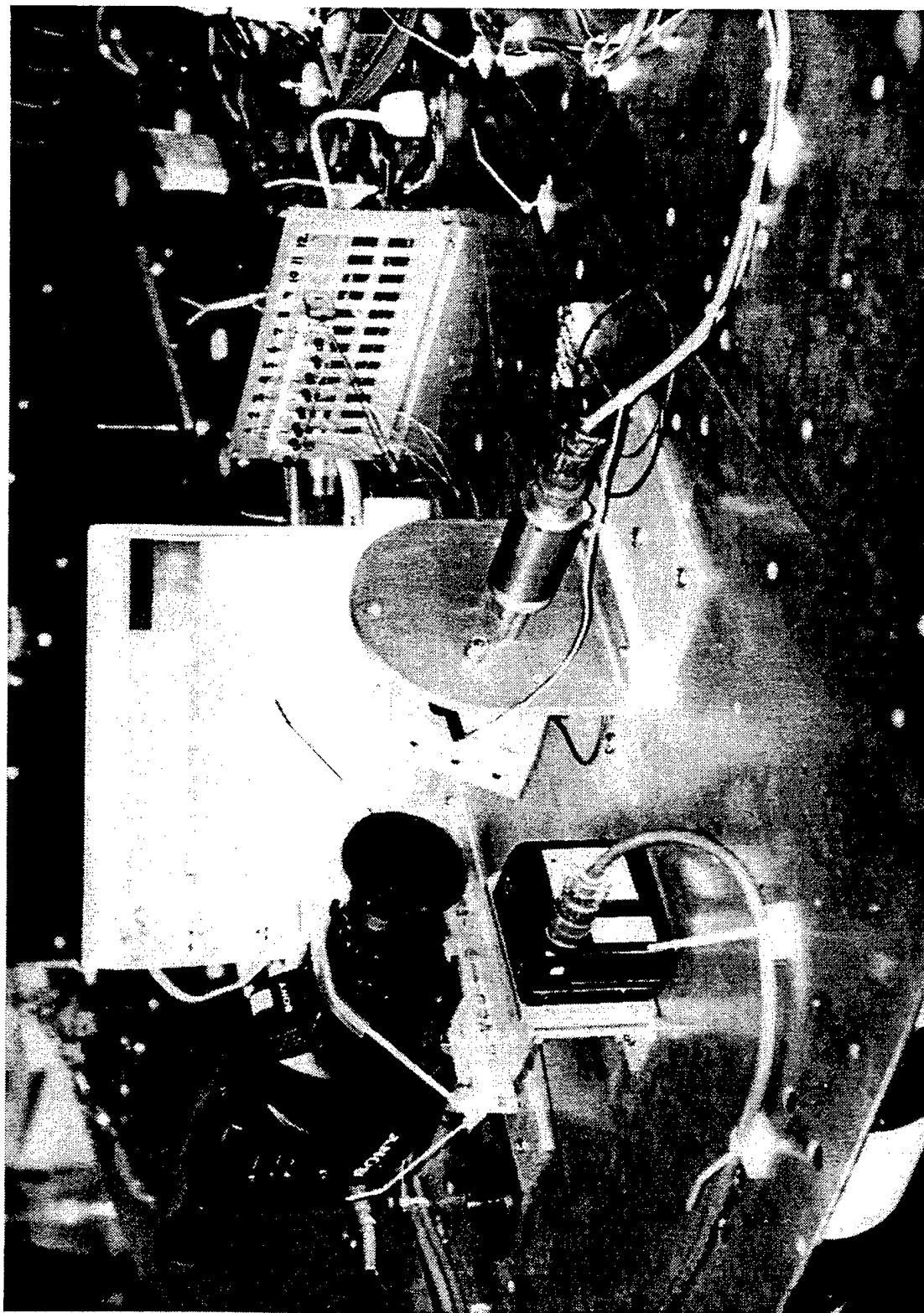
Fig. B.5 Photograph of experimental apparatus mounted on centrifuge.

179

179a
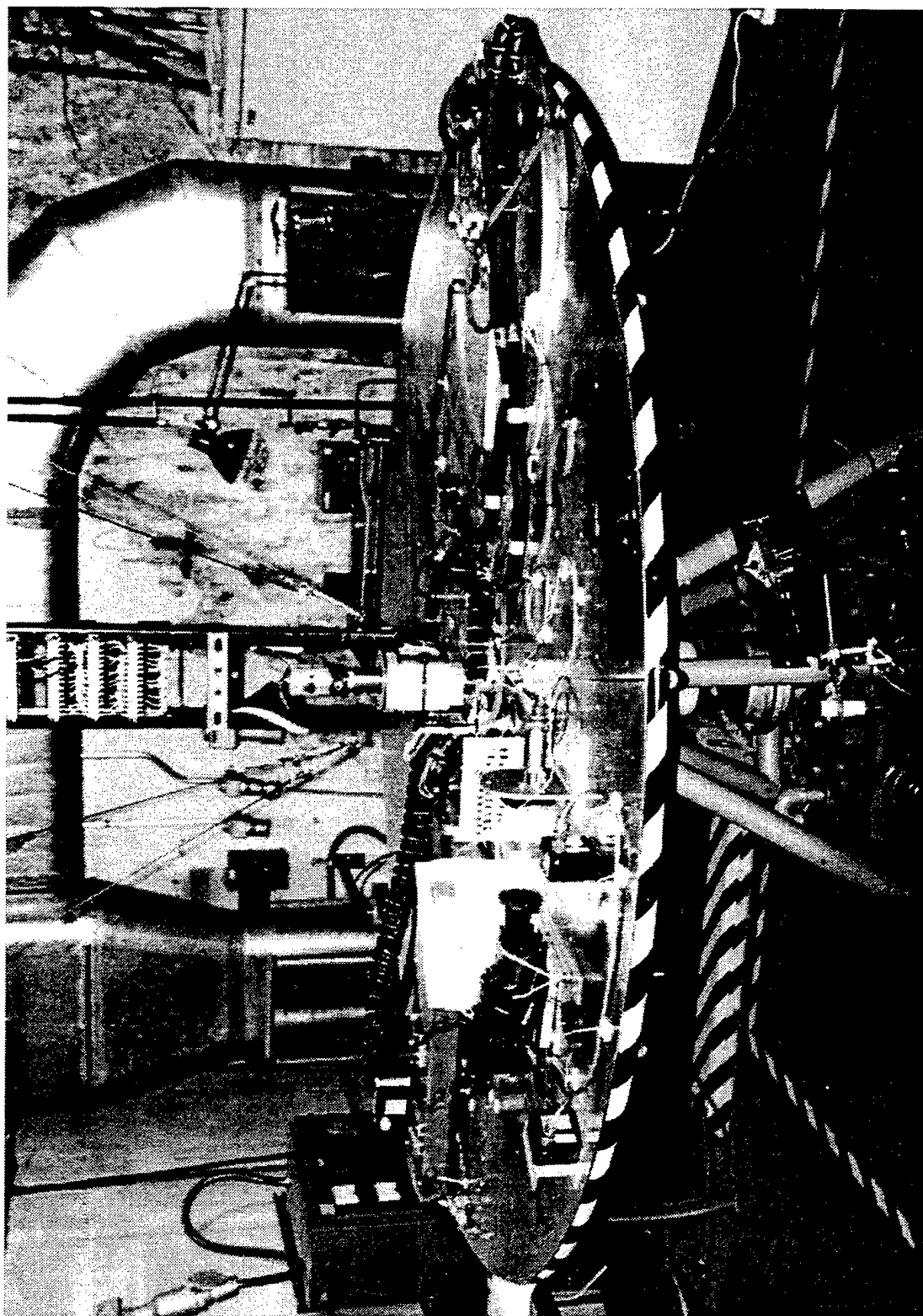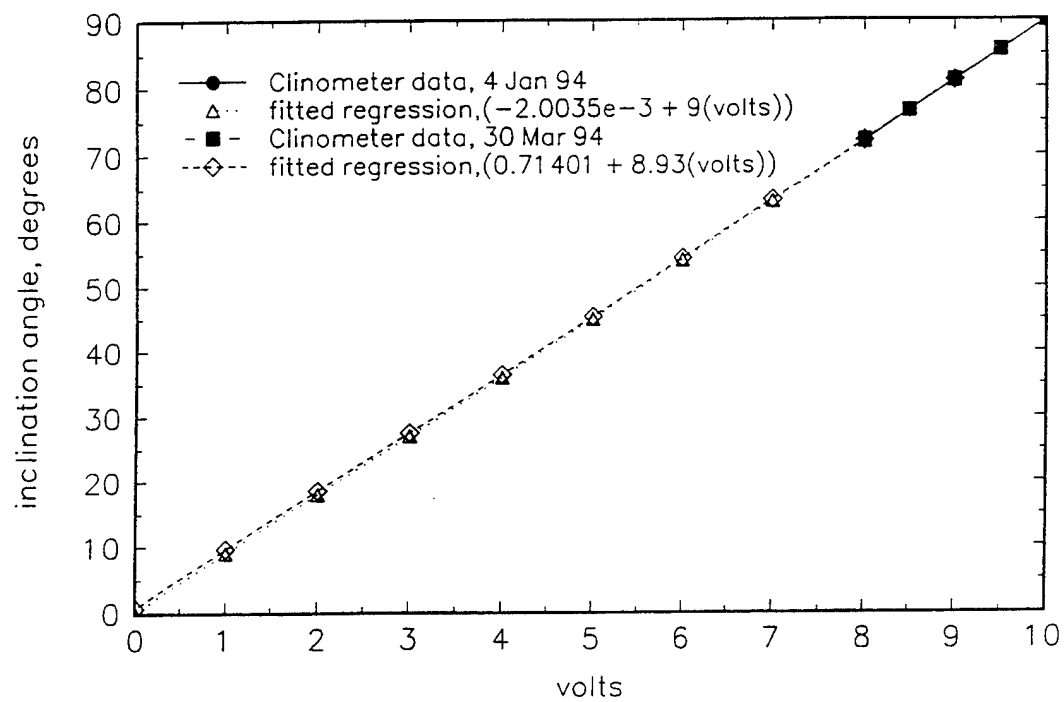
Fig. B.6 Calibration curve for angular displacement transducer.

180

$$tc1 = 0.99402*(40°C/volt)*(volt) - 0.39294$$
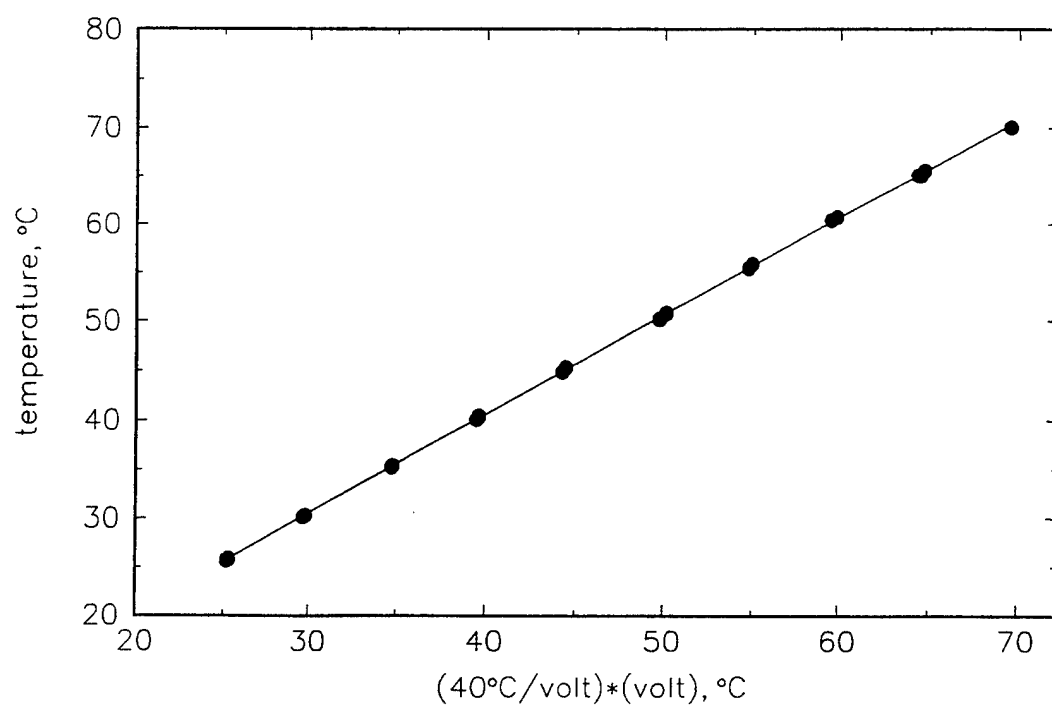
Fig. B.7 Thermocouple calibration curves: a) tc1,

$$tc2 = 1.0083*(40°C/volt)*(volt) - 2.1602$$
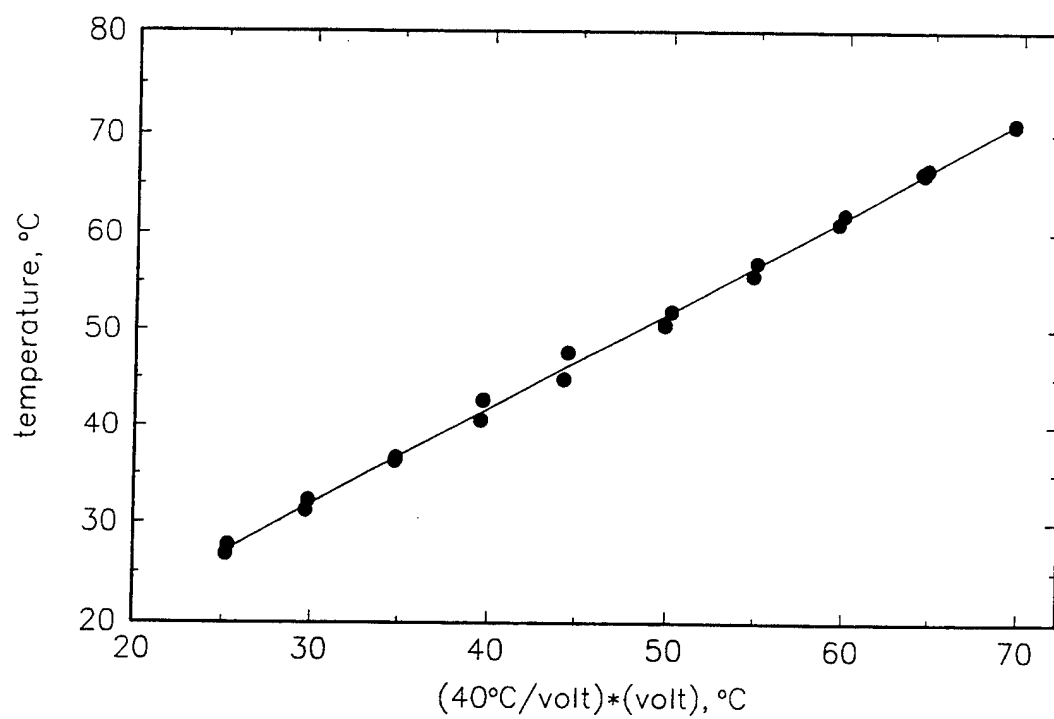
Fig. B.7(contd) b) tc2,

$$tc3 = 0.99255*(40°C/volt)*(volt) - 0.77115$$
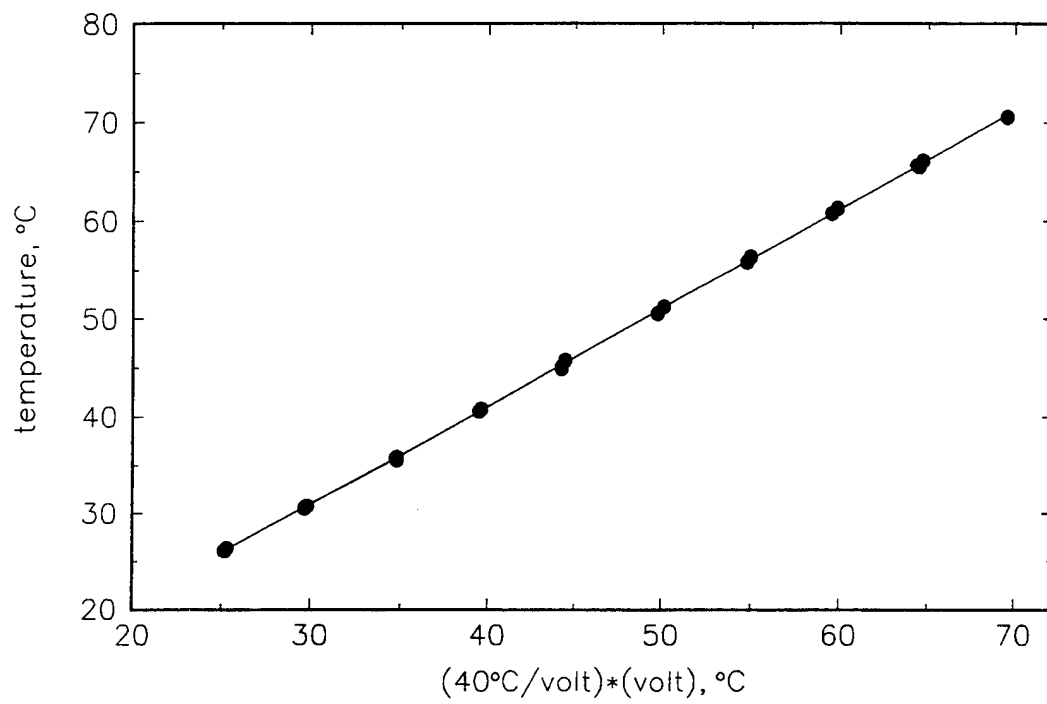
Fig. B.7(contd) c) tc3,

$$tc4 = 0.99249*(40°C/volt)*(volt) - 0.57348$$
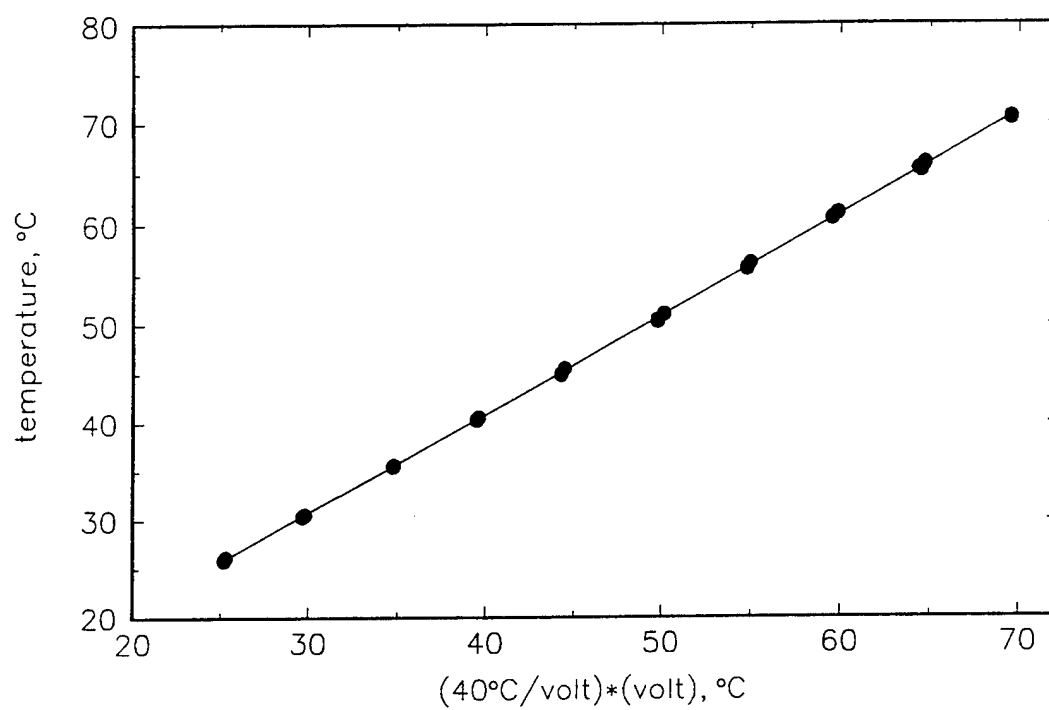
Fig. B.7(contd) d) tc4,

$$tc5 = 0.99208*(40°C/volt)*(volt) - 0.92477$$
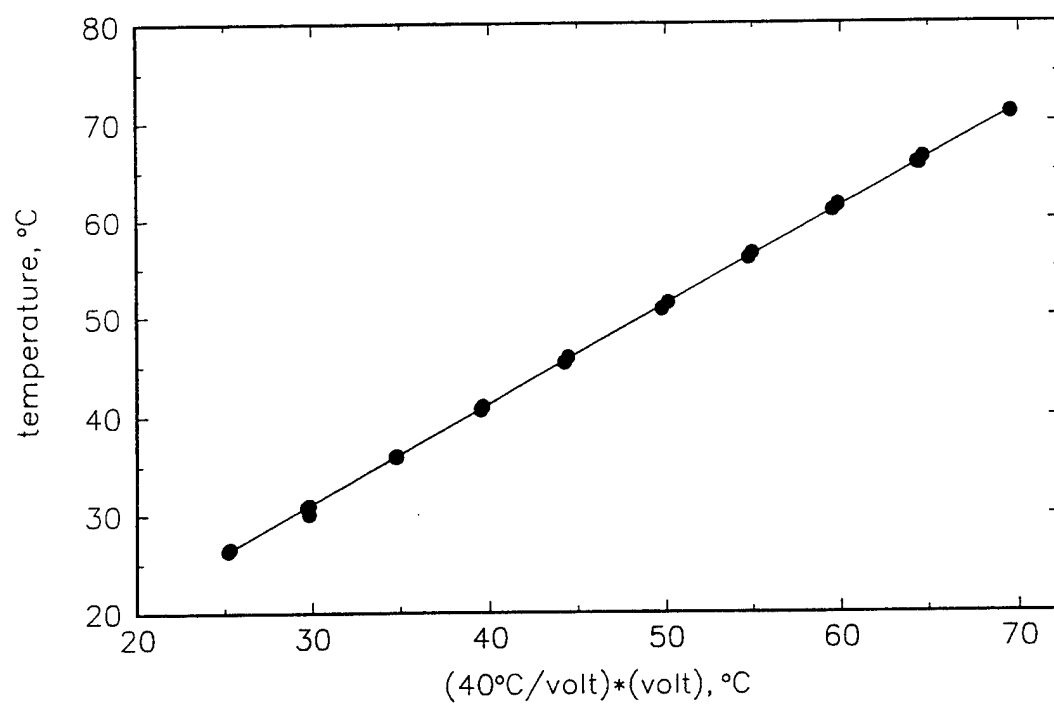
Fig. B.7(contd) e) tc5,

$$tc6 = 0.9916*(40°C/volt)*(volt) - 0.16203$$
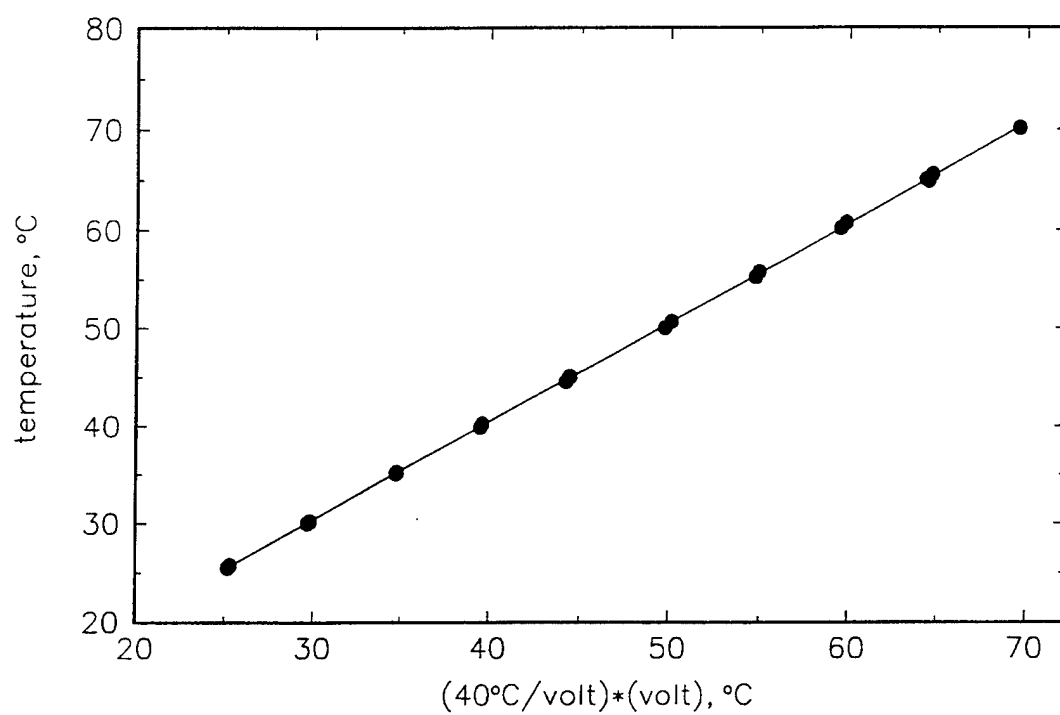
Fig. B.7(contd) f) tc6,

$$tc7 = 0.99583*(40°/volt)*(volt) - 0.9948$$
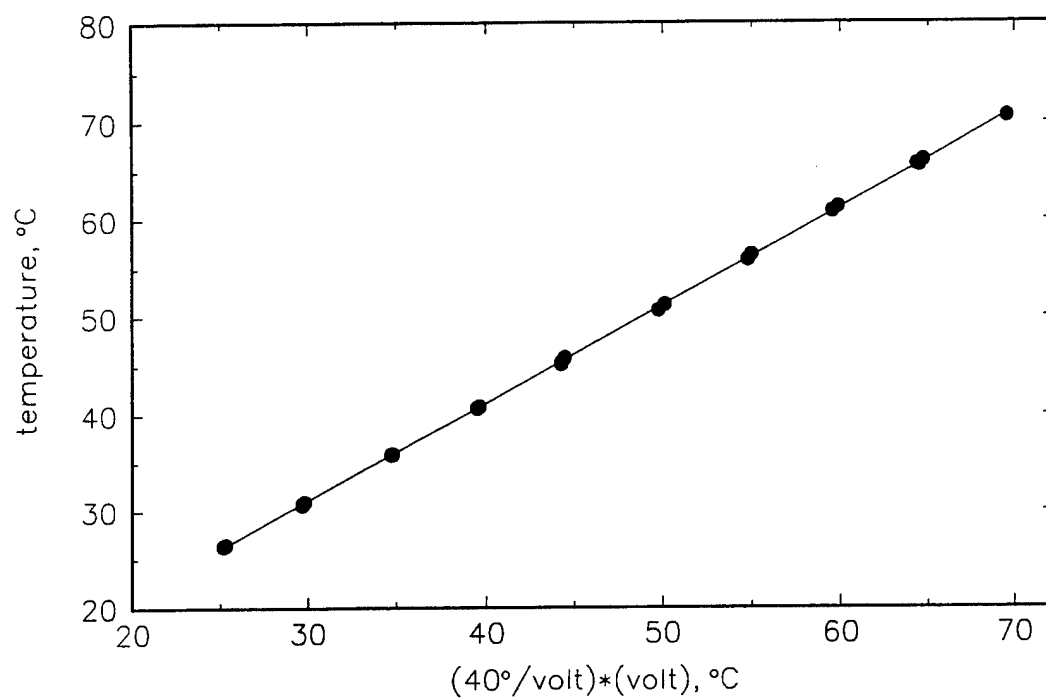
Fig. B.7(contd) g) tc7,

$$\mathrm{tc}8 = 0.99845*(40°C/\mathrm{volt})*(\mathrm{volt}) - 0.68306$$
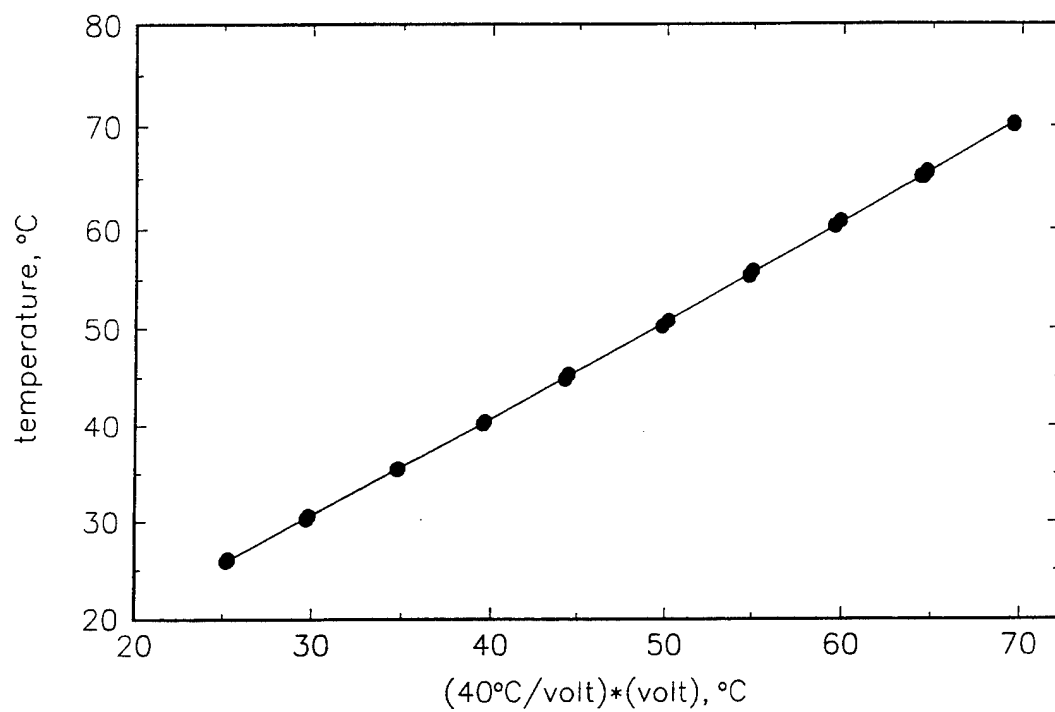
Fig. B.7(contd) h) tc8.
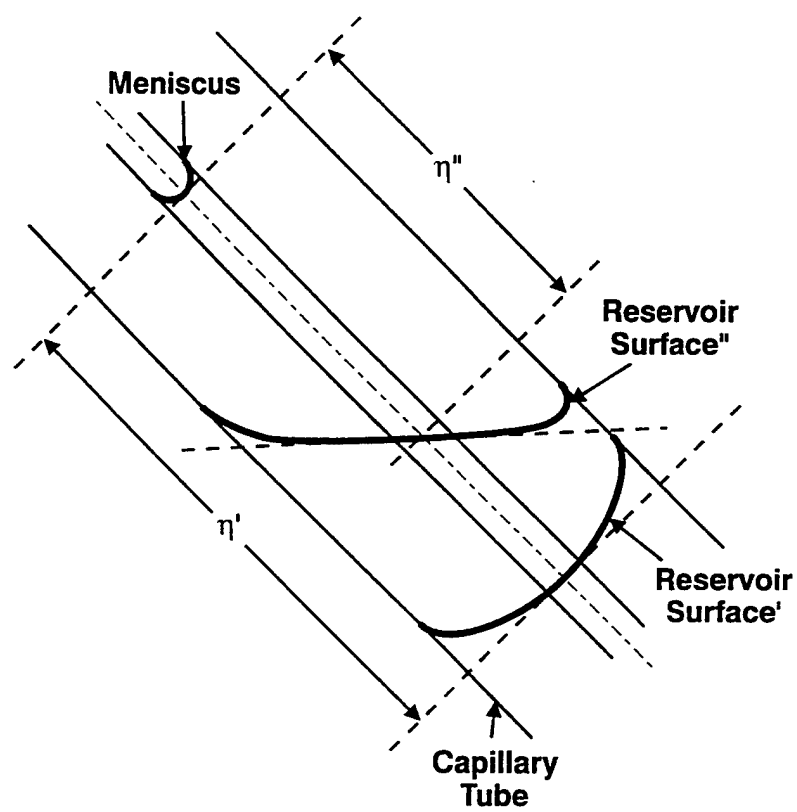
Fig. B.8 Meniscus height measurement reference specification.

Table B.1
Summary of experimental tests conducted for this investigation.

exp#	fluid	ϕ	$Q(W)$	$f(Hz)$	$a(mm)$	Bo	Ca
1	H_2O	20°	0	0.0015	0.946	2.05	1.50×10^{-6}
2		30°					1.03×10^{-6}
3		40°					7.99×10^{-7}
4		50°					6.70×10^{-7}
5		60°					5.93×10^{-7}
6	C_2H_6O	25°	0	0.0015	0.50	1.47	3.55×10^{-6}
7		30°					3.00×10^{-6}
8		40°					2.33×10^{-6}
9		50°					1.96×10^{-6}
10		60°					1.73×10^{-6}
11		30°	0	0.0015	0.25	0.3675	6.00×10^{-6}
12		40°					4.67×10^{-6}
13		50°					3.92×10^{-6}
14		60°					3.47×10^{-6}
15		25°	0	0.100	0.50	1.47	2.37×10^{-4}
16				0.050			1.18×10^{-4}
17				0.025			5.92×10^{-5}
18		30°	0	0.100	0.25	0.3675	4.00×10^{-4}
19				0.050			2.00×10^{-4}
20				0.025			1.00×10^{-4}
21				0.010			4.00×10^{-5}
22		30°	1.0	0.0015	0.50	1.47	3.00×10^{-6}
23			3.5				
24			4.0				

exp#	Re	$\dfrac{a}{h_o}$	$\dfrac{a}{h_o}\dfrac{Re\,Ca}{Bo}$	$\dfrac{Ca}{Bo}$
1	0.278	2.25×10^{-2}	4.58×10^{-9}	7.32×10^{-7}
2	0.191	3.30×10^{-2}	3.15×10^{-9}	5.02×10^{-7}
3	0.148	4.24×10^{-2}	2.44×10^{-9}	3.90×10^{-7}
4	0.124	5.05×10^{-2}	2.05×10^{-9}	3.27×10^{-7}
5	0.110	5.71×10^{-2}	1.81×10^{-9}	2.89×10^{-7}
6	6.07×10^{-2}	1.93×10^{-2}	2.83×10^{-9}	2.42×10^{-6}
7	5.13×10^{-2}	2.28×10^{-2}	2.39×10^{-9}	2.04×10^{-6}
8	3.98×10^{-2}	2.94×10^{-2}	1.85×10^{-9}	1.59×10^{-6}
9	3.35×10^{-2}	3.50×10^{-2}	1.56×10^{-9}	1.33×10^{-6}
10	2.96×10^{-2}	3.96×10^{-2}	1.38×10^{-9}	1.18×10^{-6}
11	5.13×10^{-2}	5.71×10^{-3}	4.78×10^{-9}	1.63×10^{-5}
12	3.99×10^{-2}	7.34×10^{-3}	3.72×10^{-9}	1.27×10^{-5}
13	3.35×10^{-2}	8.75×10^{-3}	3.12×10^{-9}	1.07×10^{-5}
14	2.96×10^{-2}	9.89×10^{-3}	2.76×10^{-9}	9.43×10^{-6}
15	4.05	1.93×10^{-2}	1.26×10^{-5}	1.61×10^{-4}
16	2.02		3.14×10^{-6}	8.05×10^{-5}
17	1.01		7.86×10^{-7}	4.03×10^{-5}
18	3.42	5.71×10^{-3}	2.13×10^{-5}	1.09×10^{-3}
19	1.71		5.31×10^{-6}	5.44×10^{-4}
20	0.855		1.33×10^{-6}	2.72×10^{-4}
21	0.342		2.13×10^{-7}	1.09×10^{-4}
22	5.13×10^{-2}	2.28×10^{-2}	2.39×10^{-9}	2.04×10^{-6}
23				
24				

Table B.4
An example of the raw data extracted from video information.

7 July 94   B

5.0 cm = 6.713 ± 0.0153 mm

$\measuredangle$ 50°
(C_2H_6O)
$f = 0.0015\,Hz$
$\alpha = 0.25\,mm$

Time		Height (cm)
8:58:01	0	12.5 – 13.0
11	10	12.5 – 13.0
21	20	12.5
31	30	12.0 – 12.5
41	40	12.0 – 12.5
51	50	11.5 – 12.0
8:59:01	60	11.0 – 11.5
11	70	11.0
21	80	10.5
31	90	10.0 – 10.5
41	100	9.5 – 10.0
51	110	9.0 – 9.5
9:00:01	120	8.5 – 9.0
11	130	8.0 – 8.5
21	140	8.0
31	150	7.0 – 7.5
41	160	7.0
51	170	6.5 – 7.0
9:01:01	180	6.5
11	190	
21	200	5.5 – 6.0
31	210	5.5
41	220	5.0
51	230	4.5 – 5.0
9:02:01	240	4.5 – 5.0
11	250	4.0 – 4.5
21	260	4.0
31	270	4.0
41	280	3.5 – 4.0
51	290	3.5
9:03:01	300	3.0 – 3.5
11	310	3.0 – 3.5
21	320	3.0
31	330	3.0
41	340	3.0
51	350	3.0 – 3.5
9:04:01	360	3.0 – 3.5
11	370	3.5
21	380	3.5
31	390	3.5 – 4.0
41	400	3.5 – 4.0
51	410	4.0

Time		Height (cm)
9:05:01	420	4.5
11	430	4.5 – 5.0
21	440	4.5 – 5.0
31	450	5.0 – 5.5
41	460	5.5 – 6.0
51	470	6.0
9:06:01	480	6.0 – 6.5
11	490	6.5 – 7.0
21	500	7.0
31	510	7.0 – 7.5
41	520	8.0
51	530	8.5
9:07:01	540	8.5 – 9.0
11	550	9.0 – 9.5
21	560	9.5 – 10.0
31	570	10.0
41	580	10.5
51	590	11.0
9:08:01	600	11.0 – 11.5
11	610	11.5 – 12.0
21	620	12.0
31	630	12.0 – 12.5
41	640	12.5
51	650	12.5 – 13.0
9:09:01	660	12.5 – 13.0
08	667	12.5 – 13.0

EXP 10

193

LIST OF REFERENCES

1.   Kaelble, D. H., *Physical Chemistry of Adhesion*, New York: John Wiley & Sons, 1971.

2.   Adamson, A. W., *Physical Chemistry of Surfaces*, New York: John Wiley & Sons, 1982.

3.   Israelachvili, J. N., *Intermolecular and Surface Forces*, San Diego: Academic Press, Inc., 1985.

4.   Carey, V. P., *Liquid-Vapor Phase-Change Phenomena: An Introduction to the Thermophysics of Vaporization and Condensation Processes in Heat Transfer Equipment*, Washington: Hemisphere Publishing Corp., 1992.

5.   Dussan V., E. B., "On the Spreading of Liquids on Solid Surfaces: Static and Dynamic Contact Lines," *Annual Review of Fluid Mechanics*, Vol. 11, 1979, pp. 371-400.

6.   de Gennes, P. G., "Wetting: Statics and Dynamics," *Review of Modern Physics*, Vol. 57, 1985, pp. 827-863.

7.   Cazabat, A. M., "How Does a Droplet Spread?," *Contemporary Physics*, Vol. 28, 1987, pp. 347-364.

8.   Teletzke, G. F., Davis, H. T., and Scriven, L. E., "Wetting Hydrodynamics," *Revue De Physique Appliquee*, Vol. 23, 1988, pp. 989-1007.

9.   Young, T., *Miscellaneous Works*, G. Peacock, ed. J. Murray, London, Vol. 1,

1855, p. 418.

10.   Padday, J. F., *Theory of Surface Tension, Surface and Colloid Science*, ed. E. Matijevic', New York: John Wiley & Sons, Vol. 1, 1969, pp. 39-251.

11.   Hansen, R. J. and Toong, T. Y., "Dynamic contact Angle and Its Relationship to Forces of Hydrodynamic Origin," *Journal of Colloid and Interface Science*, Vol. 37, No. 1, 1971, pp. 196-207.

12.   Concus, P., "Static Menisci in a Vertical Right Circular Cylinder," *Journal of Fluid Mechanics*, Vol. 34, 1968, pp. 481-495.

13.   Elliott, G. E. P. and Riddiford, A. C., "Dynamic Contact Angles I. The Effect of Impressed Motion," *Journal of Colloid and Interface Science*, Vol. 23, 1967, pp. 389-398.

14.   Phillips, M. C. and Riddiford, A. C., "Dynamic Contact Angles II. Velocity and Relaxation Effects For Various Liquids," *Journal of Colloid and Interface Science*, Vol. 41, No. 1, 1972, pp. 77-85.

15.   Hoffman, R. L., "A Study of the Advancing Interface I. Interface Shape in Liquid-Gas Systems," *Journal of Colloid and Interface Science*, Vol. 50, No. 2, 1975, pp. 228-240.

16.   Calvo, A., Paterson, I., Chertcoff, R., Rosen, M., and Hulin, J. P., "Dynamic Capillary Pressure Variations in Diphasic Flows Through Glass Capillaries," *Journal of Colloid and Interface Science*, Vol. 141, No. 2, 1991, pp. 384-394.

17.   de Gennes, P. G., Hua, X., and Levinson, P., "Dynamics of Wetting: Local Contact Angles," *Journal of Fluid Mechanics*, Vol. 212, 1990, pp. 55-63.

18.   Ngan, C. G. and Dussan, V., E. B., "On the Dynamics of Liquid Spreading on

Solid Surfaces," *Journal of Fluid Mechanics*, Vol. 209, 1989, pp. 191-226.

19.   Dussan, V., E. B., Ramé, E., and Garoff, S., "On Identifying the Appropriate Boundary Conditions at a Moving Contact Line: An Experimental Investigation," *Journal of Fluid Mechanics*, Vol. 230, 1991, pp. 97-116.

20.   Derjaguin, B. V., Nerpin, S. V., and Churayev, N. V., "Effect of Film Transfer Upon Evaporation of Liquids From Capillaries," *Bulletin R.I.L.E.M.*, Vol. 29, 1965, pp. 93-98.

21.   Holm, F. W. and Goplen, S. P., "Heat Transfer in the Meniscus Thin-Film Transition Region." *Journal of Heat Transfer*, Vol. 101, 1979, pp. 543-547.

22.   Moosman, S. and Homsy, G. M., "Evaporating Menisci of Wetting Fluids." *Journal of Colloid and Interface Science*, Vol. 73, No. 1, 1980, pp. 212-223.

23.   Sen, A. K. and Davis, S. H., "Steady Thermocapillary Flows in Two-Dimensional Slots." *Journal of Fluid Mechanics*, Vol. 121, 1982, pp. 163-186.

24.   Swanson, L. W. and Herdt, G. C., "Model of the Evaporating Meniscus in a Capillary Tube," *Journal of Heat Transfer*, Vol. 114, 1992, pp. 434-441.

25.   Hallinan, K. P., Chebaro, H. C., Kim, S. J., and Chang, W. S., "Evaporation from an Extended Meniscus for Nonisothermal Interfacial Conditions," *Journal of Thermophysics and Heat Transfer*, Vol. 8, No. 4, 1994, pp. 709-716.

26.   Pratt, D. M. and Hallinan, K. P., "An Investigation of Thermocapillary Effects on a Heated, Capillary Re-Supplied Meniscus for Low Bond Numbers," 3rd Latin American Symposium on Fluid Mechanics, Feb. 1995, Caracas, Vz.

27.   Li, D. and Slattery, J. C., "Analysis of the Moving Apparent Common Line and Dynamic Contact Angle Formed by a Draining Film," *Journal of Colloid and Interface Science*, Vol. 143, No. 2, 1990, pp. 382-396.

28.   West, G. D., "On Resistance to the Motion of a Thread of Mercury in a Glass Tube," *Proceedings Royal Society of London A*, Vol. 86, 1911-1912, pp. 20.

29.   Washburn, E. W., "The Dynamics of Capillary Flow," *Physical Review*, Vol. 17, 1921, pp. 273-283.

30.   Kafka, F. Y. and Dussan V., E. B., "On the Interpretation of Dynamic Contact Angles in Capillaries," *Journal of Fluid Mechanics*, Vol. 95, 1979, pp. 539-564.

31.   Oker, E. and Merte, H., Jr., "Semi-Transparent Gold Film as Simultaneous Surface Heater and Resistance Thermometer for Nucleate Boiling Studies," *Journal of Heat Transfer*, Vol. 103, 1981, pp. 65-68.

32.   Yerkes, K. L., Chang, W. S., and Beam, J. E., "Heat Pipe Performance with Transient Heat Flux and Body Force Effects," *Advances in Heat Pipe Science and Technology, Proceedings of the 8th International Heat Pipe Conference*, Beijing, China, September 14-18, 1992, pp. 205-213.

33.   Doebelin, E. O., *Measurement Systems Application and Design*, New York: McGraw-Hill, 1983.